2009-02-21

Polymer Microfluidic Devices for Bioanalysis

Xuefei Sun
Brigham Young University - Provo

POLYMERIC MICROFLUIDIC DEVICES FOR BIOANALYSIS

by

Xuefei Sun

A dissertation submitted to the faculty of

Brigham Young University

in partial fulfillment of the requirements for the degree of

Doctor of Philosophy

Department of Chemistry and Biochemistry

Brigham Young University

April 2009

BRIGHAM YOUNG UNIVERSITY

GRADUATE COMMITTEE APPROVAL

of a dissertation submitted by

Xuefei Sun

This dissertation has been read by each member of the following graduate committee and by majority vote has been found to be satisfactory.

Date	Milton L. Lee, Chair
Date	Adam T. Woolley
Date	Matthew R. Linford
Date	H. Dennis Tolley
Date	Daniel Maynes

BRIGHAM YOUNG UNIVERSITY

As chair of the candidate's graduate committee, I have read the dissertation of Xuefei Sun in its final form and have found that (1) its format, citations and bibliographical style are consistent and acceptable and fulfill university and department style requirements; (2) its illustrative materials including figures, tables, and charts are in place; and (3) the final manuscript is satisfactory to the graduate committee and is ready for submission to the university library.

Date	Milton L. Lee Chair, Graduate Committee

Accepted for the Department

David V. Dearden Graduate Coordinator

Accepted for the College

Thomas W. Sederberg Associate Dean, College of Physical and Mathematical Sciences

ABSTRACT

POLYMERIC MICROFLUIDIC DEVICES FOR BIOANALYSIS

Xuefei Sun

Department of Chemistry and Biochemistry

Doctor of Philosophy

Polymeric microchips have received increasing attention in chemical analysis because polymers have attractive properties, such as low cost, ease of fabrication, biocompatibility and high flexibility. However, commercial polymers usually exhibit analyte adsorption on their surfaces, which can interfere with microfluidic transport in, for example, chemical separations such as chromatography or electrophoresis. Usually, surface modification is required to eliminate this problem. To perform stable and durable surface modification, a new polymer, poly(methyl methacrylate-co-glycidyl methacrylate) (PGMAMMA) was prepared for microchip fabrication, which provides epoxy groups on the surface. Whole surface atom transfer radical polymerization (ATRP) and in-channel ATRP approaches were employed to create uniform and dense poly(ethylene glycol) (PEG)-functionalized polymer brush channel surfaces for capillary electrophoresis (CE) separation of biomolecules, such as peptides and proteins. In addition, a novel microchip material was developed for bioanalysis,

which does not require surface modification, made from a PEG-functionalized copolymer. The fabrication is easy and fast, and the bonding is strong. Microchips fabricated from this material have been applied for CE separation of small molecules, peptides, proteins and enantiomers.

Electric field gradient focusing (EFGF) is an attractive technique, which depends on an electric field gradient and a counter-flow to focus, concentrate and separate charged analytes, such as peptides and proteins. I used the PEG-functionalized copolymer to fabricate EFGF substrates. The separation channel was formed in an ionically conductive and protein resistant PEG-functionalized hydrogel, which was cast in a changing cross-sectional cavity in the plastic substrate. The hydrogel shape was designed to create linear or non-linear gradients. These EFGF devices were successfully used for protein focusing, and their performance was optimized. Use of buffers containing small electrolyte ions promoted rapid ion transport in the hydrogel for achieving the designed gradients. A PEG-functionalized monolith was incorporated in the EFGF separation channel to reduce dispersion and improve focusing performance. Improvement in peak capacity was proposed using a bilinear EFGF device. Protein concentration exceeding 10,000-fold was demonstrated using such devices.

ACKNOWLEDGEMENTS

First, I give my sincere appreciation to my advisor, Dr. Milton L. Lee, for providing me with the opportunity to study in his group. His guidance, encouragement, and support provided many invaluable learning and research experiences during my five-year graduate program.

I thank my graduate committee members, Dr. Linford, Dr. Woolley, Dr. Tolley, and Dr. Maynes for their instruction and invaluable suggestions regarding my research. I also thank Dr. Warnick and Dr. Farnsworth for their help on numerical simulations and microscope operation. I am very grateful to Dr. Jikun Liu, Dr. Tao Pan and Dr. Binghe Gu, who taught me how to fabricate microchips and synthesize monoliths. I give Susan Tachka special thanks for her service and support in my research and studies. I would like to acknowledge other members of Dr. Lee's group: Dr. Yansheng Liu, Dr. Shu-ling Lin, Dr. Li Zhou, Lailiang Zhai, Dr. Jenny Armenta, Dr. Nosa Agbonkonkon, Miao Wang, Tai Truong, Yuanyuan Li, Yun Li, Yan Fang, Dan Li, and Jie Xuan. Thank you all for your friendship and help during my time at Brigham Young University.

I would like to give special thanks to my mother, Yunzhen Ji, my mother-in-law, Keqin Wang, my father-in-law, Yicheng Yang, my brother, Pengfei Sun, my sister-in-law, Ling Yu, and my dear wife, Li Yang. Their love, support and encouragement were a great motivation in my Ph.D. studies.

Finally, I thank the Department of Chemistry and Biochemistry at

Brigham Young University for providing me the opportunity and financial support to pursue my Ph.D. degree. Financial support from the National Institutes of Health is gratefully acknowledged.

TABLE OF CONTENTS

LIST OF TABLES

LIST OF FIGURES

1 INTRODUCTION

1.1 Micro-Total-Analysis Systems

1.1.1 Introduction

Although the first analytical miniaturized device, a gas chromatographic analyzer fabricated on a silicon wafer, was reported almost 30 years ago,[1] the concept of micro-total-analysis systems (μTAS) was first proposed by Manz et al. in 1990.[2] μTAS, also called "lab on a chip" devices, are miniaturized analysis systems, which integrate many components together, including sample preparation, injection, separation, and detection. Recently, the development of μTAS has become one of the hottest research fields in analytical chemistry.[3-7]

Both inorganic materials and organic polymers are used for microfabrication of μTAS. Various components of microfluidic devices, such as micropumps, micromixers, microvalves, microreactors, microcolumns, and micro-detectors have been explored. μTAS have many advantages, such as fast and high throughput analysis, comparable performance to conventional methods, small sample and reagent consumption, and easy integration of components in a single device.[8,9] Currently, μTAS are widely used in applications covering chemistry, biochemistry, environmental science, forensics, medicine, and clinical diagnostics.[10] For example, μTAS are employed for cell culture and cell handling,[11] proteins and DNA separation and analysis, particle synthesis and separation, and polymerase chain reaction.[12]

1.1.2 Fabrication of Microdevices Using Inorganic Materials

Inorganic materials used for microfabrication. In the early years of μTAS,

the dominant materials applicable for microfluidic device fabrication were inorganic materials, such as silicon,[1,13,14] glass,[15-19] and quartz.[20-22] All of these materials are widely used in the microelectronics industry and standard microfabrication techniques have already been well developed. Among these materials, silicon is seldom used for microfluidic devices because it is not transparent to visible and UV light for optical detection. Moreover, its breakdown voltage is relatively low (~500 V).[23] In comparison, glass has been the major inorganic material used in microfluidic device fabrication because it has good optical, mechanical, electrically insulating and thermal properties. In addition, glass surfaces are easy to modify because surface chemistries have been well established. Even though quartz, a pure form of silicon dioxide, has superior physical properties over other inorganic materials for microfabrication, it is not widely used in microfluidic device fabrication due to its high cost and difficult fabrication requirements. Recently, Pan et al.[24] fabricated microfluidic capillary electrophoresis devices using calcium fluoride (CaF_2), which has good optical properties and is suitable for various optical detection methods, such as UV, IR, Raman, and fluorescence. However, difficult fabrication and bonding procedures limit its general use.

Fabrication of inorganic microfluidic devices. One of the conventional fabrication techniques for inorganic materials is photolithography. In photolithography, the desired microstructures are fabricated onto inorganic substrates with the help of a photoresist, which is a light-sensitive polymer material. The fabrication procedure usually consists of substrate pretreatment, photolithography, etching and bonding.

Figure 1.1 outlines a typical photolithographic process.

First, a substrate is cleaned using boiling Piranha (H_2SO_4/H_2O_2) or NH_4F/HF solution (step 1, Figure 1.1). Then, an etch mask or sacrificial material (such as Cr/Au,[17,20] amorphous Si,[25] or SiO_2[26-29]) is attached to the substrate surface to protect some areas of the substrate during etching (step 2, Figure 1.1). Following, a layer of photoresist is spin-coated on the top of the etch mask (step 3, Figure 1.1). After soft baking, a photomask, which is a glass plate or transparent polymer sheet containing a high-resolution pattern, is placed on top of the photoresist-coated substrate. UV radiation is employed to transfer the pattern from the photomask to the photoresist layer (step 4, Figure 1.1). To allow the pattern to appear on the surface, a developing solution is used to remove some areas of the photoresist. The final feature on the substrate depends on the photoresist that is used.

There are two types of photoresist: positive and negative.[30] For a positive photoresist, the UV-exposed portion is dissolved during the development process (step 5A, Figure 1.1). The unexposed portion, which is identical to the photomask remains on the surface. In comparison, the UV-exposed portion remains on the substrate when a negative photoresist is used (step 5B, Figure 1.1) and a reversed pattern is obtained on the substrate. After photoresist development, the unprotected etch mask is removed using an etchant (step 6, Figure 1.1), and the bare substrate is further etched (step 7, Figure 1.1). Finally, all of the remnant photoresist and etch mask is removed to complete the desired microstructure on the substrate. When a positive photoresist is used, the final structure is recessed (step 8A, Figure 1.1), however, a negative

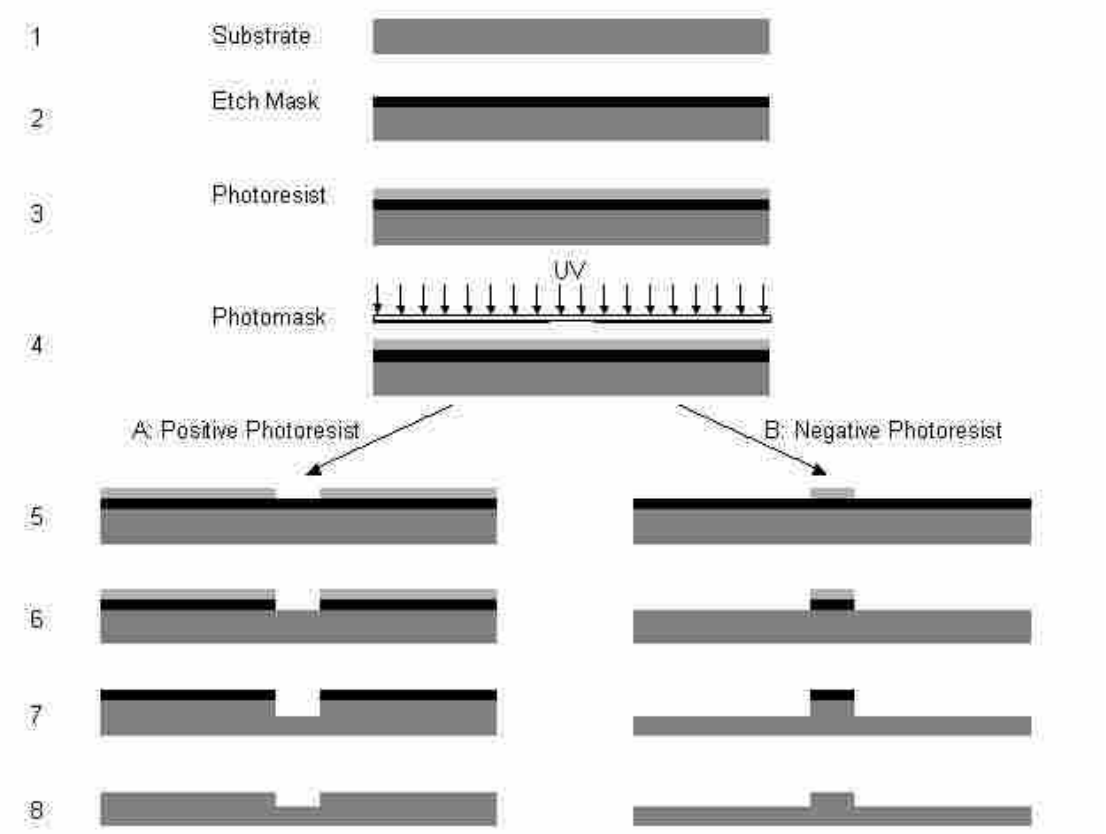

Figure 1.1. Typical photolithographic procedures for microfabrication.

photoresist gives a protruding structure (step 8B, Figure 1.1).

Currently, there are two approaches used to etch inorganic materials: wet etching and dry etching.[30] Wet etching employs liquid chemicals to dissolve the inorganic material. For example, concentrated potassium hydroxide (KOH) solution is a typical anisotropic etchant for silicon,[26-29] which preferentially attacks the <1 0 0> plane of silicon and results in the sidewalls forming an angle of 54.74^{o} with the top surface.[30] HNA solution, a mixture of HF, HNO_3 and CH_3COOH, is an isotropic etchant which generates rounded sidewalls and corners on a silicon surface. HF-containing solutions, such as HF/HNO_3,[17] HF/NH_4F,[18,20] HF/HCl,[31] and concentrated HF,[25] can be used to isotropically etch glass and quartz. The wet etching approach only produces low-aspect-ratio microstructures. Dry etching, such as deep reactive ion etching (DRIE), can create microstructures with high aspect ratios and complex patterns on the surfaces of inorganic substrates.[32,33]

In typical microfluidic device fabrication, a bonding process is needed to enclose the microchannels. Thermal bonding is the most popular technique to bond inorganic substrates. Typically, glass substrates are pretreated in hot Piranha solution to produce silanol groups on the surfaces. Then the substrates are clamped together and heated at an elevated temperature for a period of time to form siloxane bonds between silanol groups on the contacted surfaces.[30] Most glass bonding is carried out in a temperature range from 500 to 700 ^{o}C.[17,18,25] Sometimes, a temperature program is necessary for optimal bonding. The bonding of quartz substrates is usually performed at very high temperature (~ 1100 ^{o}C).[20,22] To bond silicon to silicon or glass,

electric-field-assisted thermal bonding or anodic bonding is used, which is performed at temperatures of 180 – 500 ^{o}C with assistance of an applied voltage from 200 to 1000 V.[13,33-35] Adhesive bonding is an alternative method to bond inorganic microfluidic devices.[24,36,37] This method is usually performed at relatively low temperature. However, the adhesives will impact the microchannel surface properties and, thus, affect the performance of the microfluidic device.

Thin-film fabrication. Recently, a new technique, called thin-film fabrication, was developed to fabricate inorganic microfluidic devices.[38] The procedure is briefly illustrated in Figure 1.2. First, a clean substrate, such as quartz, is coated with a composite sacrificial layer, which contains an aluminum layer and a photoresist layer (Figure 1.2 A). Then standard photolithography using a photomask is employed to pattern the sacrificial layer (Figure 1.2 B). Then, a silicon dioxide (SiO_2) layer is deposited on the patterned surface to enclose the features using plasma-enhanced chemical vapor deposition (PECVD) (Figure 1.2 C). Finally, the enclosed sacrificial layer is removed using etchants to form hollow tubular microfluidic channels. Compared with conventional microfabrication approaches, thin-film fabrication has many advantages. The most attractive advantage is elimination of the bonding procedure. Moreover, it is convenient to produce complex structures, such as multi-layer crossover microfluidic channels. This approach is also applicable to a wide range of inorganic materials for microfabrication. However, the time-consuming etching process is a major disadvantage of this approach.

Although microfabrication using inorganic materials has played an important

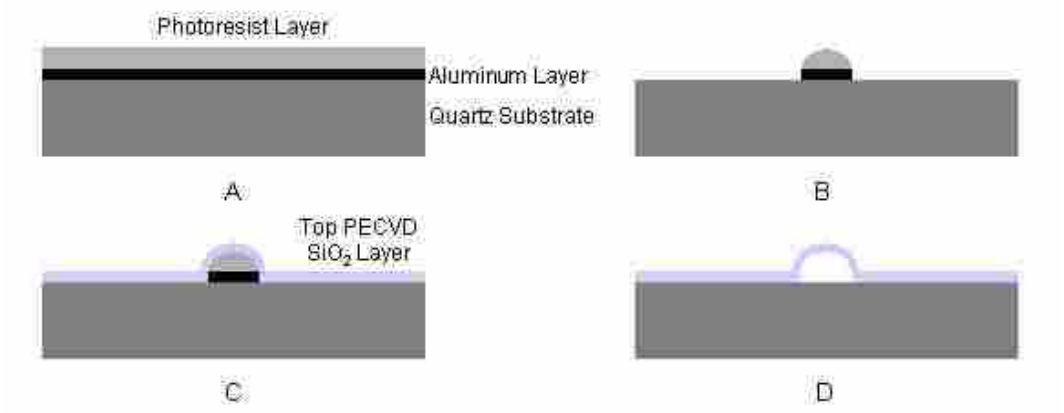

Figure 1.2. Thin-film technique for microfabrication.

role in the origin and development of μTAS, some disadvantages limit its widespread use. The fabrication process must be performed in a clean room with expensive equipment. In addition, hazardous chemicals are involved in the wet etching process.

1.1.3 Fabrication of Microdevices Using Polymeric Materials

Polymer materials used for microfabrication. The disadvantages of inorganic microfluidic devices have driven researchers and producers to seek alternative materials. Recent efforts have led to increasing use of polymeric materials in microfabrication.[39,40] Polymeric materials offer attractive mechanical and chemical properties, low cost, ease of fabrication, biocompatibility, and higher flexibility.[41] To date, many polymers have been explored for fabrication of microfluidic devices, including polydimethylsiloxane (PDMS),[42-45] poly(methyl methacrylate) (PMMA),[26-28,46,47] polystyrene (PS),[48,49] polycarbonate (PC),[50,51] polyethylene terephthalate (PET/PETG),[52,53] polyimide (PI),[54,55] cycloolefin copolymer (COC),[56-58] and polyester.[59-61] Such polymers differ in their properties; therefore, various techniques have been developed for the fabrication of microfluidic devices. Currently, two types of methods are used for microfabrication: replication technologies (such as hot embossing, injection molding and casting) and direct techniques (such as laser ablation).[62]

Template fabrication. In replication technologies, the patterns on the templates or molds are transferred to polymer substrates. First-generation microfluidic devices were fabricated using simple metal wires as templates to directly create straight channels.[46] Second-generation microfluidic devices were fabricated using

planar templates with three-dimensional features on the surfaces, which were produced using various techniques and rigid materials, including silicon,[26-28,46] metals[32,47] and polymers.[47,63-65] For silicon templates, the fabrication methods are the same as for fabrication of inorganic microfluidic devices demonstrated in Figure 1.1. Micromachining technologies (e.g., sawing, cutting, milling, and turning) are capable of producing metal templates.[47] However, these micromachining methods cannot produce complex and high aspect ratio structures. The most commonly used methods for metal template fabrication are electroplating techniques, by which a thick metal layer (nickel or nickel alloy) is grown on a silicon substrate which is patterned using standard photolithographic methods. The substrates are removed to obtain the final metal templates.[32] The LIGA technique, which is a German acronym for lithographie (lithography), galvanoformung (electroplating), and abformung (molding), is a complicated method to produce high-quality templates.[30]

Some polymers with high mechanical strength, such as polyetheretherketone (PEEK), SU-8, and polyetherimide (PEI), can also be used to produce templates. For example, SU-8 templates were fabricated on silicon or glass substrates using photolithography.[63] PEI templates were produced using a hot embossing method.[47] PMMA templates were created from an original negative glass master using a thermal imprinting technique.[64] Recently, a rapid and non-photolithographic approach was presented to generate microfluidic patterns with deep and rounded channels, which leverages the inherent shrinkage properties of polystyrene thermoplastic sheets (Shrinky Dinks).[65]

Hot embossing. Currently the most widely used replication method to fabricate polymeric microfluidic devices is hot embossing.[26-28,46] This method is suitable for thermoplastic polymers, such as PMMA, PC, PET, PS and COC. Generally, a template and a planar polymer substrate are mounted together (Figure 1.3 A). Then the temperature is elevated above the polymer glass transition temperature (T_g) to soften it, and the pattern on the template is embossed into the polymer substrate with assistance of high pressure (Figure 1.3 B). Finally, the assembly is cooled to release the patterned substrate from the template (Figure 1.3 C). During hot embossing, vacuum conditions are usually necessary to prevent the generation of air bubbles between the template and substrate. Also, thermally induced stresses should be minimized to eliminate replication defects.

Injection molding. Injection molding is another commonly used method for fabrication of thermoplastic polymer microdevices.[66] This process starts with raw polymer resins. The resins are melted in a chamber at an elevated temperature and injected into a mold cavity under a high pressure. The cavity is then cooled to allow ejection of the replica. Compared with hot embossing, injection embossing is easier for mass production. Moreover, the cycle time for injection molding is shorter, and it is convenient to integrate other components, such as optical fibers, into the microdevices. One challenge of this method is that the process temperature and pressure should be well controlled to prevent deviations in the replica structure.

Casting. Casting or soft lithography is a simple and flexible replication method for microfabrication.[67] This method does not need special facilities, but can

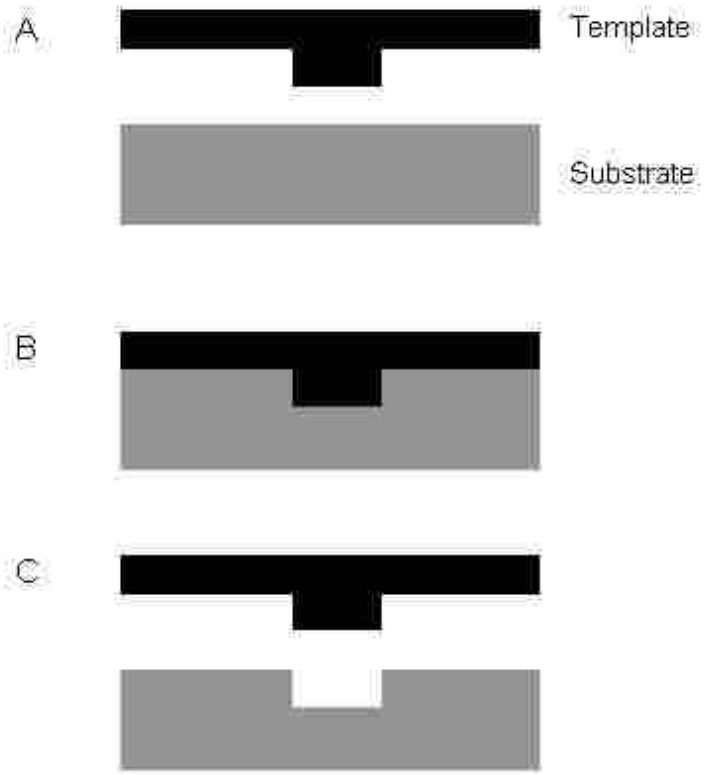

Figure 1.3. Fabrication of polymeric microfluidic devices using hot embossing.

fabricate complex three-dimensional microstructures.[68-70]

The earliest miniaturized PDMS separation device was fabricated using a casting method.[43] PDMS is the most commonly used elastomer for microfabrication. In the casting process, the PDMS monomer is thoroughly mixed with a curing agent and the generated bubbles are removed with vacuum. Then the viscous liquid is poured into a cartridge containing a template. After it is cured, the PDMS slab with desired pattern is peeled off the template. Usually, casting is done under mild conditions, therefore, various materials such as metal, silicon and polymer can serve as templates.

Besides PDMS, many other polymers can also be used in casting, such as solvent-resistant photocurable perfluoropolyether (PFPE),[71] thermoset polyester (TPE)[59] and poly(ethylene glycol) functionalized acrylic copolymers.[72,73]

Solvent imprinting. Recently, a new approach called solvent imprinting was developed to rapidly fabricate microstructures on hard polymer substrates.[74] First, a good solvent for the polyme is spread on the planar polymeric substrate surface (Figure 1.4 A). After a while, a template is pressed into the solvent-coated surface (Figure 1.4 B). When the pattern is transferred to the polymer surface, the substrate is detached from the template (Figure 1.4 C). This procedure is similar to hot embossing, however, solvent imprinting is performed at room temperature and its cycle time is shorter. Furthermore, this method is easily combined with solvent bonding to enclose the microchannels.

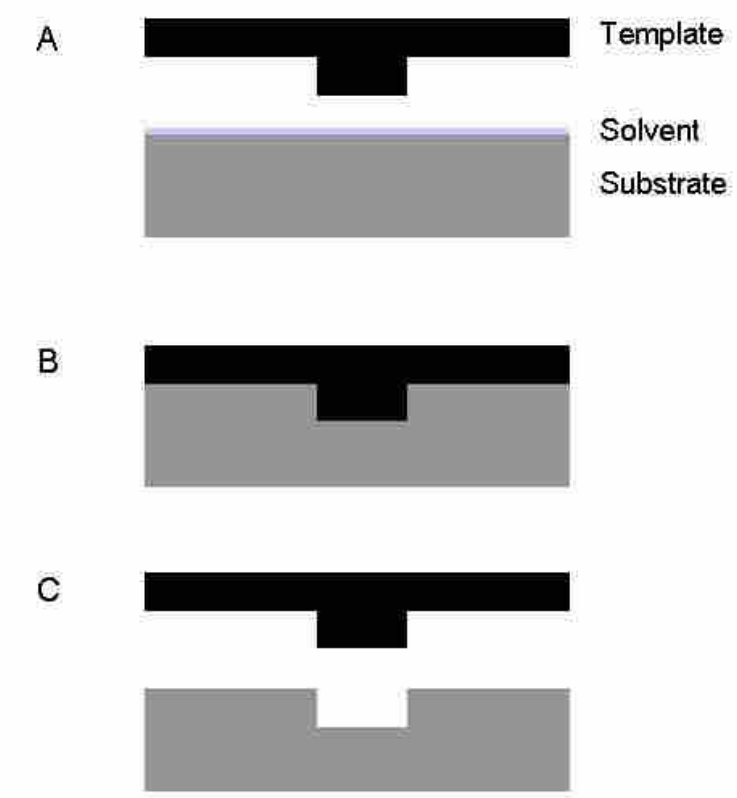

Figure 1.4. Fabrication of microfluidic devices using solvent imprinting.

Laser ablation. In contrast to replication technologies, direct techniques do not depend on templates, which fabricate microdevices individually. Laser ablation or laser micromachining is such a method.[75-78] In this process, the energy of a laser, such as a UV excimer laser or CO_2 infrared laser, is used to break the polymeric bonds and remove the decomposed polymer fragments from the ablation region to form channels. Complex patterns can be fabricated by moving a computer-controlled stage on which the polymer substrate is positioned.

With this technique, a wide range of polymer materials, including PC,[75] PS,[75] PET,[76] PMMA,[77,78] and PETG,[52,75] have been structured. During laser ablation, channel surfaces are simultaneously modified due to photochemical reactions.[79] However, the channel surfaces are rougher than those fabricated using replication methods. Another consideration is that generated polymer fragments may deposit onto the surface to change the local surface properties.

Microfluidic tectonics. Microfluidic tectonics (μFT) is the fabrication and assembly of microfluidic components into a universal platform, in which the microchannels and other components are formed using liquid-phase photopolymerization or laminar flow.[80-83] Typically, a monomer solution containing photoinitiator is filled into a cartridge assembled with microfluidic connections and posts (Figure 1.5 A). Then the cartridge is exposed to UV light with a photomask placed on the top (Figure 1.5 B). The unblocked areas are polymerized (Figure 1.5 C), and the solution under the masked area is finally flushed out to form the channels (Figure 1.5 D).

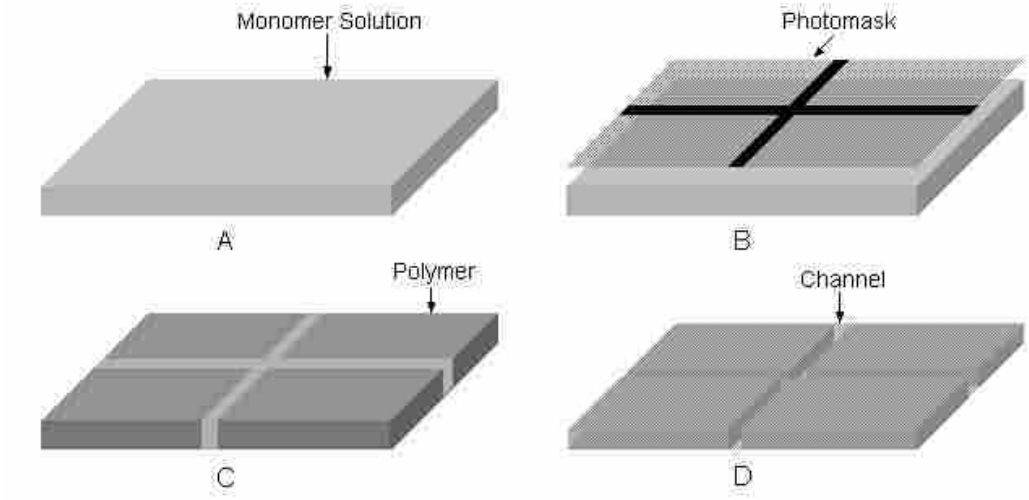

Figure 1.5. Diagram of microfluidic tectonics process.

In this procedure, templates and bonding are not required, and the fabrication consumes only a short period of time. Moreover, some complicated structures, such as valves, pumps and sensors, can be integrated easily by using different photomasks, UV exposure steps and monomers. Membranes or metal wire can be directly fabricated in the microchannels using laminar flow. However, the μFT technique cannot be used to fabricate features smaller than 100 μm due to the lower resolution in fabrication than traditional techniques. During photopolymerization, diffraction of UV light at the edge of the photomask may initiate partial polymerization in regions close to the pattern edge. In addition, free radicals may diffuse to regions under the photomask to cause undesired polymerization. Therefore, monomers that are used should induce polymerization with low shrinkage and fast reaction rate.

SU-8 photolithography. SU-8 is successfully used to fabricate microchannels by applying UV-patterning of SU-8 and adhesive bonding.[84] First, a layer of SU-8 is spin-coated on a wafer and reservoirs are exposed on this layer. Then a second SU-8 layer is coated on top of the first SU-8 layer, followed by patterning using a standard photolithographic approach. The thickness of the second layer defines the depth of the microchannels. Post-exposure bake and development are performed for both SU-8 layers. Finally, a layer of SU-8 spin-coated on a bottom plate wafer is used as an adhesive layer to enclose the microchannels. SU-8 has high thermal stability and optical transparency, good mechanical strength and chemical resistance. However, the electroosmotic flow (EOF) of SU-8 microchannels is large and pH-dependent.

Thermal bonding. Thermal bonding is a broadly used approach to enclose

microfluidic channels.[26,27,46,48-51] Typically, a patterned plate and a cover plate are clamped together. Appropriate pressure is applied to the assembly at elevated temperature around the T_g of the polymer. After a while, the temperature is lowered and the bonded microfluidic device is released from the clamp.

Although thermal bonding is simple and easy to perform, the bonding is often not strong enough, and delamination occurs. Moreover, since the bonding is performed around the T_g of the polymer, channel deformation usually happens, which limits the application of this method to fabrication of high aspect ratio or large dimension structures.

Solvent bonding. Solvent bonding is an alternative bonding method for polymer microfluidic devices.[28,32,47,85] In this method, good solvents for the polymer are employed to dissolve a thin layer of one polymer substrate, which can adhere to the other substrate strongly because the flexible polymer chains at the interface infiltrate into each other and entangle together. Currently, three solvent bonding approaches as shown in Figure 1.6 have been developed. In approach A,[85] a thin layer of solvent is spin-coated on the cover plate (Figure 1.6 A1). Then the patterned substrate is brought into contact with the cover plate (Figure 1.6 A2). After a while, the two substrates are bonded together and enclosed microchannels are formed (Figure 1.6 A3). In approach B,[32] a thin layer of solvent is spin-coated on a glass or silicon wafer, and a patterned substrate stamp is placed on the coated surface (Figure 1.6 B1) to wet all except the recessed areas (Figure 1.6 B2). Then, the solvent-coated substrate and a blank substrate are placed together (Figure 1.6 B3) for a while to bond

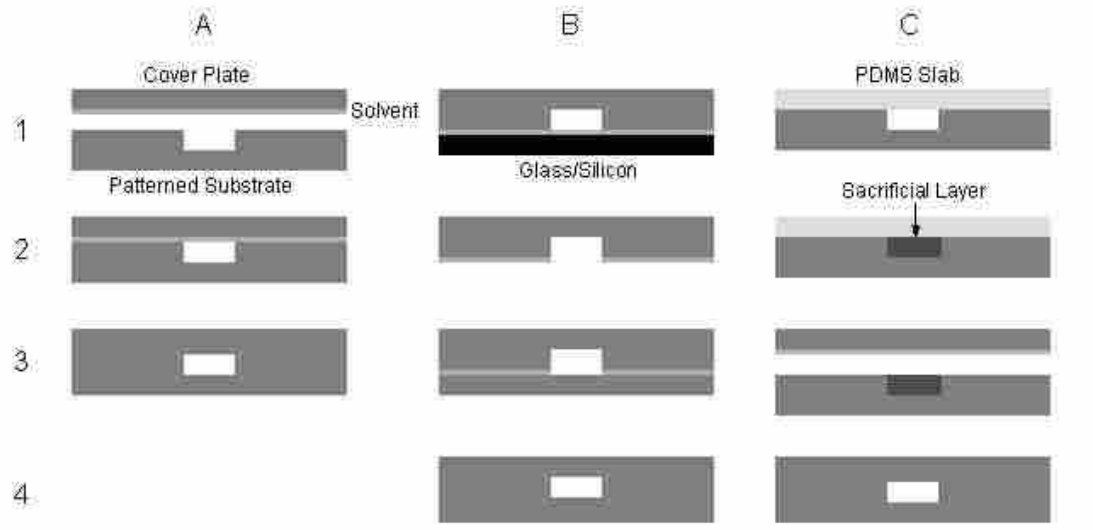

Figure 1.6. Solvent bonding of polymeric microdevices.

them to each other (Figure 1.6 B4).

Solvent bonding is performed at room temperature and can give high bonding strength. However, sometimes the solvent flows into the channels to deform and even block the channels. To avoid these problems, a phase-changing sacrificial layer was reported to protect the channels (Figure 1.6 C).[28] After the channels are temporarily enclosed using a PDMS slab (Figure 1.6 C1), a sacrificial material is introduced into the channels in a fluidic state, and then changed to the solid phase by decreasing the temperature (Figure 1.6 C2). Similar to approach A, a cover plate spin-coated with a thin layer of solvent is pressed onto the patterned substrate after detaching the PDMS slab (Figure 1.6 C3). When the two substrates are bonded together tightly, the sacrificial material is removed by changing it back to the fluidic state from the microchannels. Wax[28] and water[47] have been used as sacrificial materials to fabricate PMMA microfluidic devices.

Adhesive bonding. Adhesive bonding is an approach similar to solvent bonding, however, the adhesive works as a glue and does not dissolve the polymer substrate.[86-88] One consideration is that the residual adhesive on the channel surface may alter the surface properties, leading to sample adsorption and electroosmotic flow (EOF).

Resin-gas injection bonding. Recently, a new technique, resin-gas injection, has been explored for bonding of polymer microfluidic devices (Figure 1.7).[89] Initially, a patterned substrate and a cover plate are assembled together (Figure 1.7 A). A monomer solution containing photoinitiator is introduced into the microchannels

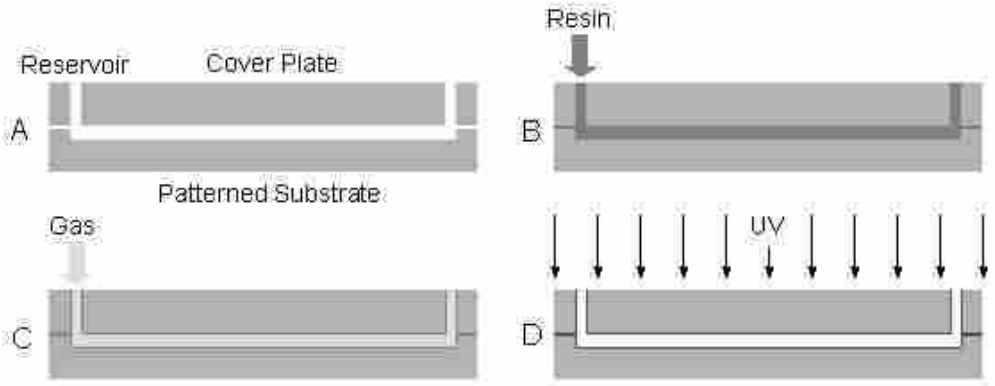

Figure 1.7. Resin-gas injection bonding.

through a reservoir. The solution fills all of the channels, reservoirs and gaps between the patterned substrate and cover plate (Figure 1.7 B). Then nitrogen gas or vacuum is employed to remove the solution in the channels (Figure 1.7 C), and the residual monomer solution in the gaps and on the surfaces is cured using UV radiation (Figure 1.7 D). In this way, the microfluidic devices are bonded together and the channel surfaces are modified simultaneously.

Lamination. Lamination is a simple and rapid method to seal microchannels using thin polymer films. For example, photoablated polymer devices were sealed by thermal lamination with a PET/PE film at 125 ^{o}C using a standard industrial lamination instrument.[75]

Chemical bonding. Chemical bonding depends on a suitable reaction to form chemical bonds between two contact surfaces. This approach provides strong and permanent bonding, however, specific methods must be developed for specific polymers.

To ensure that PDMS is covalently bonded with substrates, such as glass, silicon or PDMS itself, a low power O_2 plasma has been used to treat their surfaces. During O_2 plasma treatment, the surfaces are activated by cleaving siloxane bonds on the surfaces into silanol groups. After plasma treatment, the PDMS substrate is quickly brought into contact with the other complementary substrate to form covalent bonds at the interface.[43,45] Commercial PDMS kits employ a different chemical bonding mechanism. One part of the kit contains a PDMS polymer with vinyl groups and a platinum catalyst, while the other part contains a cross-linker with silicon

hydride groups. When these two PDMS polymers contact, the vinyl groups react with the silicon hydride groups in the presence of the catalyst at an elevated temperature to form covalent bonds.[90,91]

Thermoset polyester (TPE) microchannels are also enclosed using chemical bonding.[59] TPE substrates are fabricated using a casting approach by UV exposure of TPE resin solution containing both photoinitiator and thermal initiator. Then the patterned substrate and cover plate are assembled, exposed to UV radiation, and heated to initiate polymerization between the unsaturated polyester backbones.

Recently, a poly(ethylene glycol)-functionalized acrylic copolymer was used to fabricate microfluidic devices with UV-assisted chemical bonding.[72,73] Partially polymerized planar substrates of this material were given various features after UV exposure of the cast monomer solution. Since polymerization was not taken to completion, active species or groups were left on the prepolymer surfaces. When the two substrates were assembled together and further exposed to UV light, reactions at the interface ensued for bonding. The obtained devices were applied for bioanalysis without further surface modification.

1.2 Microchip Electrophoresis Separation

1.2.1 Introduction

The electrophoretic separation technique is based on the principle that, under an applied potential field, analytes migrate at different velocities due to their net charges and sizes.[92] Historically, electrophoresis has been performed in various

support media, such as paper, cellulose acetate and slab gels. In the early 1980s, capillary electrophoresis (CE) emerged as a high resolution form of electrophoresis.[93,94] Since then, CE has experienced rapid development to become a popular separation method. Several operation modes of CE have been developed, including capillary zone electrophoresis (CZE), capillary gel electrophoresis (CGE), capillary isoelectric focusing (CIEF), capillary isotachophoresis (CITP), and micellar electrokinetic capillary chromatography (MEKC). CE has been successfully used for separation of nucleic acids, proteins, peptides, saccharides, inorganic ions, and small organic molecules.

After the introduction of μTAS, CE separation was successfully combined with μTAS. To date, although microchip liquid chromatography (LC) has also shown excellent performance,[55] microchip CE has been the dominant separation technique in μTAS,[95] including CZE,[96,97] CGE,[98,99] CITP,[100] CIEF,[101,102] MEKC,[103] and 2-D microchip CE.[32,104-106] The most mature application of microchip CE is DNA analysis.[19,107] Recently, protein separation using microchips has received increasing attention.[27,101,108-111]

1.2.2 Fundamental Theory of Capillary Electrophoresis

Electrophoretic mobility. The fundamental theory of modern CE was first described by Jorgenson and Lukacs.[93,94] When a voltage (V) is applied over a capillary with length L, an electric field (E) is established, which drives an analyte to the electrode of opposite charge. The analyte migration velocity (u_{ep}) is expressed as

$$u_{ep} = \mu_{ep} E = \mu_{ep} \frac{V}{L} \tag{1.1}$$

where μ_{ep} is the electrophoretic mobility of the analyte. Therefore, analytes are separated in CE according to their different electrophoretic mobilities. Generally, electrophoretic mobility depends on the analyte and on the local environment, as expressed in equation 1.2.

$$\mu_{ep} = \frac{q}{6\pi\eta r} \tag{1.2}$$

where q is the charge of the analyte, η is the buffer viscosity, and r is the hydrodynamic radius of the analyte. Because different analytes have distinct q and r, their electrophoretic mobilities are also different. It should be mentioned that electrophoretic mobility also relies on the buffer conditions, such as pH value and temperature.

Practically, electrophoretic mobility of an analyte is determined in experiment by measuring the migration time (t_m) through a distance (L_m) when a voltage (V) is applied over a capillary with total length L

$$\mu_{ep} = \left(\frac{L_m}{t_m}\right)\left(\frac{L}{V}\right) \tag{1.3}$$

Electroosmotic flow. Electroosmotic flow (EOF) is used to describe the movement of a liquid in contact with a solid surface when an electric field is applied.[92] EOF occurs in fused silica capillaries where acidic silanol groups on the surface dissociate to form a negatively charged layer when in contact with an electrolyte solution (Figure 1.8). Hydrated cations in the solution are attracted to this layer and arranged into two layers. As illustrated in Figure 1.8, one layer is tightly

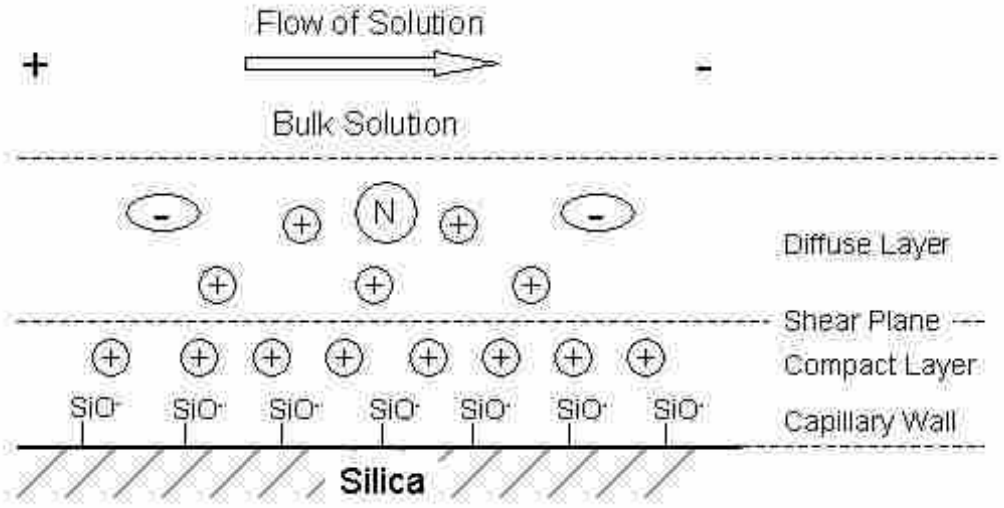

Figure 1.8. Electric double layer on a silica capillary surface and creation of EOF.

attracted (compact layer), the other is more loosely attracted (diffuse layer). The boundary between these two electrical layers is the shear plane. When an electric field is applied, the diffuse layer breaks away at the shear plane and moves toward the cathode, dragging with it the bulk buffer solution, thereby resulting in EOF.

The EOF velocity (u_{EOF}) is given by

$$u_{EOF} = \mu_{EOF} E \tag{1.4}$$

where E is the electric field intensity, and μ_{EOF} is the EOF mobility, which is defined by

$$\mu_{EOF} = \frac{\varepsilon \varsigma}{\eta} \tag{1.5}$$

where ε is the permittivity of the buffer solution and ς (zeta potential) is the electrical potential at the shear plane. The zeta potential depends upon the surface properties and the pH value of the buffer solution. In addition to fused silica, polymeric channel surfaces also generate EOF due to the presence of charged functional groups.[112]

If EOF is considered in CE, the total or effective migration velocity of an analyte (u_{Total}) is the vector sum of both the electrophoretic and EOF velocities, as expressed in equation 1.6,

$$\vec{u}_{Total} = \vec{u}_{EOF} + \vec{u}_{ep} = (\vec{\mu}_{EOF} + \vec{\mu}_{ep}) \times \vec{E} = \vec{\mu}_{Total} \times \vec{E} \tag{1.6}$$

where μ_{Total} is the effective mobility of the analyte.

Separation efficiency and resolution. When an analyte migrates from the injection point to the detection point, its migration time is given by

$$t_m = \frac{L_m}{u_{Total}} = \frac{L_m}{\mu_{Total} E} = \frac{L_m L}{\mu_{Total} V} \tag{1.7}$$

During this time, diffusion occurs. According to Einstein's equation, the spatial variance of the analyte band (σ^2) is defined by

$$\sigma^2 = 2Dt_m \tag{1.8}$$

where D is the effective diffusivity of the analyte. The separation efficiency of CE may be expressed in terms of the number of theoretical plates (N) as given in equation 1.9.[92]

$$N = \frac{{L_m}^2}{\sigma^2} = \frac{{L_m}^2}{2Dt_m} = \frac{\mu_{Total} V}{2D} = \frac{\left|\vec{\mu}_{EOF} + \vec{\mu}_{ep}\right| V}{2D} \tag{1.9}$$

where the migration distance, L_m, equals the total length of the column, L. Experimentally, the efficiency may be determined using[92]

$$N = 5.54\left(\frac{t_m}{w_{1/2}}\right)^2 \tag{1.10}$$

where $w_{1/2}$ is the width of the peak at half height.

The resolution (R_s) of two analytes in CE is defined as[92]

$$R_s = \frac{2\left(t_2 - t_1\right)}{w_1 + w_2} = \frac{t_2 - t_1}{4\sigma} \tag{1.11}$$

where t is the migration time, w is the baseline width in time, and σ is the standard deviation. A better description of resolution was derived by Jorgenson and Lukacs as follows: [92]

$$R_s = 0.177\left(\mu_1 - \mu_2\right)\left[\frac{V}{D\left(\bar{\mu}_{ep} + \mu_{EOF}\right)}\right]^{1/2} \tag{1.12}$$

where $\bar{\mu}_{ep}$ is the average mobility of the two analytes for which the resolution is being calculated.

From equations 1.7, 1.9 and 1.12, a high applied voltage results in fast separation, high efficiency and high resolution. But too high voltage will generate Joule heating and compromise the separation performance. High effective mobility can contribute to high efficiency. Usually, efficiency is also affected by injection length, diffusion and dispersion. When the EOF velocity decreases or moves in the opposite direction from the electrophoretic velocity, the resolution increases.

1.2.3 Sample Injection and Separation in Microchip Electrophoresis

Figure 1.9 shows a typical design of a microchip CE system, where a sample plug formed at the intersection of the channel cross is injected into the long channel for separation. Due to the scale of the channel dimensions, a very small amount of sample can be injected in order to obtain efficient separation. Currently, electrokinectic injection is broadly used in microchip CE and various operation modes have been demonstrated.

Cross injection. The first method introduced in microchip CE is cross injection.[15] A voltage is applied across reservoirs 1 and 2 to form a sample stream as illustrated in Figure 1.10 A. After sample fills the intersection volume, the injection voltage is turned off and a separation voltage is applied across reservoirs 3 and 4 to direct the plug at the intersection region into the downstream channel for separation. It is somewhat difficult to control the injected sample size reproducibly using this technique.

Single T injection. The simplest injection mode is single T injection.[113] As shown in Figure 1.11, a voltage is applied over reservoirs 1 and 3 to drive the sample

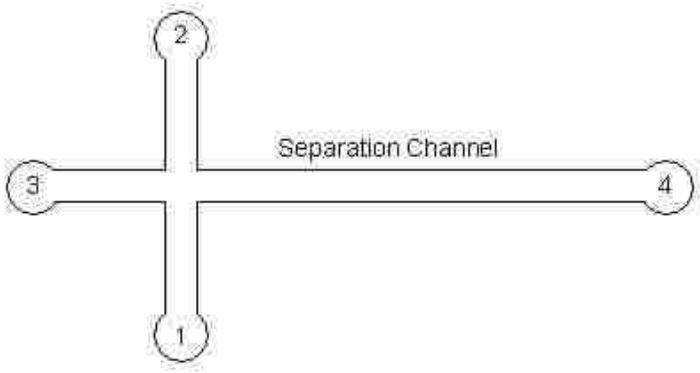

Figure 1.9. Schematic of a typical microchip design.

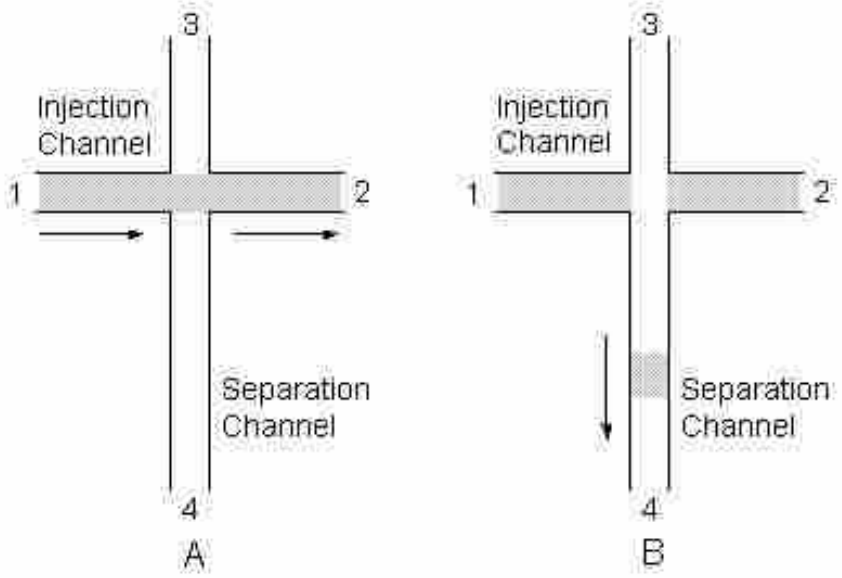

Figure 1.10. Cross injection. (A) Loading and (B) injection and separation.

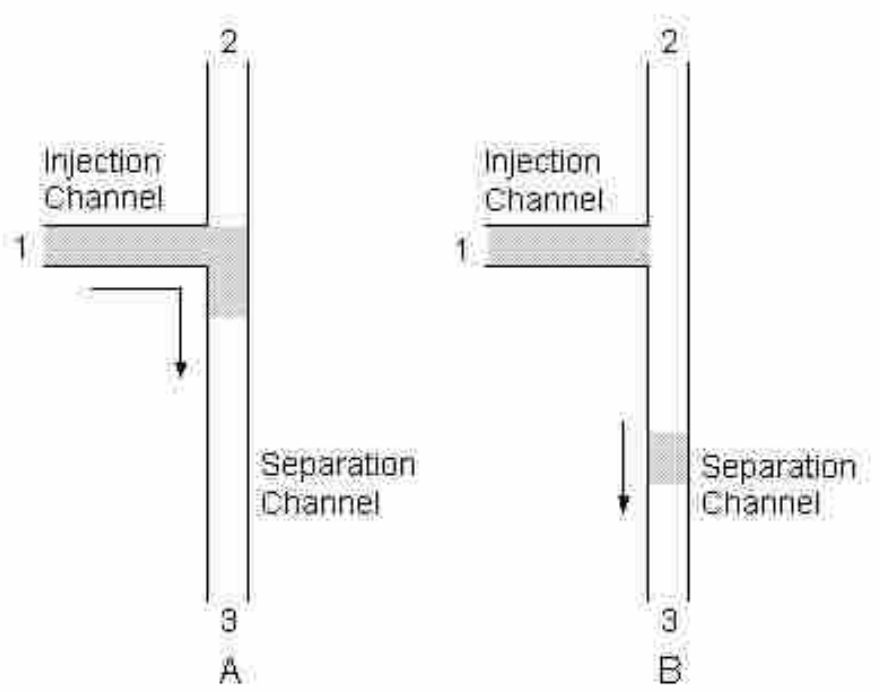

Figure 1.11. Single T injection. (A) Loading and (B) injection and separation.

flow into the separation channel. After a short period, the voltage is switched across reservoirs 2 and 3, and the voltage on reservoir 1 is left floating. In this way, a sample plug is injected and then separated. This technique leads to “injection bias”, in which analytes with high mobilities are injected in higher relative concentration than in the original sample.

Double T injection. To avoid injection bias and obtain reproducible sample size, double T injection was introduced (Figure 1.12).[16,114] During sample loading, a voltage is applied across reservoirs 1 and 2 to produce a sample stream through the intersection volume while reservoirs 3 and 4 are allowed to float. After a short period of time, voltage across reservoirs 3 and 4 is applied. At the same time, reservoirs 1 and 2 are allowed to float. By this procedure, a sample plug is injected into the separation channel for analysis. A serious problem with this technique is leaking of the sample from the injection channel to the separation channel during operation because of convection and diffusion.

Pinched injection. To minimize sample leakage, an approach called pinched injection was developed (Figure 1.13).[18,115] In typical operation, a potential is applied from reservoirs 1, 3 and 4 to reservoir 2 to create a stream of sample ions migrating from reservoir 1 to reservoir 2 (Figure 1.13 A). After a well-defined sample stream is formed, an identical and relatively low potential is applied on reservoirs 1 and 2 to drive sample back toward the reservoirs. Simultaneously, a high voltage is applied across reservoirs 3 and 4 to inject a sample plug into the separation channel (Figure 1.13 B). This technique not only avoids sample leakage, but also gives good

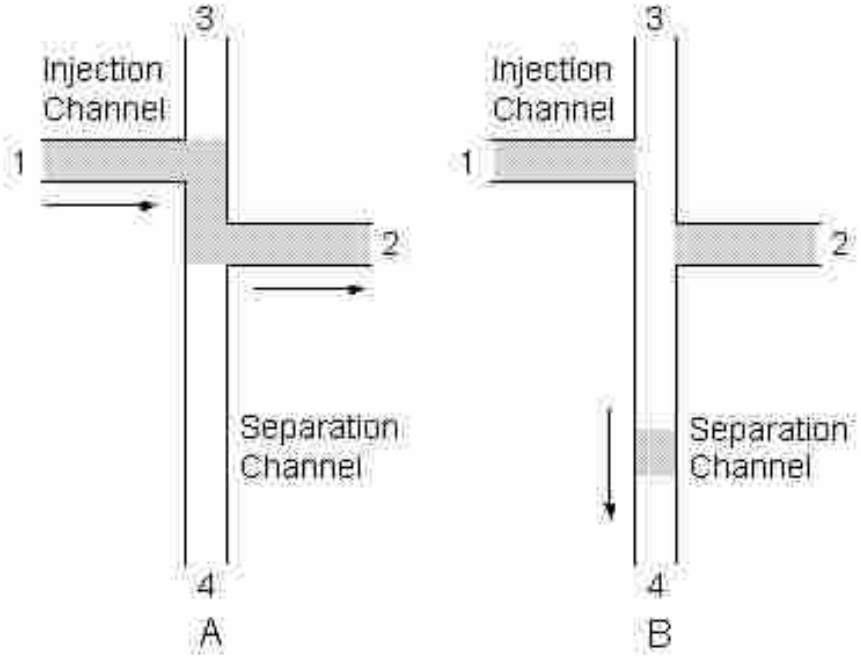

Figure 1.12. Double T injection. (A) Loading and (B) injection and separation.

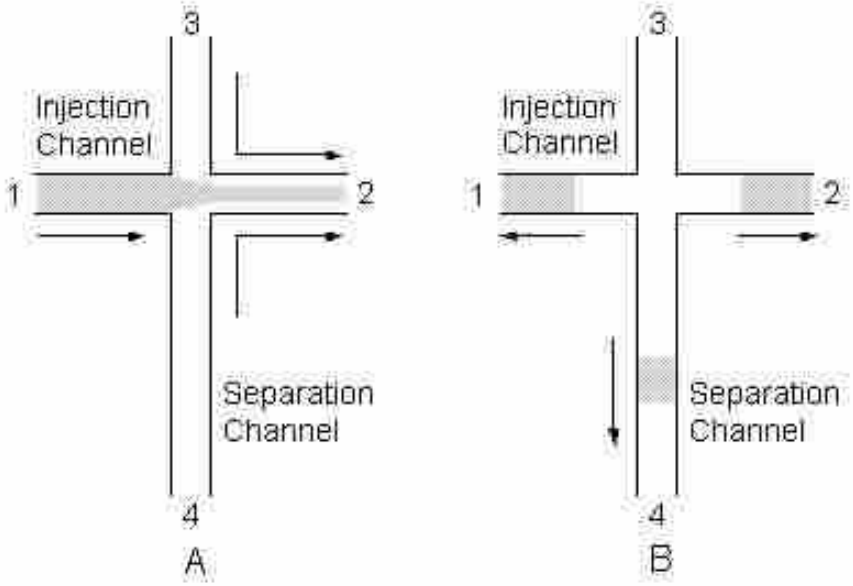

Figure 1.13. Pinched injection. (A) Loading and (B) injection and separation.

reproducibility.

Double L injection. Double L injection is another low leakage injection technique.[116] This method uses "L" shape voltage application twice to control the sample movement as shown in Figure 1.14. The first "L" shape voltage is applied across reservoirs 1 and 3 to form an ion stream (Figure 1.14 A). Then the first voltage is turned off and the second "L" shape voltage is applied across reservoirs 2 and 4 to drive the sample plug formed at the intersection into the separation channel (Figure 1.14 B).

Gated injection. Gated injection is a repetitive injection technique.[117] As illustrated in Figure 1.15, there are three steps involved. First, two "L" shape voltages are applied. One is across reservoirs 2 and 3 to form a sample ion stream while the other is across reservoirs 1 and 4 to form a buffer stream to prevent leakage (Figure 1.15 A). Next, the voltage across 1 and 4 is turned off for a short time to allow a small amount of the sample to enter the separation channel (Figure 1.15 B). Then, the voltage across 1 and 4 is applied again and a sample plug is injected into the separation channel (Figure 1.15 C). Using this method, various sample amounts can be injected by controlling the injection time.

1.2.4 Detection Approaches in Microchip Electrophoresis

Optical detection. UV-absorbance detection is the most commonly used optical detection method for conventional CE and HPLC. Even though this detection method has been used in inorganic microchip CE, it has not been successfully applied to polymeric microchips because of strong UV adsorption by commodity polymeric

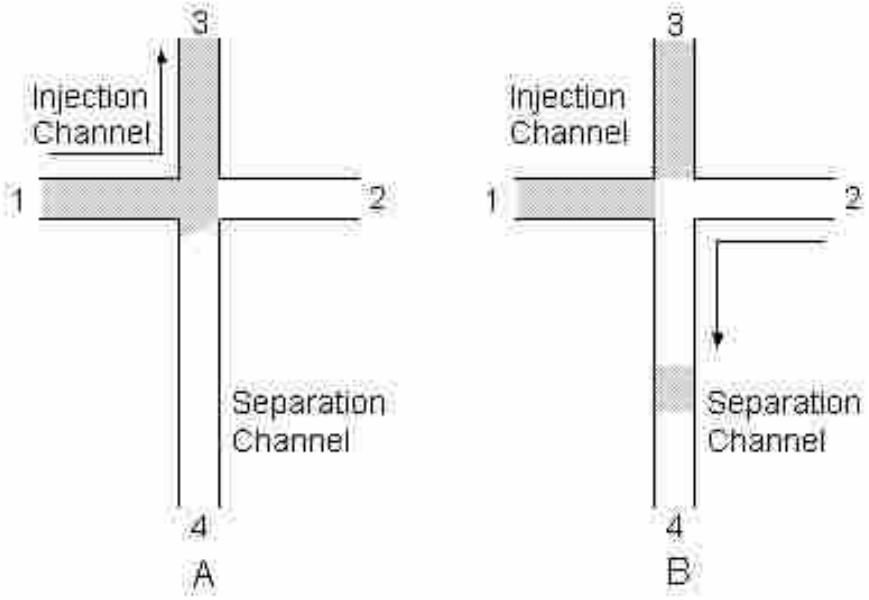

Figure 1.14. Double L injection. (A) Loading and (B) injection and separation.

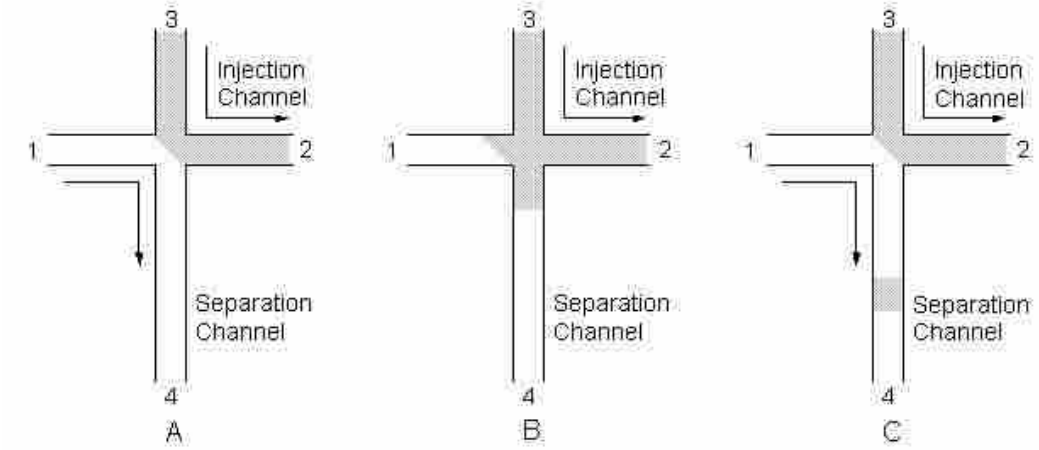

Figure 1.15. Gated injection. (A) Loading, (B) injection, and (C) separation.

substrates.

So far, laser induced fluorescence (LIF) detection is the most popular method for polymeric microchip CE.[26-28,74,113,118] Typically, this method uses a laser with visible wavelength, such as 488 nm, to excite and then emit another visible wavelength. Common polymer substrates are transparent to these wavelengths, which provides high sensitivity and low detection limits. Unfortunately, most analytes including proteins and peptides do not exhibit native fluorescence when excited using a visible laser. Analytes should be tagged with fluorescent dyes for microchip CE detection. Several fluorescent dyes have been used for labeling, such as fluorescein isothiocyanate (FITC).

In addition to UV and LIF, two-photon excited fluorescence (TPEF) detection has been used for quartz microchip CE to detect native fluorescence of analytes.[119] In a typical TPEF process, a fluorophore absorbs two photons sequentially within an extremely short period (~ 1 fs), which are produced by a tightly focused laser beam. After excited to a high energy state, the fluorophore emits fluorescence with a shorter wavelength than the excitation light, which makes it easy to discriminate between the excitation light (visible) and the fluorescence signal. TPEF has potential application in polymer microchip CE detection.

Electrochemical detection. Electrochemical detection is another widely used detection method for microchip CE.[120] Compared with optical methods, electrochemical detection is simple and less expensive. Most importantly, electrodes can be integrated in the microchips using standard photolithography to obtain high

sensitivity and fast response time (~300 ms). Presently, electrochemical detection has been used in both inorganic and polymeric microchips for detection of DNA, proteins, peptides, amino acids, and other samples. There are several operation modes for electrochemical detection, including conductometry, amperometry, and voltammetry.

Mass spectrometry. Mass spectrometry (MS) is a very powerful technique in analytical chemistry. It provides high sensitivity, fast analysis, and small sample consumption. Another advantage of MS is the capability to identity analytes, which is very useful for bioanalysis. A major challenge is the interface for coupling the microchip with MS.[121,122] To date, the most commonly used interface is electrospray ionization (ESI).[102]

1.3 Surface Modification of Polymeric Microfluidic Devices

1.3.1 Introduction

In microfluidic devices, the surface characteristics are important to consider due to the high surface-to-volume ratio. Especially in microchip CE, the channel surface has a significant impact on separation performance. Normally, the polymer surface is charged when in contact with buffer solutions, resulting in EOF in the presence of an electric field. Furthermore, most polymeric surfaces tend to adsorb biomolecules through hydrophobic, electrostatic or other interactions, which compromises separation power and reproducibility. Therefore, it is necessary to modify the microdevice surface as part of the fabrication protocol.[123] Two methods have been commonly used for modification: dynamic adsorption and permanent

surface modification.[124-127]

1.3.2 Dynamic Adsorption Methods

Dynamic adsorption is a simple and rapid surface modification technique that has been used widely to control analyte adsorption and to manipulate EOF for separation of proteins, DNA, or oligosaccharides with polymeric microdevices. Using this approach, surface modifiers are introduced into the separation buffer, which are then physically adsorbed to the channel surface. Many species can serve as surface modifiers, including neutral polymers, charged compounds, surfactants, and nanoparticles.

Among the candidate additives, neutral hydrophilic polymers are the most effective surface modifiers. It was reported that certain neutral polymers with hydroxyl groups, such as poly(ethylene glycol) (PEG), hydroxyethylcellulose (HEC), hydroxypropyl methylcellulose (HPMC), and methylcellulose (MC), could be used to suppress adsorption and improve separation of oligosaccharides in PMMA microchips.[128] Hybrid dynamic adsorption using *n*-dodecyl β-D-maltoside (DDM) and MC in PMMA microchannels was developed for analysis of carbohydrates.[129] Fast protein separation was performed in PMMA microchips dynamically coated with polydimethylacrylamide.[130] Some native fluorescent proteins were isolated in an MC coated PDMS microchip using isoelectric focusing.[131] Hydroxypropyl cellulose (HPC) was employed to dynamically coat PMMA microchannels for separation of amino acids and peptides.[28] To reduce DNA adsorption, poly(ethylene glycol)-poly(propylene glycol)-poly(ethylene glycol) (PEG-PPG-PEG) triblock

copolymer and a mixture containing HPMC, mannitol, glucose and glycerol were used to dynamically coat PMMA microchip surfaces.[132,133]

Charged compounds used for dynamic coating include polymers, such as polybrene (PB), dextran sulfate (DS),[134] poly(styrene sulfonate) (PSS) and poly(allylamine hydrochloride) (PAH),[49] quaternary ammonium derivatized starch,[135] proteins[136] and low-molecular weight species, such as various amines.[128] These have been adsorbed on the channel surface to manipulate the EOF. Polyelectrolyte multilayers (PEMs) have been reported for microchip surface modification. For example, negatively charged PSS and positively charged PAH can be alternately coated on PMMA, PS and PETG surfaces to form PEMs.[48,49] Makamba et al.[137] exposed hydrophobic PDMS to hydrolyze poly(styrene-*alt*-maleic anhydride) (h-PSMA). The h-PSMA strongly interacted with the hydrophobic PDMS surface through the benzene rings while the carboxylic groups extended away from the surface. Subsequently, polyethyleneimine (PEI) and poly(acrylic acid) (PAA) were alternately adsorbed on the surface to form PEMs. The PEMs were then cross-linked by carbodiimide coupling to form amide bonds between the PEI and PAA layers. Finally, a PEG layer was immobilized on the PEMs surface to form a stable permanently hydrophilic, protein-resistant, thin-film coating on the PDMS surface. Proteins, such as albumin and lysozyme, were used for modification of PDMS microchips to enhance separation of neurotransmitters and environmental pollutants.[136]

Other commonly used species for dynamic coating are various surfactants, in

which the hydrophobic segments attach to the polymer surface and the hydrophilic segments extend outward to alter the surface properties. Reported surfactants used for dynamic coating include sodium dodecyl sulfate (SDS), dodecyltrimethylammonium chloride, tetrabutylammonium chloride, cetyltrimethylammonium bromide, Brij 35, Brij 76, and Brij 78.[128,132,138-140]

Recently, nanoparticles have also been used for dynamic adsorption on polymer microchip surfaces. Usually, nanoparticles are employed together with neutral polymers or charged polymers. For example, a coating containing gold nanoparticles (GNPs), poly(ethylene oxide) (PEO), and poly(vinyl pyrrolidone) (PVP) was applied to PMMA microchip for analysis of DNA.[141] PDMS microchannel surfaces have been modified by successive coating with chitosan, GNPs, and albumin.[136]

Although dynamic adsorption is convenient, surface modifiers can influence separation and detection. Sometimes they are detrimental in applications that require coupling to mass spectrometry or to miniaturized chemical reactors. Therefore, permanent surface modification is preferred.

1.3.3 Permanent Surface Modification Methods

Permanent surface modification involves specific chemical reactions to change the surface composition, for instance, attaching protein resistant polymer layers on the surface. Many efforts have been devoted to permanent surface modification of polymeric materials to improve the performance of microdevices.[127]

Plasma-assisted modification. An oxygen plasma is a simple and fast tool to

modify polymeric surfaces. Plasma treatment renders the PDMS surfaces hydrophilic through surface oxidation reactions to form a layer of silanol groups.[67] However, the hydrophilicity disappears after a short time (~3 h) due to hydrophobic recovery.[43] Recently, a new method called two-step extraction/oxidation was developed to generate relatively stable hydrophilicity.[142] First, PDMS was extracted using a series of solvents to remove unreacted oligomers in the bulk. Then, the oligomer-free PDMS was oxidized in an air plasma to generate a layer of hydrophilic SiO_2 on the surface, which was stable for at least 7 days. This method improved the performance of PDMS microchip electrophoresis and also increased the EOF.

The silanols produced by oxygen plasma treatment can be employed for further modification to generate stable hydrophilic layers. Papra et al.[143] grafted PEG-functionalized silanes on an oxygen plasma-treated PDMS microchip surface to resist TRITC-labeled IgG adsorption. Wang et al.[108] treated an oxygen plasma activated PDMS microchip surface with (3-methacryloxypropyl)trimethoxysilane to introduce methacrylic groups, and then polyacrylamide was attached on the surface through reaction with the immobilized methacrylic double bonds. These microchips were used for two-dimensional protein separation after further coating with methylcellulose. Wu et al.[144] introduced amino groups on the plasma pretreated PDMS surface by reaction with 3-aminopropyl-triethoxysilane (APTES). Then some epoxy-containing hydrophilic copolymers, such as poly(AAM-co-GMA) and PVA-g-GMA, were grafted on the surface by reaction between the amino groups and epoxy groups. The surface obtained was hydrophilic and protein-adsorption resistant.

Besides PDMS, an oxygen plasma has been used to treat other polymeric microdevice surfaces, such as PMMA,[27] COC[145] and TPE[59].

UV-light assisted modification. UV radiation is another widely used tool to activate and treat polymer surfaces. UV light assisted graft polymerization is attractive for surface modification of microfluidic devices since it requires few steps and low light penetration into the bulk polymer substrate. For instance, a PDMS surface was exposed to UV light to generate radicals that initiated polymerization from the surface. Several hydrophilic polymers, including polyacrylic acid, polyacrylamide, polydimethylacrylamide, poly(2-hydroxylethyl acrylate) and poly(poly(ethylene glycol)monomethoxyl acylate), were grafted on PDMS microdevice surfaces to improve the separation performance.[109,110,146] The one-step UV light photografting process required a relatively long exposure time, and the microchannels were prone to clog with the polymers generated in the solution. Moreover, it was difficult to achieve reproducible surface modification using this method. To overcome these problems, Hu et al.[111] proposed an alternative strategy called surface-directed graft polymerization. In this two-step process, a photoinitiator was first absorbed onto the PDMS surface. Then, a monomer solution without initiator was introduced into the channel. A polymer layer was formed on the surface when exposed to UV radiation. No clogging was observed in the channel because polymerization on the surface was enhanced by the trapped initiators and, therefore, was faster than in the bulk solution. The resultant microfluidic device exhibited stable EOF and improved separation performance.

PMMA and PC microchips were treated with UV light and ozone to generate hydroxyl and carboxyl groups on their surfaces, which were further used to introduce methacrylate functionality by reacting with 3-methacryloxypropyltrimethoxysilane. Polyacrylamide was then UV light grafted onto the chemically modified surfaces.[147] The carboxyl groups could also be used to attach amine groups to the surface for further modification.[148] Polyacrylamide was UV grafted onto the inner wall of COC microchips for isoelectric focusing of proteins.[101] UV-initiated photografting was also performed on polybutylmethacrylate (PBMA), PS, hydrogenated polystyrene (PS-H), polypropylene (PP), and other polymeric substrates.[149]A pulsed UV excimer laser (KrF, 248 nm) below the ablation threshold was also employed to produce carboxyl groups on the PMMA surface without changing the physical surface morphology. The UV laser-treated PMMA microchip exhibited an increase in EOF and a decrease in band broadening during electrokinetic flow.[150] An ArF excimer laser (193 nm) was used to modify PET microchannels for EOF control.[76]

Modification using other energy sources. In addition to plasma and UV radiation, other energy sources have also been employed to oxidize PDMS surfaces. For example, a Tesla coil was used to generate sufficient ozone to oxidize PDMS surfaces.[151] The Si-OH and/or COOH groups formed by oxidation resulted in an increase in the EOF. An amine-terminated surface was produced by exposing the oxidized PDMS substrate to a solution of 3-aminopropyl triethoxysilane (APTES). A cross-linked amine-terminated layer was formed on the surface, which resulted in a decrease in EOF compared with the native PDMS surface.

Sol-gel modification. A unique sol gel method was reported to modify PDMS microchips, in which nanometer SiO_2 particles were uniformly distributed in the matrix.[152] The first step was to swell a sealed PDMS microchip in tetraethyl orthosilicate (TEOS), which became trapped in the expanded matrix. Then the swelled microchip was immersed in an aqueous solution containing ethylamine to catalyze the formation of SiO_2 particles and shrink the microchip back to its original form. After removal from the ethylamine solution, the PDMS microchip was dried in an oven. Compared with the original PDMS microchip, the modified chip exhibited increased and stable EOF. Moreover, both the hydrophobicity and adsorption proterties of the surface were reduced.

Chemical modification. PDMS microchips have been modified using cerium (IV)-catalyzed polymerization.[153,154] The silanol groups on the PDMS surface were activated using cerium (IV) to form radicals, which initiated polymerization from the surface. Poly(vinylsulfonic acid), poly(acrylic acid), poly(2-acrylamido-2-methylpropanesulfonic acid), poly(4-styrenesulfonic acid), and poly(stearyl methacrylate) were successfully coated on microfabricated collocated monolith support microchip structures for capillary electrochromatography of peptides.

In addition to oxygen plasma and UV radiation treatment, the PDMS surface can be oxidized in acidic H_2O_2 solution to produce silanol groups. The hydrophilic silanol-covered PDMS surface can be further modified by reaction with silanes. Using this approach, functional groups such as PEG and amine can be introduced onto PDMS surfaces for minimization of nonspecific protein adsorption and attachment of

biomolecules, respectively. Surface-grafted amino groups can be converted to isothiocyanate groups for further attachment of peptides, DNA and proteins. The biomolecule-grafted PDMS microchannels can be used for cell immobilization and incubation, DNA hybridization and immunoassay.[155]

Henry et al. chemically modified PMMA surfaces using aminolysis.[156] The ester groups on the PMMA surface reacted with N-lithiodiaminoethane or N-lithiodiaminopropane to yield an amine-terminated surface. The EOF in the aminated PMMA microchannels was reversed compared to the original PMMA. The terminal amine groups could be used for further treatment, such as reaction with *n*-octadecane-1-isocyanate to achieve a $C_{18}H_{37}$-modified PMMA microchannel surface, which was used for CEC separation of oligonucleotides.[157] Waddell et al.[158] and Wang et al.[159] reacted the amine groups with glutaric dialdehyde, and then reacted the resulting aldehyde groups with amino-modified oligonucleotides to immobilize them on the surface.

PETG microchips were treated with NaOH solution, which hydrolyzed the ester groups in PETG backbone chains to produce carboxylic groups. These carboxylate moieties were then used as a means for further modification, such as reaction with amine group-containing reagents.[52]

Bulk modification. Wang et al.[160] reported a bulk modification approach to control surface chemistry and performance of PMMA microchips during the fabrication process. Some alkylmethacrylate modifiers, such as methacrylic acid (MAA), 2-sulfoethyl methacrylate (2-SEMA), and 2-aminoethyl methacrylate

(2-AEMA), were added to MMA monomer solutions to produce copolymers with different surface properties and charges. This resulted in significant enhancement and/or modulation of the EOF. For example, an MAA-modified PMMA microchip showed an increase in EOF and a 2-AEMA-modified microchip exhibited a reversal of EOF compared with untreated PMMA microchips. This simple one-step method that couples the fabrication and modification processes could be easily extended to other polymers to achieve diverse surface chemistries for specific applications. Liu et al. prepared a surface reactive polymer (PGMAMMA) by copolymerization of GMA and MMA. The epoxy groups present on this copolymer surface could be used for further modification, such as photografting of polyacrylamide and aminolysis.[29] Xu et al. used a similar process to bulk modify polyester microchips. Olefinic alcohols were incorporated into an unsaturated polyester matrix, which was then cured with addition of curing agent to initiate cross-linking.[161] Zhou et al. blended PMMA with acrylonitrile-butadiene-styrene (ABS) to fabricate microchips using injection-molding.[162]

Luo et al. doped 0.5 wt % undecylenic acid (UDA) into a PDMS prepolymer to fabricate microchips.[163] This modification did not change the hydrophobicity of the PDMS surface, but increased the EOF. The UDA-doped PDMS microchip was then hydrodynamically coated with n-dodecyl-β-D-maltoside (DDM) to minimize protein adsorption on the surface. These microchips could then be used for electrophoretic separation of immunocomplexes.

1.3.4 Atom Transfer Radical Polymerization

Atom transfer radical polymerization. Unfortunately, among the methods reported to permanently modify the microchip inner surface, few were effective for high-efficiency separations of proteins, indicating that more uniform polymer layers with higher surface coverage are needed. Recently, atom transfer radical polymerization (ATRP) has been used to grow polymers on planar surfaces or spherical particles, which appears to provide the desired higher surface coverage.

Different from traditional radical polymerization, ATRP is a transition metal catalyzed free radical living polymerization method, which produces well-defined polymers of low polydispersity.[164,165] A general mechanism for ATRP is shown in Figure 1.16.[164] A free radical ($R^{\cdot}$) is generated from an organic halide (R-X, where X is a halogen atom) through a one-electron oxidation with concomitant abstraction of X from R-X, which is a reversible redox process catalyzed by a transition metal complex (M_t^n-Y/Ligand, where Y is another ligand or a counter ion). The generated radicals react with monomers to propagate the polymer chains in a manner similar to traditional radical polymerization. Termination reactions also occur through radical coupling and disproportionation. Typically, few growing polymer chains undergo termination and other side reactions because of fast initiation and rapid reversible deactivation. The radicals react rapidly with the oxidized metal complexes (X-M_t^{n+1}-Y/Ligand) to reduce the stationary concentration of radicals and thereby minimize the contribution of termination. Therefore, ATRP is a living polymerization method. In ATRP, one polymer chain forms per molecule of organic halide and the

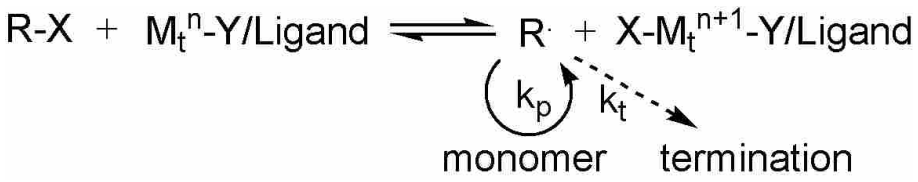

Figure 1.16. Atom transfer radical polymerization.

generated polymer chains are uniform and well controlled by the reaction conditions.

Surface-initiated ATRP for microchip surface modification.

Surface-initiated ATRP (SI-ATRP) is a well-controlled "grafting from" polymerization technique that produces uniform and dense polymer brushes on various surfaces. Huang et al. grafted a polyacrylamide film on nanoporous silicasurfaces using SI-ATRP to separate proteins by size exclusion.[166] They also used SI-ATRP to graft linear or cross-linked polyacrylamide films on fused silica capillary inner walls without clogging for capillary electrophoresis of proteins.[167] Leinweber et al. used a similar method to graft poly(2-hydroxyethyl methacrylate) (PHEMA) on a capillary surface to lower the EOF and to separate proteins with high efficiency.[168] Miller et al. further derivatized the grafted PHEMA layer with ethylenediamine or octanoyl chloride to afford better resolution of phenols and anilines.[169] Unsal et al. used SI-ATRP to graft poly(3-sulfopropyl methacrylate) (PSPM) onto hydrolyzed porous poly(glycidyl methacrylate-co-ethylene dimethacrylate) (poly(GMA-co-EDMA)) particles for use as an ion-exchange chromatographic stationary phase.[170]

SI-ATRP has also been applied to modify microchip surfaces. Xiao et al.[171] carried out microchannel confined SI-ATRP to graft a thin polyacrylamide layer inside a PDMS microchannel. The patterned PDMS surface was oxidized using a UV/ozone plasma and then bonded with the ATRP initiator. Finally, an aqueous solution containing acrylamide, catalyst and ligand was introduced into the enclosed microchannel to perform ATRP. The resultant microchip was successfully used for

electrophoretic separation of proteins.

Liu et al.[27] employed an oxygen plasma to oxidize PMMA and generate hydroxyl groups on the surface. Following plasma treatment, an ATRP initiator was anchored by reaction of 2-bromoisobutyryl bromide with the hydroxyl groups. Then a PEG-functionalized monomer, poly(ethylene glycol) methyl ether methacrylate (PEGMEMA), was polymerized from the surface through SI-ATRP. The coupled PEG-containing layer resisted protein adsorption and reduced EOF. Efficient and reproducible CE of proteins was obtained using the resultant PMMA microchips.

Recently, Pan et al.[118] developed a new technique called in-channel ATRP to modify TPE microdevices, which were fabricated using a casting method. An ATRP initiator was first immobilized on the channel surface through the existing hydroxyl groups. Then a dilute PEG-functionalized monomer solution containing catalyst and ligand was introduced into the microchannel to perform ATRP. The resultant PEG-grafted TPE microchannel exhibited low, pH-stable EOF, low protein adsorption, and efficient separation of amino acids and peptides. This microdevice was also used to separate phosducin-like protein and phosphorylated phosducin-like protein to evaluate the efficiency of phosphorylation.

1.4 Electric Field Gradient Focusing

1.4.1 Introduction

With completion of the sequencing of the human genome, scientists have turned their attention to proteomics, which involves the study of proteins in organisms

including identification of amino acid sequences, tertiary structures and functions in biological systems.[172,173] Identification of a target protein or biomarker of a disease, such as cancer, can significantly help to develop an efficient drug to treat the disease. However, protein analysis is a major challenge because of the vast number of proteins in biological systems and their dynamic nature. It has been estimated that 500,000 to 1 million proteins are expressed in humans.[174] They have different molecular weights, isoelectric points (*pI*) and other properties. Most importantly, the dynamic range of protein abundance ranges from >> mg/mL to << pg/mL, exceeding approximately ten orders of magnitude.[175] Moreover, proteins interact with each other or with other ligands, and they are frequently modified by post-translational reactions, such as phosphorylation, carbamylation, glycosylation, deamidation, etc.[176] All of these challenges make complete characterization of a proteome nearly impossible with current analytical techniques. Therefore, sophisticated analytical techniques are needed to analyze such complex mixtures. For the first step of protein analysis, protein isolation, the techniques must offer fast and high throughput separations with high peak capacity, large dynamic detection range, low detection limits, and reliable resolution.

Currently, the most widely used approach for large-scale separation of protein mixtures is two-dimensional (2-D) gel electrophoresis.[177-179] Although this technique can provide over 1,000 discrete bands per gel, it has a number of limitations. This method is time-consuming and labor-intensive. It cannot provide sufficient resolution and reproducibility. It cannot analyze proteins with extreme *pI* values and

hydrophobicity. Moreover, the detection limits of this technique are not sufficient to analyze lower-abundance proteins, which have potential value for clinical diagnosis. Because of this, researchers have been developing alternative techniques such as 2-D liquid chromatography (LC) and mass spectrometry (MS) for peak identification.[180] Most of the newer techniques are combinations of liquid chromatography (LC) and electrophoresis. Both LC and electrophoresis are linear techniques widely used in separation science. However, they have some inherent limitations. For example, the injected sample plugs broaden as the separation continues, which impacts the separation efficiency and resolution. Another problem is that samples are diluted during the separation, which complicates the determination of trace analytes.[181] To circumvent these limitations, a nonlinear technique, termed equilibrium gradient focusing, was introduced by Giddings and Dahlgren.[182] In this method, the net force applied on an analyte, as a result of an external gradient field and an opposing force, changes monotonically along the channel and reverses its direction at an equilibrium point where the net force is zero. All analyte molecules of the same kind are drawn to the equilibrium point and are focused and concentrated. A good example of such a technique used for separation of proteins is isoelectric focusing (IEF), which is based on the establishment of a pH gradient in a separation column.

1.4.2 Principles of Electric Field Gradient Focusing

Electric field gradient focusing (EFGF), another member of the family of equilibrium gradient focusing techniques, depends on an electric field gradient and a counter-flow to focus, concentrate and separate charged analytes, such as peptides and

proteins.[181,183-188] The constant counter flow is opposite to the electrophoretic force that drives the analytes. When the electrophoretic velocity of a particular analyte is equal and opposite to the velocity of the counter flow, the analyte is focused in a narrow band because at this position the net force on it is zero (Figure 1.17). Since analytes with different electrophoretic mobilities have unique equilibrium positions, EFGF separates analytes according to their electrophoretic mobilities, similar to the way IEF separates analytes according to isoelectric points. However, EFGF avoids protein precipitation that often occurs in IEF when proteins reach their isoelectric points and, therefore, can be applied to a broad range of proteins.

The basic theory of EFGF developed by Tolley et al.[186,187] was derived starting from the general transport equation

$$J = \left(u + \mu E(x)\right)c(x) - D_T \frac{\partial c(x)}{\partial x} \tag{1.13}$$

where J is the flux density of the analyte, u is the velocity of the counter hydrodynamic flow, μ is the electrophoretic mobility of the analyte, $E(x)$ is the electric field intensity at point x, $c(x)$ is the concentration of the analyte at point x, and D_T is the dispersion coefficient that represents the sum of all contributions to effective diffusion.

The electric field gradient at point x is expressed as

$$q(x) = -\frac{\partial E(x)}{\partial x} \tag{1.14}$$

When the analyte is focused at point x_0 (i.e., its equilibrium point), the flux is set equal to zero

$$J = 0 \tag{1.15}$$

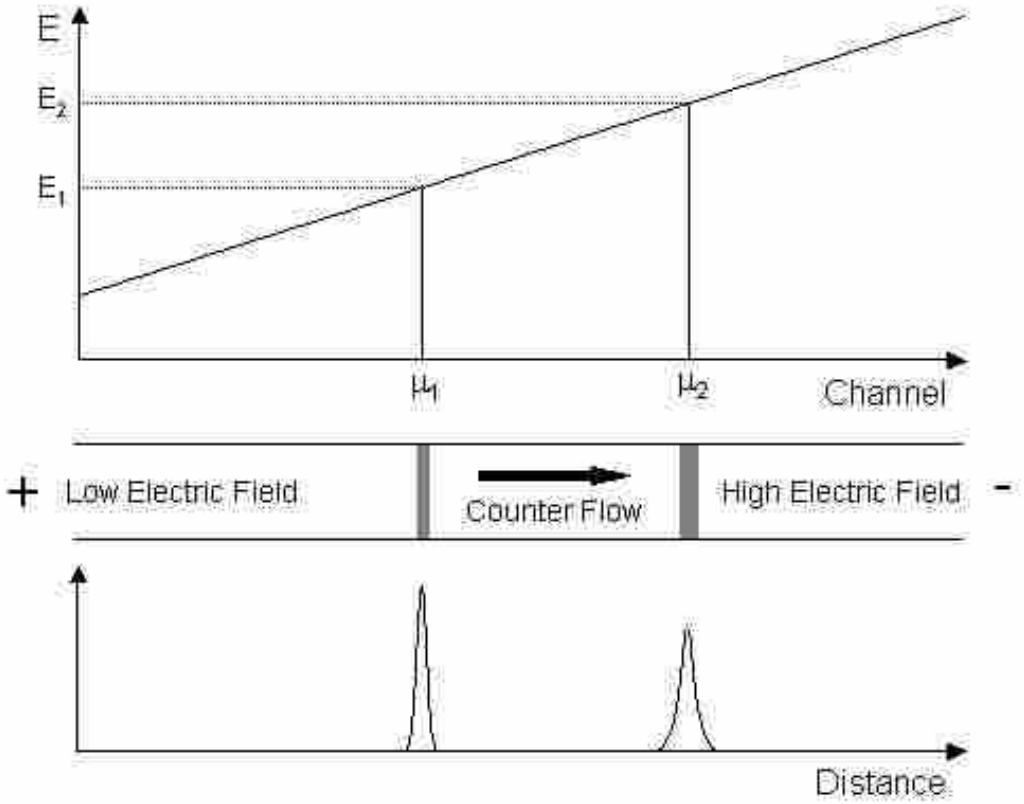

Figure 1.17. Schematic representation of an EFGF separation.

and

$$u + \mu E(x_0) = 0 \tag{1.16}$$

From equations 1.13 to 1.16, the standard deviation (σ) of the focused band is obtained as

$$\sigma = \sqrt{\frac{D_T}{\mu q(x_0)}} \tag{1.17}$$

The resolution (R_s) can be expressed as

$$R_s = \frac{\Delta x}{4\sigma} = \frac{|u|}{4} \cdot \left(\frac{\bar{\mu}}{q(x_0) D_T} \right)^{1/2} \cdot \frac{\Delta \mu}{\bar{\mu}^2} \tag{1.18}$$

and the peak capacity (n) can be expressed as

$$n = \frac{L}{4\sigma} = \frac{L}{4} \sqrt{\frac{\mu q(x_0)}{D_T}} \tag{1.19}$$

where $\Delta\mu$ is the mobility difference between two analytes, $\bar{\mu}$ is the average mobility of the two analytes, and L is the length of the separation channel.

Equations 1.17 and 1.18 indicate that both the width of the focused band and resolution are inversely proportional to $\sqrt{q(x_0)}$, which indicates that a steeper gradient will generate a narrower band and lower resolution, while a shallower gradient will produce higher resolution and broader bands. From equation 1.19, for a fixed separation channel length, the peak capacity is high when the electric field gradient is steep. At first glance, it appears that the peak capacity and resolution cannot be improved simultaneously. To solve this problem, Tolley et al. proposed a nonlinear electric field gradient, in which the first section of the gradient is relatively steep and the second section is rather shallow.[186,187] Thus, analytes will be tightly stacked with narrow bandwidths in the first segment to achieve high peak capacity

and then moved sequentially to the second segment where they are resolved. A bilinear gradient profile shown in Figure 1.18 illustrates this design. Based on such a profile, computer simulation demonstrates dynamic improvement of peak capacity.[186] However, long separation time is required. The alternative is to use parallel EFGF arrays which can achieve high peak capacity within relatively short separation time.

1.4.3 Approaches to Establish the Electric Field Gradient

A major challenge in EFGF is establishment of the desired electric field gradient along the separation channel. When a voltage is applied across the channel ends, the electric field strength along the channel, $E(x)$, depends on the current, *I*, buffer conductivity, $\sigma(x)$, and cross-sectional area normal to the field, $A(x)$, by

$$E(x) = \frac{I}{\sigma(x)A(x)} \tag{1.20}$$

According to this equation,[184] it is possible to obtain an electric field gradient when the buffer conductivity, $\sigma(x)$ or cross-sectional area, $A(x)$ is gradually changed because the current is constant in the channel. Currently, several methods have been reported to create an electric field gradient, including the use of a conductive changing cross-sectional area around a separation channel, a buffer conductivity gradient in a column, a temperature gradient along a column filled with a buffer that has a temperature-dependent conductivity, and electrodes along a channel for digital field gradient focusing.[181]

Changing cross-sectional area. Koegler and Ivory[183,184] first reported a preparative scale EFGF device, in which a size exclusion resin-packed dialysis tube was mounted in the center of a poly(methyl methacrylate) (PMMA) cylinder (Figure

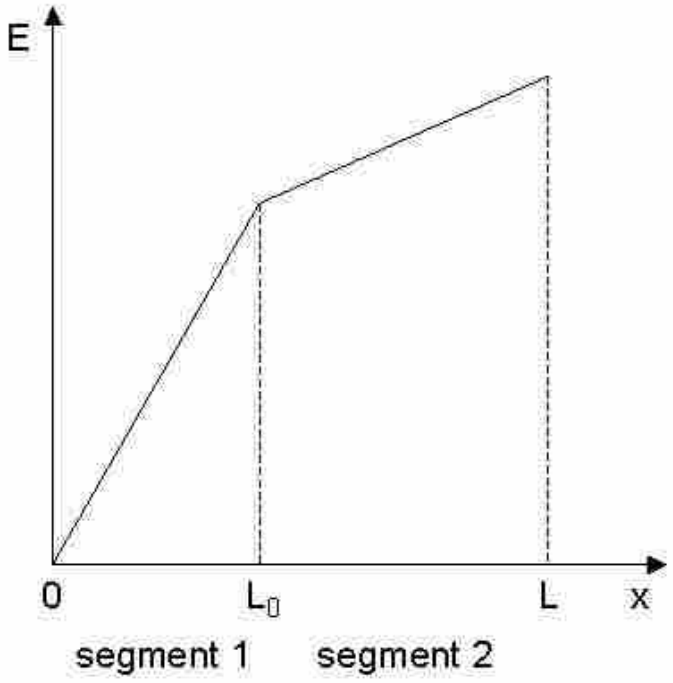

Figure 1.18. Bilinear electric field gradient profile.

1.19). The inner surface of the cylinder was conically shaped to generate the electric field gradient along the dialysis tube. Proteins were focused in the dialysis tube when a counter flow was pumped through the tube and a voltage was applied along the shaped chamber. This system was cumbersome to set up and gave mediocre results. Humble et al.[189] improved this design and made capillary-based planar devices for analytical scale EFGF (Figure 1.20). The separation channel was created using a small diameter wire as template to form a channel surrounded by an ionically conductive acrylic copolymer that freely allowed passage of small ions but restricted migration of biomacromolecules into the gel. This nanoporous copolymer was shaped to form a linear electric field gradient by changing the cross-sectional area. With the use of these devices, a 10,000-fold concentration factor was obtained for green fluorescent protein (GFP), and several proteins were separated. Although the fabrication of these devices was easy and reproducible, limitations included low peak capacity and low resolution, primarily due to flow dispersion in the channel. Recently, Kelly et al.[190] miniaturized this capillary-based EFGF device into a PMMA microchip format, in which a microchannel was imprinted on the bottom plate and a shaped cavity of changing cross-sectional area was cut into the top plate. The same ionically conductive copolymer was polymerized in the shaped cavity using phase-changing sacrificial layers to protect the microchannel. This microchip EFGF device was used to separate various proteins and peptides. Compared with the capillary-based system, the microchip EFGF device offered 3-fold improved resolution of proteins.

Liu et al.[88] used a different approach to fabricate a micro electric field gradient

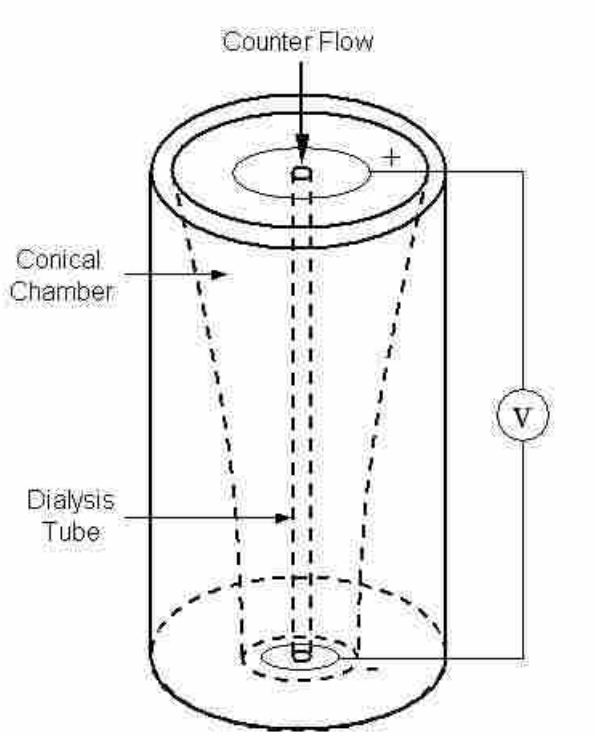

Figure 1.19. EFGF device of Koegler and Ivory.[184]

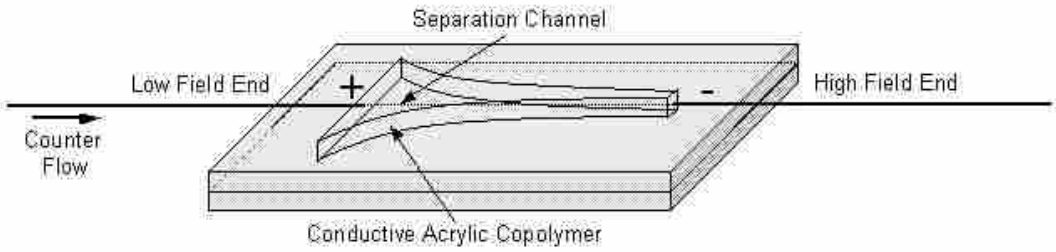

Figure 1.20. EFGF device of Humble at al.[189]

focusing (μEFGF) device out of poly(glycidyl methacrylate-co-methyl methacrylate). A weir structure was fabricated between the separation channel and changing cross-section electric field gradient generating channel (Figure 1.21). A buffer ion-permeable membrane made from a poly(ethylene glycol) (PEG)-functionalized copolymer was positioned on the weir to separate the two microchannels. GFP was concentrated 4,000-fold using this μEFGF device. Separation and selective elution of one component from a mixture containing three proteins was also investigated. Unfortunately, the fabrication procedure and chemistry were complex and the membrane strongly influenced the behavior of the μEFGF device.

Conductivity gradient. Greenlee and Ivory[191] proposed another EFGF form, termed conductivity gradient focusing, which used a dialysis membrane to divide the electrolyte chamber into two regions: separation channel and purge channel (Figure 1.22). A high conductivity electrolyte was introduced into the separation channel with a low velocity, which also acted as the counter flow for focusing. Simultaneously, a low conductivity buffer was introduced into the adjacent purge channel with a high velocity. Thus, an axial conductivity gradient was created along the separation channel as the buffer ions diffused from the higher conductivity buffer through the membrane to the lower conductivity buffer. An electric field gradient could be established by applying a voltage along the channel. In the free solution experiments, the proteins formed contiguous bands. When focusing in a packed channel, the resolution was improved. Following this idea, an analytical scale EFGF device based on a dialysis hollow fiber was fabricated by Wang et al.[192] An online UV absorbance

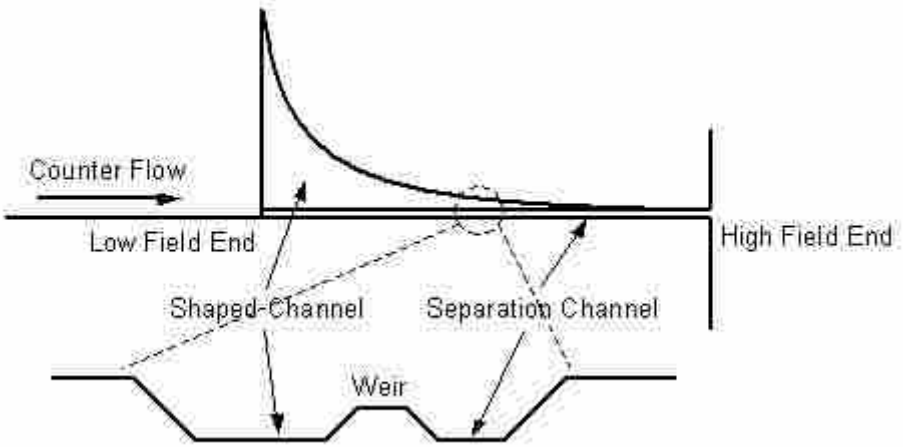

Figure 1.21. Diagram of the μEFGF device of Liu at al.[88]

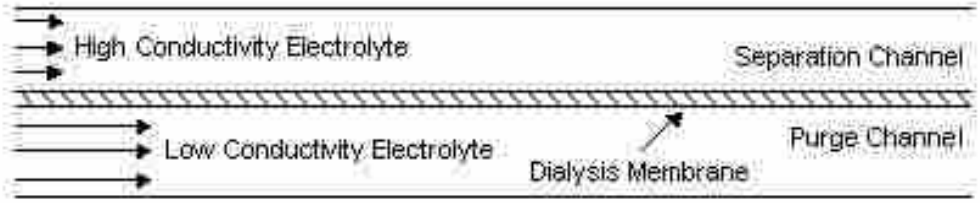

Figure 1.22. Diagram of the EFGF device of Greenlee.[191]

detector was used to detect protein focusing and voltage-controlled elution. Later, this system was applied for protein analysis, including protein concentration, desalting, and purification of protein samples.[193] This EFGF system provided a concentration factor as high as 15,000 for bovine serum albumin (BSA). Recently, this hollow fiber based system was coupled to the capillary-based EFGF device to form a tandem EFGF system, which can trap and concentrate specific proteins of interest based on their mobilities while desalting and removing unwanted components.[194]

Temperature gradient focusing. Temperature gradient focusing (TGF) is a third form of EFGF, which was recently reported (Figure 1.23).[195-197] In TGF, a temperature gradient is employed to produce an electric field gradient due to the dependence of the buffer conductivity on temperature. The temperature gradient could be induced by external heating or internal Joule heating.[198] One advantage of TGF is that a membrane is not required. Therefore, TGF can be applied to focus and separate various analytes, including proteins,[195] DNA,[199] enantiomers,[200] small dye molecules[195,201] and amino acids,[202] in both capillaries and microchannels. However, the short channel used in TGF limits the peak capacity, and only a few buffer solutions can be used to generate the temperate gradient. Also the temperature gradient is constrained by the buffer and analytes.

Digital field gradient focusing. Digital field gradient focusing is the fourth form of EFGF, in which an array of electrodes is used to generate the electric field gradient.[203-206] The electrode voltages were individually controlled by a computer, and a dialysis membrane is used to isolate the electrodes and separation channel. In this

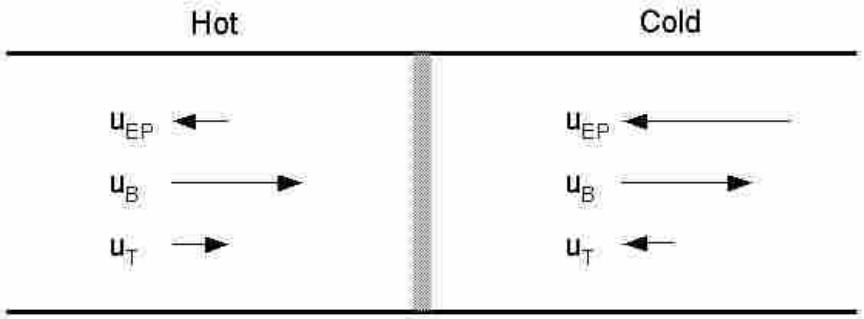

Figure 1.23. Diagram of TGF.

design, the field gradient profile can be dynamically adjusted using the computer. It is possible to manipulate the field during separation to achieve better resolution and narrower bands. However, this system is fairly complicated and the number of electrodes affects the resolving power. Recently, this multielectrode design was miniaturized on a poly(dimethylsiloxane) (PDMS) microchip.[207] Two side channels separated from the main fluidic channel with a dialysis fiber were used to replace the metal electrodes and create the field gradient. A constant electroosmotic flow was used as the counter flow to balance the electrophoresis. Myers and Bartle[208] fabricated a miniaturized dynamic field gradient focusing device for protein separation and focusing. The separation channel was in contact with a parallel electric field channel with five individual electrodes through a porous glass membrane. A porous monolith was filled in the separation channel to reduce diffusional band broadening caused by hydrodynamic flow.

1.5 Dissertation Overview

My research focused on polymeric microchips for CE and EFGF. Chapter 2 describes surface modification of PGMAMMA microchips using SI-ATRP. A PEG-functionalized polymer layer was grafted on the polymer surface using three different surface activation methods. Chapter 3 demonstrates in-channel ATRP surface modification of PGMAMMA microchips. Chapter 4 focuses on a new polymeric microchip for CE separation that does not require surface modification. In Chapter 5, an EFGF device made of PEG-functionalized polymers is introduced for protein

focusing and separation. Chapter 6 describes the performance optimization of this EFGF device. Chapter 7 describes work done to construct and evaluate EFGF devices with non-linear electric field gradients. Finally, Chapter 8 summarizes the conclusions of this dissertation and gives suggestions of future work that could be pursued.

1.6 References

1. Terry, S. C.; Jerman, J. H.; Angell, J. B. *IEEE Trans. Electron Devices* **1979**, *26*, 1880-1886.
2. Manz, A.; Graber, N.; Widmer, H. M. *Sens. Actuators B* **1990**, *1*, 244-248.
3. Reyes, D. R.; Iossifidis, D.; Auroux, P.-A.; Manz, A. *Anal. Chem.* **2002**, *74*, 2623-2636.
4. Auroux, P.-A.; Iossifidis, D.; Reyes, D. R.; Manz, A. *Anal. Chem.* **2002**, *74*, 2637-2652.
5. Vilkner, T.; Janasek, D.; Manz, A. *Anal. Chem.* **2004**, *76*, 3373-3386.
6. Dittrich, P. S.; Tachikawa, K.; Manz, A. *Anal. Chem.* **2006**, *78*, 3887-3907.
7. West, J.; Becker, M.; Tombrink, S.; Manz, A. *Anal. Chem.* **2008**, *80*, 4403-4419.
8. Tang, T.; Badal, M. Y.; Ocvirk, G.; Lee, W. E.; Bader, D. E.; Bekkaoui, F.; Harrison, D. J. *Anal. Chem.* **2002**, *74*, 725-733.
9. Broyles, B. S.; Jacobson, S. C.; Ramsey, J. M. *Anal. Chem.* **2003**, *75*, 2761-2767.
10. Verpoorte, E. *Electrophoresis* **2002**, *23*, 677-712.
11. McClain, M. A.; Culbertson, C. T.; Jacobson, S. C.; Allbritton, N. L.; Sims, C.

E.; Ramsey, J. M. *Anal. Chem.* **2003**, *75*, 5646-5655.

12. Roper, M. G.; Easley, C. J.; Landers, J. P. *Anal. Chem.* **2005**, *77*, 3887-3894.
13. Kamholz, A. E.; Weigl, B. H.; Finlayson, B. A.; Yager, P. *Anal. Chem.* **1999**, *71*, 5340-5347.
14. Lambertus, G. R.; Fix, C. S.; Reidy, S. M.; Miller, R. A.; Wheeler, D.; Nazarov, E.; Sacks, R. *Anal. Chem.* **2005**, *77*, 7563-7571.
15. Manz, A.; Harrison, D. J.; Verpoorte, E. M. J.; Fettinger, J. C.; Paulus, A.; Ludi, H.; Widmer, H. M. *J. Chromatogr. A* **1992**, *593*, 253-258.
16. Harrison, D. J.; Manz, A.; Fan, Z.; Ludi, H.; Widmer, H. M. *Anal. Chem.* **1992**, *64*, 1926-1932.
17. Fan, Z. H.; Harrison, D. J. *Anal. Chem.* **1994**, *66*, 177-184.
18. Jacobson, s. C.; Hergenroder, R.; Koutny, L. B.; Warmack, R. J.; Ramsey, J. M. *Anal. Chem.* **1994**, *66*, 1107-1113.
19. Woolley, A. T.; Mathies, R. A. *Proc. Natl. Acad. Sci. USA* **1994**, *91*, 11348-11352.
20. Jacobson, S. C.; Moore, A. W.; Ramsey, J. M. *Anal. Chem.* **1995**, *67*, 2059-2063.
21. He, B.; Tait, N.; Regnier, F. *Anal. Chem.* **1998**, *70*, 3790-3797.
22. Tokeshi, M.; Minagawa, T.; Kitamori, T. *Anal. Chem.* **2000**, *72*, 1711-1714.
23. Borrello, L.; Bernardini, J.; Dell'Orso, R.; Dutta, S.; Fallica, P. G.; Giassi, A.; Messineo, A.; Militaru, O.; Segneri, G.; Starodumov, A.; Teodorescu, L.; Tonelli, G.; Valvo, G.; Verdini, P. G. *IEEE Trans. Nucl. Sci.* **2002**, *49*, 1035-1039.

24. Pan, T.; Kelly, R. T.; Asplund, M. C.; Woolley, A. T. *J. Chromatogr. A* **2004**, *1027*, 231-235.

25. Simpson, P. C.; Roach, D.; Woolley, A. T.; Thorsen, T.; Johnston, R.; Sensabaugh, G. F.; Mathies, R. A. *Proc. Natl. Acad. Sci. USA* **1998**, *95*, 2256-2261.

26. Kelly, R. T.; Woolley, A. T. *Anal. Chem.* **2003**, *75*, 1941-1945.

27. Liu, J.; Pan, T.; Woolley, A. T.; Lee, M. L. *Anal. Chem.* **2004**, *76*, 6948-6955.

28. Kelly, R. T.; Pan, T.; Woolley, A. T. *Anal. Chem.* **2005**, *77*, 3536-3541.

29. Liu, J.; Sun, X.; Lee, M. L. *Anal. Chem.* **2005**, *77*, 6280-6287.

30. Madou, M. J. *Fundamentals of Microfabrication: The Science of Miniaturization*; CRC Press: Boca Raton, FL, 2002.

31. Haab, B. B.; Mathies, R. A. *Anal. Chem.* **1999**, *71*, 5137-5145.

32. Griebel, A.; Rund, S.; Schonfeld, F.; Dorner, W.; Konrad, R.; Hardt, S. *Lab Chip* **2004**, *4*, 18-23.

33. Wang, Y.-C.; Stevens, A. L.; Han, J. *Anal. Chem.* **2005**, *77*, 4293-4299.

34. Petersson, F.; Nilsson, A.; Jonsson, H.; Laurell, T. *Anal. Chem.* **2005**, *77*, 1216-1221.

35. Fonslow, B. R.; Bowser, M. T. *Anal. Chem.* **2005**, *2005*, 5706-5710.

36. Wang, H. Y.; Foote, R. S.; Jacobson, S. C.; Schneibel, J. H.; Ramsey, J. M. *Sens. Actuators B* **1997**, *45*, 199-207.

37. Huang, Z.; Sanders, J. C.; Dunsmor, C.; Ahmadzadeh, H.; Landers, J. P. *Electrophoresis* **2001**, *22*, 3924-3929.

38. Peeni, B. A.; Conkey, D. B.; Barber, J. P.; Kelly, R. T.; Lee, M. L.; Woolley, A. T.; Hawkins, A. R. *Lab Chip* **2005**, *5*, 501-505.

39. Soper, S. A.; Ford, S. M.; Qi, S.; McCarley, R. L.; Kelly, K.; Murphy, M. C. *Anal. Chem.* **2000**, *72*, 643A-651A.

40. Becker, H.; Locascio, L. E. *Talanta* **2002**, *56*, 267-287.

41. Shadpour, H.; Musyimi, H.; Chen, J.; Soper, S. A. *J. Chromatogr. A* **2006**, *1111*, 238-251.

42. Effenhauser, C. S.; Bruin, G. J. M.; Paulus, A.; Ehrat, M. *Anal. Chem.* **1997**, *69*, 3451-3457.

43. Duffy, D. C.; McDonald, J. C.; Schueller, O. J. A.; Whitesides, G. M. *Anal. Chem.* **1998**, *70*, 4974-4984.

44. McDonald, J. C.; Whitesides, G. M. *Acc. Chem. Res.* **2002**, *35*, 491-499.

45. McDonald, J. C.; Duffy, D. C.; Anderson, J. R.; Chiu, D. T.; Wu, H.; Schueller, O. J. A.; Whitesides, G. M. *Electrophoresis* **2000**, *21*, 27-40.

46. Martynova, L.; Locascio, L. E.; Gaitan, M.; Kramer, G. W.; Christensen, R. G.; MacCrehan, W. A. *Anal. Chem.* **1997**, *69*, 4783-4789.

47. Koesdjojo, M. T.; Tennico, Y. H.; Remcho, V. T. *Anal. Chem.* **2008**, *80*, 2311-2318.

48. Barker, S. L. R.; Tarlov, M. J.; Canavan, H.; Hickman, J. J.; Locascio, L. E. *Anal. Chem.* **2000**, *72*, 4899-4903.

49. Barker, S. L. R.; Ross, D.; Tarlov, M. J.; Gaitan, M.; Locascio, L. E. *Anal. Chem.* **2000**, *72*, 5925-5929.

50. Liu, Y.; Ganser, D.; Schneider, A.; Liu, R.; Grodzinski, P.; Kroutchinina, N. *Anal. Chem.* **2001**, *73*, 4196-4201.

51. Vreeland, W. N.; Locascio, L. E. *Anal. Chem.* **2003**, *75*, 6906-6911.

52. Henry, A. C.; Waddell, E. A.; Shreiner, R.; Locascio, L. E. *Electrophoresis* **2002**, *23*, 791-798.

53. Malmstadt, N.; Yager, P.; Hoffman, A. S.; Stayton, P. S. *Anal. Chem.* **2003**, *75*, 2943-2949.

54. Giordano, B. C.; Ferrance, J.; Swedberg, S.; Huhmer, A. F. R.; Landers, J. P. *Anal. Biochem.* **2001**, *291*, 124-132.

55. Yin, H.; Killeen, K.; Brenen, R.; Sobek, D.; Werlich, M.; Goor, T. V. D. *Anal. Chem.* **2005**, *77*, 527-533.

56. Gustafsson, O.; Mogensen, K. B.; Kutter, J. P. *Electrophoresis* **2008**, *29*, 3145-3152.

57. Kameoka, J.; Craighead, H. G.; Zhang, H.; Henion, J. *Anal. Chem.* **2001**, *73*, 1935-1941.

58. Pu, Q.; Oyesanya, O.; Thompson, B.; Liu, S.; Alvarez, J. C. *Langmuir* **2007**, *23*, 1577-1583.

59. Fiorini, G. S.; Lorenz, R. M.; Kuo, J. S.; Chiu, D. T. *Anal. Chem.* **2004**, *76*, 4697-4704.

60. Uchiyama, K.; Xu, W.; Qiu, J.; Hobo, T. *Fresenius J. Anal. Chem.* **2001**, *371*, 209-211.

61. Xu, W.; Uchiyama, K.; Shimosaka, T.; Hobo, T. *J. Chromatogr. A* **2001**, *907*,

279-289.

62. Becker, H.; Gartner, C. *Electrophoresis* **2000**, *21*, 12-26.

63. Zhang, C.-X.; Manz, A. *Anal. Chem.* **2001**, *73*, 2656-2662.

64. Li, H.-F.; Lin, J.-M.; Su, R.-G.; Cai, Z. W.; Uchiyama, K. *Electrophoresis* **2005**, *26*, 1825-1855.

65. Grimes, A.; Breslauer, D. N.; Long, M.; Pegan, J.; Lee, L. P.; Khine, M. *Lab Chip* **2008**, *8*, 170-172.

66. McCormick, R. M.; Nelson, R. J.; Alonso-Amigo, M. G.; Benvegnu, D. J.; Hooper, H. H. *Anal. Chem.* **1997**, *69*, 2626-2630.

67. Xia, Y.; Whitesides, G. M. *Angew. Chem. Int. Ed.* **1998**, *37*, 550-575.

68. Anderson, J. R.; Chiu, D. T.; Jackman, R. J.; Cherniavskaya, O.; McDonald, J. C.; Wu, H.; Whitesides, S. H.; Whitesides, G. M. *Anal. Chem.* **2000**, *72*, 3158-3164.

69. Unger, M. A.; Chou, H.-P.; Thorsen, T.; Scherer, A.; Quake, S. R. *Science* **2000**, *288*, 113-116.

70. Wu, H.; Odom, T. W.; Chiu, D. T.; Whitesides, G. M. *J. Am. Chem. Soc.* **2003**, *125*, 554-559.

71. Rolland, J. P.; Dam, R. M. V.; Schorzman, D. A.; Quake, S. R.; DeSimone, J. M. *J. Am. Chem. Soc.* **2004**, *126*, 2322-2323.

72. Kim, P.; Jeong, H. E.; Khademhosseini, A.; Suh, K. Y. *Lab Chip* **2006**, *6*, 1432-1437.

73. Liu, J.; Sun, X.; Lee, M. L. *Anal. Chem.* **2007**, *79*, 1926-1931.

74. Sun, X.; Peeni, B. A.; Yang, W.; Becerril, H. A.; Woolley, A. T. *J. Chromatogr. A* **2007**, *1162*, 162-166.

75. Roberts, M. A.; Rossier, J. S.; Bercier, P.; Girault, H. *Anal. Chem.* **1997**, *69*, 2035-2042.

76. Bianchi, F.; Chevolot, Y.; Mathieu, H. J.; Girault, H. H. *Anal. Chem.* **2001**, *73*, 3845-3853.

77. Klank, H.; Kutter, J. P.; Geschke, O. *Lab Chip* **2002**, *2*, 242-246.

78. Bowden, M.; Geschke, O.; Kutter, J. P.; Diamond, D. *Lab Chip* **2003**, *3*, 221-223.

79. Pugmire, D. L.; Waddell, E. A.; Haasch, R.; Tarlov, M. J.; Locascio, L. E. *Anal. Chem.* **2002**, *74*, 871-878.

80. Beebe, D. J.; Moore, J. S.; Yu, Q.; Liu, R. H.; Kraft, M. L.; Jo, B.-H.; Devadoss, C. *Proc. Natl. Acad. Sci. USA* **2000**, *97*, 13488-13493.

81. Kenis, P. J. A.; Ismagilov, R. F.; Whitesides, G. M. *Science* **1999**, *285*, 83-85.

82. Beebe, D. J.; Moore, J. S.; Bauer, J. M.; Yu, Q.; Liu, R. H.; Devadoss, C.; Jo, B.-H. *Nature* **2000**, *404*, 588-590.

83. Kenis, P. J. A.; Ismagilov, R. F.; Takayama, S.; Whitesides, G. M.; Li, S.; White, H. S. *Acc. Chem. Res.* **2000**, *33*, 841-847.

84. Sikanen, T.; Tuomikoski, S.; Ketola, R. A.; Kostiainen, R.; Franssila, S.; Kotiaho, T. *Lab Chip* **2005**, *5*, 888-896.

85. Wang, J.; Pumera, M.; Chatrathi, M. P.; Escarpa, A.; Konrad, R.; Griebel, A.; Dorner, W.; Lowe, H. *Electrophoresis* **2002**, *23*, 596-601.

86. Meng, z.; Qi, S.; Soper, S. A.; Limbach, P. A. *Anal. Chem.* **2001**, *73*, 1286-1291.

87. Wu, H.; Huang, B.; Zare, R. N. *Lab Chip* **2005**, *5*, 1393-1398.

88. Liu, J.; Sun, X.; Farnsworth, P. B.; Lee, M. L. *Anal. Chem.* **2006**, *78*, 4654-4662.

89. Lai, S.; Cao, X.; Lee, L. J. *Anal. Chem.* **2004**, *76*, 1175-1183.

90. Thorsen, T.; Maerkl, S. J.; Quake, S. R. *Science* **2002**, *298*, 580-584.

91. Liu, J.; Hansen, C.; Quake, S. R. *Anal. Chem.* **2003**, *75*, 4718-4723.

92. Weston, A.; Brown, P. R. *HPLC and CE: Principles and Practice*; Academic Press: San Diego, CA, 1997.

93. Jorgenson, J. W.; Lukacs, K. D. *Anal. Chem.* **1981**, *53*, 1298-1302.

94. Jorgenson, J. W.; Lukacs, K. D. *Science* **1983**, *222*, 266-272.

95. Dolnik, V.; Liu, S.; Jovanovich, S. *Electrophoresis* **2000**, *21*, 41-54.

96. Mourzina, Y.; Steffen, A.; Kalyagin, D.; Carius, R.; Offenhausser, A. *Electrophoresis* **2005**, *26*, 1849-1860.

97. Zuborova, M.; Demianova, Z.; Kaniansky, D.; Masar, M.; Stanislawski, B. *J. Chromatogr. A* **2003**, *990*, 179-188.

98. Hong, J. W.; Hosokawa, K.; Fujii, T.; Seki, M.; Endo, I. *Biotechnol. Prog.* **2001**, *17*, 958-962.

99. Brahmasandra, S. N.; Ugaz, V. M.; Burke, D. T.; Mastrangelo, C. H.; Burns, M. A. *Electrophoresis* **2001**, *22*, 300-311.

100. Huang, H.; Xu, F.; Dai, Z.; Lin, B. *Electrophoresis* **2005**, *26*, 2254-2260.

101. Li, C.; Yang, Y.; Craighead, H. G.; Lee, K. H. *Electrophoresis* **2005**, *26*,

1800-1806.

102. Wen, J.; Lin, Y.; Xiang, F.; Matson, D. W.; Udseth, H. R.; Smith, R. D. *Electrophoresis* **2000**, *21*, 191-197.

103. Kutter, J. P.; Jacobson, S. C.; Ramsey, J. M. *Anal. Chem.* **1997**, *69*, 5165-5171.

104. Li, Y.; Buch, J. S.; Rosenberger, F.; DeVoe, D. L.; Lee, C. S. *Anal. Chem.* **2004**, *76*, 742-748.

105. Shadpour, H.; Soper, S. A. *Anal. Chem.* **2006**, *78*, 3519-3527.

106. Rocklin, R. D.; Ramsey, R. S.; Ramsey, J. M. *Anal. Chem.* **2000**, *72*, 5244-5249.

107. Kelly, R. T.; Woolley, A. T. *Anal. Chem.* **2005**, *77*, 96A-102A.

108. Wang, Y.-C.; Choi, M. H.; Han, J. *Anal. Chem.* **2004**, *76*, 4426-4431.

109. Hu, S.; Ren, X.; Barchman, M.; Sims, C. E.; Li, G. P.; Allbritton, N. *Anal. Chem.* **2002**, *74*, 4117-4123.

110. Hu, S.; Ren, X.; Bachman, M.; Sims, C. E.; Li, G. P.; Allbritton, N. *Electrophoresis* **2003**, *24*, 3679-3688.

111. Hu, S.; Ren, X.; Barchman, M.; Sims, C. E.; Li, G. P.; Allbritton, N. *Anal. Chem.* **2004**, *76*, 1865-1870.

112. Kirby, B. J.; Hasselbrink, E. F. *Electrophoresis* **2004**, *25*, 203-213.

113. Harrison, D. J.; Fluri, K.; Seiler, K.; Fan, Z.; Effenhauser, C. S.; Manz, A. *Science* **1993**, *261*, 895-897.

114. Effenhauser, C. S.; Manz, A.; Widmer, H. M. *Anal. Chem.* **1993**, *65*, 2637-2642.

115. Thomas, C. D.; Jacobson, S. C.; Ramsey, J. M. *Anal. Chem.* **2004**, *76*, 6053-6057.

116. Fu, L.-M.; Lin, C.-H. *Anal. Chem.* **2003**, *75*, 5790-5796.

117. Ermakov, S. V.; Jacobson, S. C.; Ramsey, J. M. *Anal. Chem.* **2000**, *72*, 3512-3517.

118. Pan, T.; Fiorini, G. S.; Chiu, D. T.; Woolley, A. T. *Electrophoresis* **2007**, *28*, 2904-2911.

119. Zugel, S. A.; Burke, B. J.; Regnier, F. E.; Lytle, F. E. *Anal. Chem.* **2000**, *72*, 5731-5735.

120. Vandaveer, W. R.; Pasas-Farmer, S. A.; Fischer, D. J.; Frankerfeld, C. N.; Lunte, S. M. *Electrophoresis* **2004**, *25*, 3528-3549.

121. Tachibana, Y.; Otsuka, K.; Terabe, S.; Arai, A.; Suzuki, K.; Nakamura, S. *J. Chromatogr. A* **2003**, *1011*, 181-192.

122. Wang, Y.-X.; Zhou, Y.; Balgley, B. M.; Cooper, J. W.; Lee, C. S.; DeVoe, D. L. *Electrophoresis* **2005**, *26*, 3631-3640.

123. Pallandre, A.; Lambert, B. D.; Attia, R.; Jonas, A. M.; Viovy, J.-L. *Electrophoresis* **2006**, *27*, 584-610.

124. Dolnik, V. *Electrophoresis* **2004**, *25*, 3589-3601.

125. Doherty, E. A. S.; Meagher, R. J.; Albarghouthi, M. N.; Barron, A. E. *Electrophoresis* **2003**, *24*, 34-54.

126. Belder, D.; Ludwig, M. *Electrophoresis* **2003**, *24*, 3595-3606.

127. Liu, J.; Lee, M. L. *Electrophoresis* **2006**, *27*, 3533-3546.

128. Dang, F.; Zhang, L.; Hagiwara, H.; Mishina, Y.; Baba, Y. *Electrophoresis* **2003**, *24*, 714-721.

129. Dang, F.; Kakehi, K.; Cheng, J.; Tabata, O.; Kurokawa, M.; Nakajima, K.; Ishikawa, M.; Baba, Y. *Anal. Chem.* **2006**, *78*, 1452-1458.

130. Tabuchi, M.; Kuramitsu, Y.; Nakamura, K.; Baba, Y. *Anal. Chem.* **2003**, *75*, 3799-3805.

131. Cui, H.; Horiuchi, K.; Dutta, P.; Ivory, C. F. *Anal. Chem.* **2005**, *77*, 1303-1309.

132. Song, L.; Fang, D.; Kobos, R. K.; Pace, S. J.; Chu, B. *Electrophoresis* **1999**, *20*, 2847-2855.

133. Xu, F.; Jabasini, M.; Baba, Y. *Electrophoresis* **2002**, *23*, 3608-3614.

134. Liu, Y.; Fanguy, J. C.; Bledsoe, J. M.; Henry, C. S. *Anal. Chem.* **2000**, *72*, 5939-5944.

135. Kato, M.; Gyoten, Y.; Sakai-Kato, K.; Nakajima, T.; Toyo'oka, T. *Anal. Chem.* **2004**, *76*, 6792-6796.

136. Wang, A.-J.; Xu, J.-J.; Chen, H.-Y. *J. Chromatogr. A* **2006**, *1107*, 257-264.

137. Makamba, H.; Hsieh, Y.-Y.; Sung, W.-C.; Chen, S.-H. *Anal. Chem.* **2005**, *77*, 3971-3978.

138. Ocvirk, G.; Munroe, M.; Tang, T.; Oleschuk, R.; Westra, K.; Harrison, D. J. *Electrophoresis* **2000**, *21*, 107-115.

139. Wang, S.-C.; Perso, C. E.; Morris, M. D. *Anal. Chem.* **2000**, *72*, 1704-1706.

140. Badal, M. Y.; Wong, M.; Chiem, N.; Salimi-Moosavi, H.; Harrison, D. J. *J. Chromatogr. A* **2002**, *947*, 277-286.

141. Lin, Y.-W.; Chang, H.-T. *J. Chromatogr. A* **2005**, *1073*, 191-199.

142. Vickers, J. A.; Caulum, M. M.; Henry, C. S. *Anal. Chem.* **2006**, *78*, 7446-7452.

143. Papra, A.; Bernard, A.; Juncker, D.; Larsen, N. B.; Michel, B.; Delamarche, E. *Langmuir* **2001**, *17*, 4090-4095.

144. Wu, D.; Zhao, B.; Dai, Z.; Qin, J.; Lin, B. *Lab Chip* **2006**, *6*, 942-947.

145. Gaudioso, J.; Craighead, H. G. *J. Chromatogr. A* **2002**, *971*, 249-253.

146. Hu, S.; Ren, X.; Barchman, M.; Sims, C. E.; Li, G. P.; Allbritton, N. *Langmuir* **2004**, *20*, 5569-5574.

147. Zangmeister, R. A.; Tarlov, M. J. *Langmuir* **2003**, *19*, 6901-6904.

148. Witek, M. A.; Wei, S.; Vaidya, B.; Adams, A. A.; Zhu, L.; Strvjewski, W.; McCarley, R. L.; Soper, S. A. *Lab Chip* **2004**, *4*, 464-472.

149. Rohr, T.; Ogletree, D. F.; Svec, F.; Frechet, J. M. J. *Adv. Funct. Mater.* **2003**, *13*, 264-270.

150. Johnson, T. J.; Ross, D.; Gaitan, M.; Locascio, L. E. *Anal. Chem.* **2001**, *73*, 3656-3661.

151. Wang, B.; Abdulali-Kanji, Z.; Dodwell, E.; Horton, J. H.; Oleschuk, R. D. *Electrophoresis* **2003**, *24*, 1442-1450.

152. Roman, G. T.; Hlaus, T.; Bass, K. J.; Seelhammer, T. G.; Culbertson, C. T. *Anal. Chem.* **2005**, *77*, 1414-1422.

153. Slentz, B. E.; Penner, N. A.; Regnier, F. E. *J. Chromatogr. A* **2002**, *948*, 225-233.

154. Sung, W.-C.; Huang, S.-Y.; Liao, P.-C.; Lee, G.-B.; Li, C.-W.; Chen, S.-H. *Electrophoresis* **2003**, *24*, 3648-3654.

155. Sui, G.; Wang, J.; Lee, C.-C.; Lu, W.; Lee, S. P.; Leyton, J. V.; Wu, A. M.; Tseng,

H.-R. *Anal. Chem.* **2006**, *78*, 5543-5551.

156. Henry, A. C.; Tutt, T. J.; Galloway, M.; Davidson, Y. Y.; McWhorter, C. S.; Soper, S. A.; McCarley, R. L. *Anal. Chem.* **2000**, *72*, 5331-5337.
157. Galloway, M.; Stryjewski, W.; Henry, A.; Ford, S. M.; Llopis, S.; McCarley, R. L.; Soper, S. A. *Anal. Chem.* **2002**, *74*, 2407-2415.
158. Waddell, E.; Wang, Y.; Stryjewski, W.; McWhorter, S.; Henry, A. C.; Evans, D.; McCarley, R. L.; Soper, S. A. *Anal. Chem.* **2000**, *72*, 5907-5917.
159. Wang, Y.; Vaidya, B.; Farquar, H. D.; Stryjewski, W.; Hammer, R. P.; McCarley, R. L.; Soper, S. A.; Cheng, Y.-W.; Barany, F. *Anal. Chem.* **2003**, *75*, 1130-1140.
160. Wang, J.; Jr., A. M.; Chatrathi, M. P.; Chen, G.; Mittal, N.; Spillman, S. D.; Obeidat, S. *Lab Chip* **2005**, *5*, 226-230.
161. Xu, W.; Uchiyama, K.; Hobo, T. *Chromatography* **2002**, *23*, 131-138.
162. Zhou, X.-M.; Dai, Z.-P.; Liu, X.; Luo, Y.; Wang, H.; Lin, B.-C. *J. Sep. Sci.* **2005**, *28*, 225-233.
163. Luo, Y.; Huang, B.; Wu, H.; Zare, R. N. *Anal. Chem.* **2006**, *78*, 4588-4592.
164. Matyjaszewski, K.; Xia, J. *Chem. Rev.* **2001**, *101*, 2921-2990.
165. Kamigaito, M.; Ando, T.; Sawamoto, M. *Chem. Rev.* **2001**, *101*, 3689-3745.
166. Huang, X.; Wirth, M. J. *Anal. Chem.* **1997**, *69*, 4577-4580.
167. Huang, X.; Doneski, L. J.; Wirth, M. J. *Anal. Chem.* **1998**, *70*, 4023-4029.
168. Leinweber, F. C.; Stein, J.; Otto, M. *Fresenius J. Anal. Chem.* **2001**, *370*, 781-788.
169. Miller, M. D.; Baker, G. L.; Bruening, M. L. *J. Chromatogr. A* **2004**, *1044*,

323-330.

170. Unsal, E.; Elmas, B.; Caglayan, B.; Tuncel, M.; Patir, S.; Tuncel, A. *Anal. Chem.* **2006**, *78*, 5868-5875.

171. Xiao, D.; Le, T. V.; Wirth, M. J. *Anal. Chem.* **2004**, *76*, 2055-2061.

172. Figeys, D. *Anal. Chem.* **2003**, *75*, 2891-2905.

173. Smith, J. C.; Lambert, J.-P.; Elisma, F.; Figeys, D. *Anal. Chem.* **2007**, *79*, 4325-4344.

174. Binz, P.-A.; Muller, M.; Walther, D.; Bienvenut, W. V.; Gras, R.; Hoogland, C.; Bouchet, G.; Gasteiger, E.; Fabbretti, R.; Gay, S.; Palagi, P.; Wilkins, M. R.; Rouge, V.; Tonella, L.; Paesano, S.; Rossellat, G.; Karmime, A.; Bairoch, A.; Sanchez, J.-C.; Appel, R. D.; Hochstrasser, D. F. *anal. Chem.* **1999**, *71*, 4981-4988.

175. Zhou, M.; Lucas, D. A.; Chan, K. C.; Issaq, H. J.; Petricoin, E. F.; Liotta, L. A.; Veenstra, T. D.; Conrads, T. P. *Electrophoresis* **2004**, *25*, 1289-1298.

176. Sarioglu, H.; Lottspeich, F.; Walk, T.; Jung, G.; Eckerskorn, C. *Electrophoresis* **2000**, *21*, 2209-2218.

177. O'Farrell, P. H. *J. Biol. Chem.* **1975**, *250*, 4007-4021.

178. Gorg, A.; Obermaier, C.; Boguth, G.; Harder, A.; Scheibe, B.; Wildgruber, R.; Weiss, W. *Electrophoresis* **2000**, *21*, 1037-1053.

179. Hancock, W. S.; Wu, S.-L.; Shieh, P. *Proteomics* **2002**, *2*, 352-359.

180. McDonald, W. H.; Ohi, R.; Miyamoto, D. T.; Mitchison, T. J.; Yates, J. R. *Int. J. Mass Spectrom.* **2002**, *219*, 245-251.

181. Kelly, R. T.; Woolley, A. T. *J. Sep. Sci.* **2005**, *28*, 1985-1993.

182. Giddings, J. C.; Dahlgren, K. *Sep. Sci.* **1971**, *6*, 345-356.

183. Koegler, W. S.; Ivory, C. F. *J. Chromatogr. A* **1996**, *726*, 229-236.

184. Koegler, W. S.; Ivory, C. F. *Biotechnol. Prog.* **1996**, *12*, 822-836.

185. Ivory, C. F. *Sep. Sci. Technol.* **2000**, *35*, 1777-1793.

186. Tolley, H. D.; Wang, Q.; LeFebre, D. A.; Lee, M. L. *Anal. Chem.* **2002**, *74*, 4456-4463.

187. Wang, Q.; Tolley, H. D.; LeFebre, D. A.; Lee, M. L. *Anal. Bioanal. Chem.* **2002**, *373*, 125-135.

188. Shackman, J. G.; Ross, D. *Electrophoresis* **2007**, *28*, 556-571.

189. Humble, P. H.; Kelly, R. T.; Woolley, A. T.; Tolley, H. D.; Lee, M. L. *Anal. Chem.* **2004**, *76*, 5641-5648.

190. Kelly, R. T.; Li, Y.; Woolley, A. T. *Anal. Chem.* **2006**, *78*, 2565-2570.

191. Greenlee, R. D.; Ivory, C. F. *Biotechnol. Prog.* **1998**, *14*, 300-309.

192. Wang, Q.; Lin, S.-L.; Warnick, K. F.; Tolley, H. D.; Lee, M. L. *J. Chromatogr. A* **2003**, *985*, 455-462.

193. Lin, S.-L.; Tolley, H. D.; Lee, M. L. *Chromatographia* **2005**, *62*, 277-281.

194. Lin, S.-L.; Li, Y.; Tolley, H. D.; Humble, P. H.; Lee, M. L. *J. Chromatogr. A* **2006**, *1125*, 254-262.

195. Ross, D.; Locascio, L. E. *Anal. Chem.* **2002**, *74*, 2556-2564.

196. Shackman, J. G.; Munson, M. S.; Ross, D. *Anal. Bioanal. Chem.* **2007**, *387*, 155-158.

197. Shackman, J. G.; Munson, M. S.; Kan, C.-W.; Ross, D. *Electrophoresis* **2006**, *27*, 3420-3427.

198. Kim, S. M.; Sommer, G. J.; Burns, M. A.; Hasselbrink, E. F. *Anal. Chem.* **2006**, *78*, 8028-8035.

199. Balss, K. M.; Ross, D.; Begley, H. C.; Olsen, K. G.; Tarlov, M. J. *J. Am. Chem. Soc.* **2004**, *126*, 13474-13479.

200. Balss, K. M.; Vreeland, W. N.; Phinney, K. W.; Ross, D. *Anal. Chem.* **2004**, *76*, 7243-7249.

201. Balss, K. M.; Vreeland, W. N.; Howell, P. B.; Henry, A. C.; Ross, D. *J. Am. Chem. Soc.* **2004**, *126*, 1936-1937.

202. Hoebel, S. J.; Balss, K. M.; Jones, B. J.; Malliaris, C. D.; Munson, M. S.; Vreeland, W. N.; Ross, D. *Anal. Chem.* **2006**, *78*, 7186-7190.

203. Huang, Z.; Ivory, C. F. *Anal. Chem.* **1999**, *71*, 1628-1632.

204. Tunon, P. G.; Wang, Y.; Myers, P.; Bartle, K. D.; Bowhill, L.; Ivory, C. F.; Ansell, R. J. *Electrophoresis* **2008**, *29*, 457-465.

205. Burke, J. M.; Ivory, C. F. *Electrophoresis* **2008**, *29*, 1013-1025.

206. Tracy, N. I.; Huang, Z.; Ivory, C. F. *Biotechnol. Prog.* **2008**, *24*, 444-451.

207. Petsev, D. N.; Lopez, G. P.; Ivory, C. F.; Sibbett, S. S. *Lab Chip* **2005**, *5*, 587-597.

208. Myers, P.; Bartle, K. D. *J. Chromatogr. A* **2004**, *1044*, 253-258.

2 SURFACE MODIFICATION OF GLYCIDYL-CONTAINING POLY(METHYL METHACRYLATE) MICROCHIPS USING SURFACE-INITIATED ATOM TRANSFER RADICAL POLYMERIZATION [*]

2.1 Introduction

As reviewed in Chapter 1, among all of the reported methods for permanent modification of the polymeric microchip inner surface, the ATRP technique gives the best protein separation results, indicating that ATRP provides uniform polymer layers with high surface coverage. Unfortunately, for most commercially available polymers, surface modification is usually preceded by activating the inert polymer surface by harsh conditions or using high-energy radiation or plasma sources. Recently, a novel surface-reactive acrylic copolymer, poly(glycidyl methacrylate-*co*-methyl methacrylate) (PGMAMMA) (Figure 2.1), was synthesized in our laboratory, which introduced epoxy functionalities on the surface.[1] Several surface reactions were performed using this material, including aminolysis and photografting of polyacrylamide. The thermal properties, solvent resistance, and transparency of this material are suitable for microfabrication.

In this study, three methods were employed to activate the PGMAMMA surface, including plasma treatment, hydrolysis and aminolysis. The latter two methods were easiest to perform in the laboratory without specialized equipment. Following surface activation, an ATRP initiator was immobilized and a

[*] This chapter (except Figures 2.1 and 2.2) is reproduced with permission from *Anal. Chem.* **2008**, *80*, 856-863. Copyright 2008 American Chemical Society.

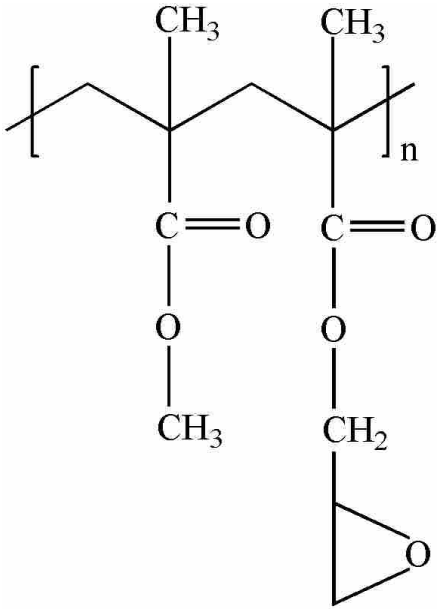

Figure 2.1. Structure of PGMAMMA.

PEG-functionalized layer was grown on the surface. Surface modified PGMAMMA microchips were used to separate peptides and proteins.

2.2 Experimental Section

2.2.1 Materials

Glycidyl methacrylate (GMA, 97%), methyl methacrylate (MMA), poly(ethylene glycol) methyl ether methacrylate (PEGMEMA, MW ~475), 2-bromoisobutyryl bromide (98%), 2,2'-azobisisobutyronitrile (AIBN, 98%), 2,2'-dipyridyl (99+%), copper(I) chloride (CuCl, 98+%), and copper(II) bromide ($CuBr_2$, 99%) were purchased from Aldrich (Milwaukee, WI) and used without further purification. Pyridine (reagent grade), heptane (reagent grade), tetrahydrofuran (THF, reagent grade), anhydrous ethylenediamine (reagent grade) and sodium silicate solution (40-42^o, Bé) were obtained from Fisher Scientific (Fair Lawn, NJ). Hydrogen peroxide (ACS grade, 30%) was purchased from Columbus Chemical Industries (Columbus, WI). Sodium carbonate, sodium bicarbonate, and sulfuric acid (96.4%) were purchased from Mallinckrodt Specialty Chemicals (Paris, KY). Isopropyl alcohol (IPA, USP grade) was obtained from AAPER Alcohol and Chemical (Shelbyville, KY). Ethylenediaminetetraacetic acid disodium salt dihydrate ($Na_2EDTA{\cdot}2H_2O$, 99+%) was obtained from Invitrogen Life Technologies (Carlsbad, CA). (Heptadecafluoro-1,1,2,2-tetrahydrodecyl)trichlorosilane was ordered from Gelest (Morrisville, PA). Fluorescein isothiocyanate (FITC), dimethyl sulfoxide (DMSO, 99.5%), tris(hydroxymethyl)aminomethane (TRIZMA, Tris),

Phe-Leu-Glu-Glu-Ile (FLEEI), Phe-Ala (FA), Phe-Gly-Gly-Phe (FGGF), Phe-Phe-Tyr-Arg (FFYR), leu enkephalin, angiotensin II fragment 3-8, angiotensin II, myoglobin, porcine thyroglobulin, β-lactoglobulin A, and FITC conjugated human serum albumin (FITC-HSA) were purchased from Sigma-Aldrich (St. Louis, MO).

Deionized water (18.2 MΩ·cm) was prepared using a Milli-Q UF Plus water purification system (Millipore, Billerica, MA). All buffers used in FITC labeling, EOF measurement and μCE separation were filtered using 0.2 μm syringe filters (Pall Gelman Laboratory, Ann Arbor, MI) before experiments. PMMA sheet (Acrylite FF) was purchased from Cyro (West Paterson, NJ). Precleaned microscope slides with dimensions of 75 × 50 × 1 mm^3 and 75 × 25 × 1 mm^3 were obtained from Fisher Scientific (Pittsburgh, PA) and Hardy Diagnostics (Santa Maria, CA), respectively.

2.2.2 Synthesis of PGMAMMA

PGMAMMA is a novel polymeric material with reactive epoxy functionalities on the surface, which has been successfully used to prepare microfluidic devices.[1,2] PGMAMMA plates were synthesized by copolymerizing MMA and GMA in glass forms (75 × 50 × 1.5 mm^3) using thermally-initiated free-radical polymerization. To prevent the polymer from sticking to the glass, the glass slides were cleaned by submersion in a boiling Piranha solution (70:30 H_2SO_4/30% aqueous H_2O_2) for 30 min and then treated with (heptadecafluoro-1,1,2,2-tetrahydrodecyl)trichlorosilane vapor. After assembling the form using sodium silicate solution as cement, an ultrasonically degassed monomer solution [(1:1 mol/mol) MMA/GMA and 0.1 % (w/w) AIBN] was introduced into the form. After sealing a glass cover over the form

using sodium silicate solution, it was placed in an oven and held at 65°C for 24 h. After the reaction was complete, the form was immersed in a water bath to dissolve the sodium silicate glue, and the glass form was disassembled to release the polymer plate. The resulting polymer plates were rinsed with IPA and deionized water, and then dried with nitrogen gas.

2.2.3 Microchip Fabrication

The procedures for fabrication of the silicon template and microchips were the same as previously reported.[1,3] Briefly, the pattern as shown in Figure 2.2A on the silicon template was embossed into the bottom PGMAMMA plate at 92 ^{o}C. The resulting plate possessed crossed microchannels; the short one was used for injection and the long one was used for separation. The top plate with four access holes was prepared using a C-200 CO_2 laser engraving system (Universal Laser Systems, Scottsdale, AZ). The top and bottom plates were then bonded together at 65^{o}C after surface modification described below. The hot embossing and bonding processes were carried out using an HP 5890 gas chromatograph oven.

2.2.4 Surface Activation of PGMAMMA

For plasma activation, the polymer substrates (PGMAMMA and PMMA) were treated with an air plasma produced in a PDC-32G plasma cleaner (Harrick Plasma, Ithaca, NY) for 3-5 min (~10.5 W and 400 mTorr), followed by immobilizing the ATRP initiator immediately. To hydrolyze the epoxy groups on the polymer surface, the substrates were placed in 0.5 M sulfuric acid solution at 40 ^{o}C for 12 h.[4] After reaction was complete, the substrates were rinsed with DI water until neutral and

dried with nitrogen gas. For aminolysis, the PGMAMMA substrates were immersed in a solution containing 20% (w/w) ethylenediamine, 40% (w/w) IPA and 40% (w/w) ethyl alcohol at room temperature for 24 h, followed by rinsing with deionized water again until neutral and dried with nitrogen gas.[1]

2.2.5 Attachment of ATRP Initiator on the PGMAMMA Surface

Immobilization of a typical ATRP initiator, 2-bromoisobutyryl bromide, on PGMAMMA and PMMA surfaces has been previously reported.[1,3] After air plasma activation, substrates were immediately immersed in a 5:1 (v/v) heptane/THF solution containing 25 mM initiator and 27.5 mM pyridine and placed on a MaxQ 2000 shaker (Barnstead International, IA) at room temperature for 6 h. For hydrolyzed and aminolyzed substrates, after cleaning and drying, the substrates were also placed in the initiator solution for 6 h. Then, the substrates were removed, rinsed thoroughly with IPA and deionized water, and dried with nitrogen gas.

2.2.6 Surface-Initiated Atom Transfer Radial Polymerization (SI-ATRP)

To avoid the negative effects of oxygen in the reaction, the ATRP process was carried out in a nitrogen-filled glove box. The initiator-anchored substrate plates were immersed in an aqueous solution containing 20% PEGMEMA 475 (v/v), 18 mM CuCl, 5.4 mM $CuBr_2$, and 46.8 mM 2,2'-dipyridyl. After reaction at room temperature for 12 h, the substrates were removed and immersed in saturated aqueous Na_2EDTA solution to quench the reaction and remove residual copper ions. All polymer plates were thoroughly rinsed with deionized water and dried with nitrogen gas before characterization and thermal bonding.

2.2.7 Electroosmotic Flow Measurement

The current monitoring approach was employed to measure the electroosmotic flow (EOF) in the PEG grafted PGMAMMA microchannel.[5] The measurement procedure and instrument were the same as used before.[1] In brief, the separation microchannel and one of the reservoirs were filled with 20 mM Tris-HCl buffer (pH 8.5), and the other reservoir was emptied using a pipette and then filled with 10 mM Tris-HCl buffer (pH 8.5). The solution levels for both reservoirs were carefully maintained the same. A voltage of 1000 V was applied over the microchannel and the current was recorded. The sampling rate for data collection was 50 Hz.

2.2.8 X-ray Photoelectron Spectroscopy (XPS)

X-ray photoelectron spectroscopy (XPS) was used to determine the elemental composition of various treated surfaces, including the initial PGMAMMA surface, initiator-bonded PGMAMMA and PMMA plates, and PEG grafted PGMAMMA surface. Before XPS experiments, all polymer samples were thoroughly rinsed with deionized water, purged with nitrogen gas, and dried under vacuum. XPS was performed using an SSX-100 X-ray photoelectron spectrometer with a monochromatic Al Kα source and a hemispherical analyzer. An electron flood gun was employed because the samples were insulating polymers. Survey scans as well as narrow scans were recorded with an 800×800 μm^2 spot size. Data acquisition and processing were implemented with the instrument software (ESCA NT 3.0).

2.2.9 Contact Angle Measurement

An NRL-100 goniometer (Ramé-hart, Mountain Lakes, NJ) was employed to

measure contact angles of activated PGMAMMA and PMMA surfaces, and initiator-bonded and PEG grafted PGMAMMA surfaces. The contact angle was determined immediately after 4 μL deionized water was dropped on the surface, reported as the mean of the left and right contact angles of the water drop.

2.2.10 FITC Labeling of Peptides and Proteins

Each peptide and protein sample was dissolved in 10 mM carbonate solution (pH 9.2), and diluted to 2 mM and 1 mg/mL, respectively. The solutions were passed through 0.2 μm syringe filters prior to use. FITC was diluted in absolute DMSO to prepare a 6 mM solution. For peptides, a 200 μL solution of each sample was combined with 50 μL of FITC solution. For proteins, 600 μL of each protein solution was thoroughly mixed with 40 μL of FITC solution. All sample-FITC solutions were allowed to react in the dark for at least 24 h at room temperature. Each sample was diluted with 10 mM Tris-HCl buffer (pH 8.5) before use.

2.2.11 CE Separation of Peptides and Proteins

The setup for CE separation, including laser induced fluorescence (LIF) detection and data acquisition, was the same as reported before.[1,3] The sampling rate for data collection was 100 Hz. Pinched injection was used for sample injection and the voltages applied to the reservoirs for both injection and separation are shown in Figures 2.2 B and C.

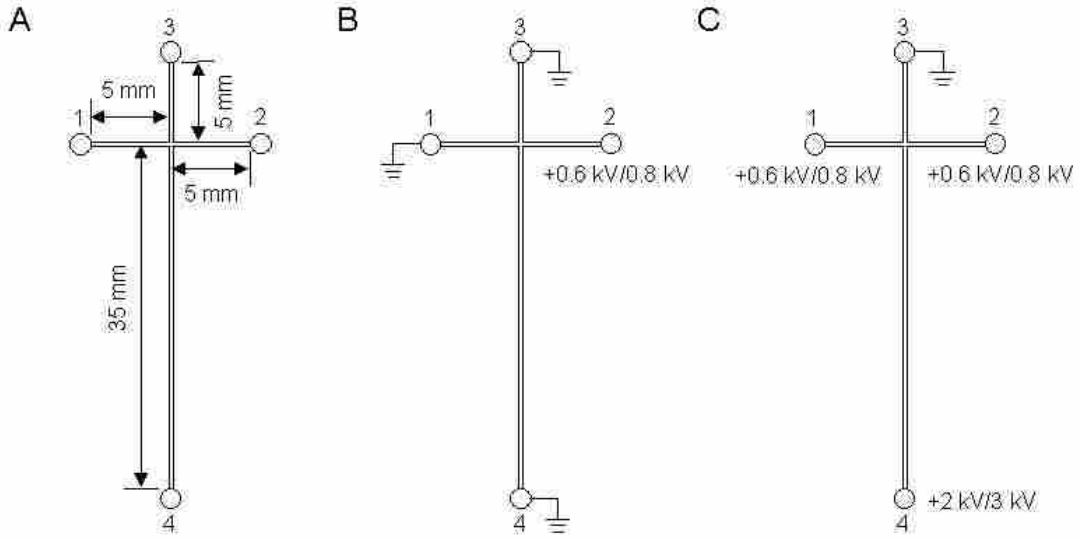

Figure 2.2. (A) Schematic diagram of microchip design used in this work, (B) voltage scheme for sample injection, (C) voltage scheme for μCE separation. (1) Sample reservoir, (2) sample waste reservoir, (3) buffer reservoir, (4) buffer waste reservoir.

2.3 Results and Discussion

2.3.1 Synthesis of PGMAMMA

PGMAMMA is a novel plastic that has physical properties similar to PMMA, such as good thermal stability and UV transparency above 300 nm. These characteristics make it suitable for fabrication of microfluidic devices.[1] Most importantly, it is easy to modify this plastic surface due to the presence of epoxy functionalities on the surface. Thus, it is feasible to obtain biocompatible surfaces using this polymer and various traditional chemical reactions.

PGMAMMA plates were first prepared in glass forms assembled with unmodified glass slides.[1] However, sometimes it was hard to remove the plastic plates out of the forms because the copolymer stuck to the glass. Occasionally, Si peaks were seen in the XPS spectra of the plastic surfaces, which indicated that the glass sometimes adhered strongly to the polymer surface. This may have resulted from interactions between the epoxy groups in the plastic and silanol groups on the glass. The presence of Si changed the polymer surface properties, affecting surface modification, microfabrication and thermal bonding. To prevent this problem, the glass slides were reacted with a perfluorinated silane vapor to produce a monolayer which was crosslinked at high temperature. These modified glass slides were then assembled into forms as before using sodium silicate solution. The monomer solution was then poured into the forms, followed by sealing them with cover plates and placing them in a GC oven at 65 ^{o}C for 24 h. After polymerization, the plastic plates were easily removed from the forms when they were immersed in a water bath. With

this treatment, no permanent adhesion or adsorption of glass or perfluorinated silane was observed on the polymer surface, as indicated by the absence of fluorine and silica peaks in the XPS spectrum of the surface (Figure 2.6 F). The contact angle of the PGMAMMA surface was $67.3^{o}\pm0.5$ (calculated from 3 measurements at 95% CL), which is close to that of PMMA.

2.3.2 Surface Activation of PGMAMMA

Various plasmas can be used to activate inert polymer surfaces, such as PDMS and PMMA.[3,6,7] Ionized oxygen or oxygen radicals in an oxygen plasma attack the polymer chains to introduce oxygen-containing functionalities onto the surface, such as hydroxyl and carboxyl groups. Such plasma treated surfaces are hydrophilic and the new generated functionalities can participate in further chemical reactions. In this work, I first used an air plasma to activate the PGMAMMA surface. Compared with PMMA, it was much easier to activate a PGMAMMA surface due to the presence of reactive epoxy functionalities. The epoxy rings opened easily to generate hydroxyl or carboxyl groups. To oxidize a PMMA surface using an oxygen plasma, pure oxygen gas should be introduced and the plasma should be maintained at 80 W.[3] For PGMAMMA, an air plasma with lower power (~10.5 W) was sufficient to activate the surface.[1] The plasma treatment time was approximately 3-5 min. If the treatment time was too long, the plastic plate deformed under the generated heat because its glass transition temperature is only 82 ^{o}C. Figure 2.3 shows that the contact angles of PGMAMMA and PMMA surfaces change with exposure time in air after 5 min air plasma treatment. The contact angles increase with exposure time, which is consistent

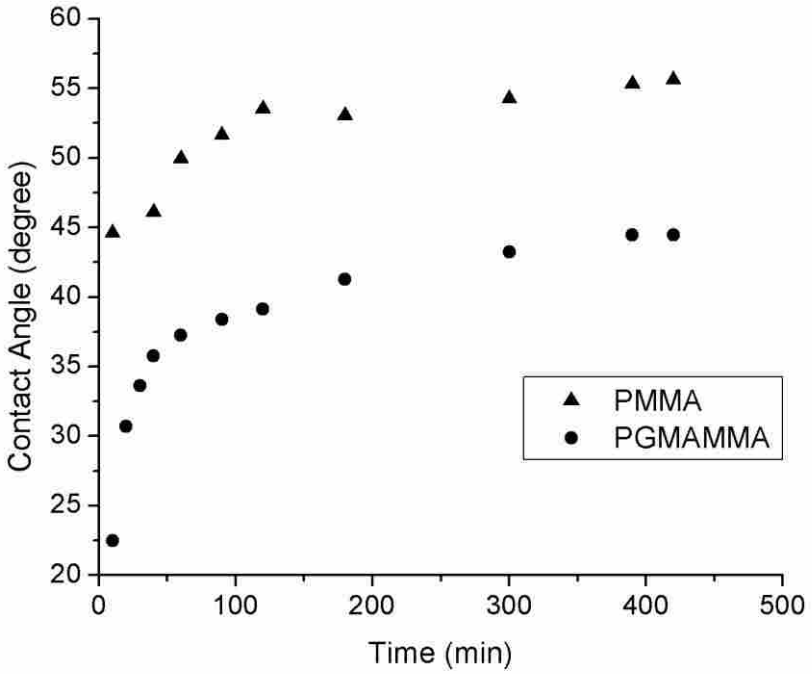

Figure 2.3. Plots of contact angle of PMMA and PGMAMMA surfaces as a function of time after 5 min plasma treatment.

with results from PDMS.[8] The recovery of hydrophobicity occurs because the hydrophilic groups or segments migrate into the bulk polymer by rotational or translational motion in order to minimize the interfacial free energy between the polymer surface and its air environment.[9] After similar treatment, the PGMAMMA surface wettability changed more than PMMA. After exposure to air for 10 min, the contact angle of the PGMAMMA surface was 22.5^{o} (Table 2.1), which was smaller than PMMA (~45^{o}). This indicates that the plasma produces more hydrophilic groups on the PGMAMMA surface than PMMA. After 7 h, the contact angle of the PMMA surface was ~55^{o}, which again was larger than PGMAMMA (~45^{o}).

In addition to plasma oxidation, the PGMAMMA surface can be activated by other means. For example, ring-opening of the epoxy groups occurs with ethylenediamine to introduce amino groups on the surface.[1] Another simple reaction is to hydrolyze the epoxy groups under acidic conditions to produce diol groups on the surface.[4] This hydrolysis reaction, which has been widely used to modify GMA copolymers, is shown in Figure 2.4. Even though surface activation by chemical treatment takes considerably longer than plasma treatment, it is much less expensive than using a plasma source, and batch processing eliminates most concerns about lengthy treatment time. After hydrolysis and aminolysis, PGMAMMA surfaces have similar contact angles (Table 2.1). Compared with plasma activation, hydrolysis and aminolysis can be carried out in most laboratories without any special equipment, and these methods generate more stable activated surfaces, which have been stored for up to 6 months without any noticeable change in reactivity.

Table 2.1. Contact angles of PGMAMMA surfaces after activation, initiator bonding, and PEG grafting. [a, b]

Treatment	Activated	Initiator bonded	PEG grafted
Plasma	22.5±1.2° [c]	56.5±0.7°	39.6±0.2°
Hydrolysis	48.7±2.6°	54.5±3.1°	39.4±0.7°
Aminolysis	48.8±3.7°	56.6±0.9°	39.3±0.1°

[a] Data were calculated from four consecutive measurements.

[b] CL% = 95%.

[c] Contact angle was measured ~10 min after 5 min plasma treatment.

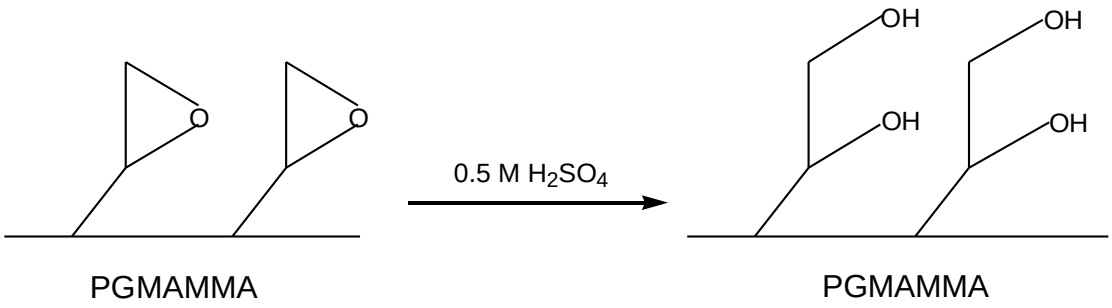

Figure 2.4. Hydrolysis of PGMAMMA under acidic conditions.

2.3.3 Surface-Initiated Atom Transfer Radical Polymerization

To generate a covalently attached polymer "brush" on a surface, two strategies have been employed: "grafting from" and "grafting to." Surface-initiated polymerization is a "grafting from" technique in which polymer chains are grown directly from initiator sites on the surface. This method achieves much higher grafting density than a "grafting to" technique. ATRP has been implemented in various surface-initiated polymerization studies to date.[10-14] This technique produces well-controlled polymer brush growth under mild conditions. In this work, I took advantage of surface-initiated atom transfer radical polymerization (SI-ATRP) to generate a protein-adsorption resistant polymer brush on the PGMAMMA surface.

To perform SI-ATRP, I first covered the polymeric substrate surface with ATRP initiator. The three surface activation methods described above introduce either hydroxyl or amino groups on the PGMAMMA surface, which are used to anchor the ATRP initiator.[10] The reactions are shown in Figure 2.5. After reaction, a transferable halogen (bromine) is attached on the surface, which acts as the ATRP initiator. The contact angles of initiator-bound surfaces (~56^{o}) increased in comparison to activated surfaces (Table 2.1) because more hydrophobic groups replaced the hydroxyl or amino groups. Figures 2.6 A-C show XPS spectra of initiator-anchored PGMAMMA surfaces, which were activated using different methods. Figure 2.6 D is the XPS spectrum of an initiator-bound PMMA surface that was first treated with an air plasma; no evidence of bromine can be found. In contrast, three bromine peaks (Br 3s, Br 3p and Br 3d) are easily recognized for treated PGMAMMA surfaces. From XPS narrow

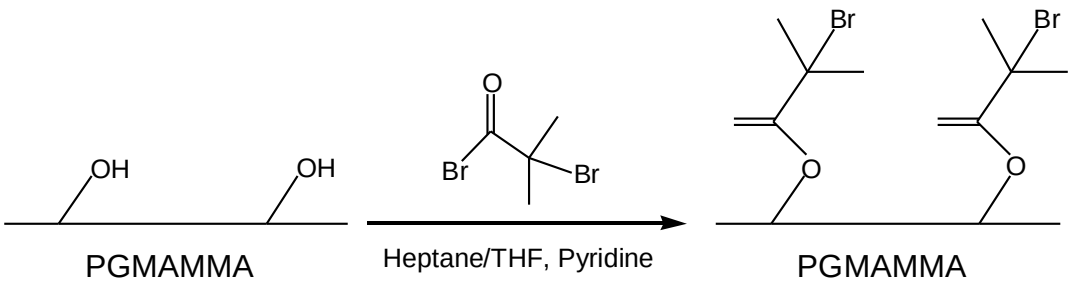

Figure 2.5. Bonding of ATRP initiator on PGMAMMA surface.

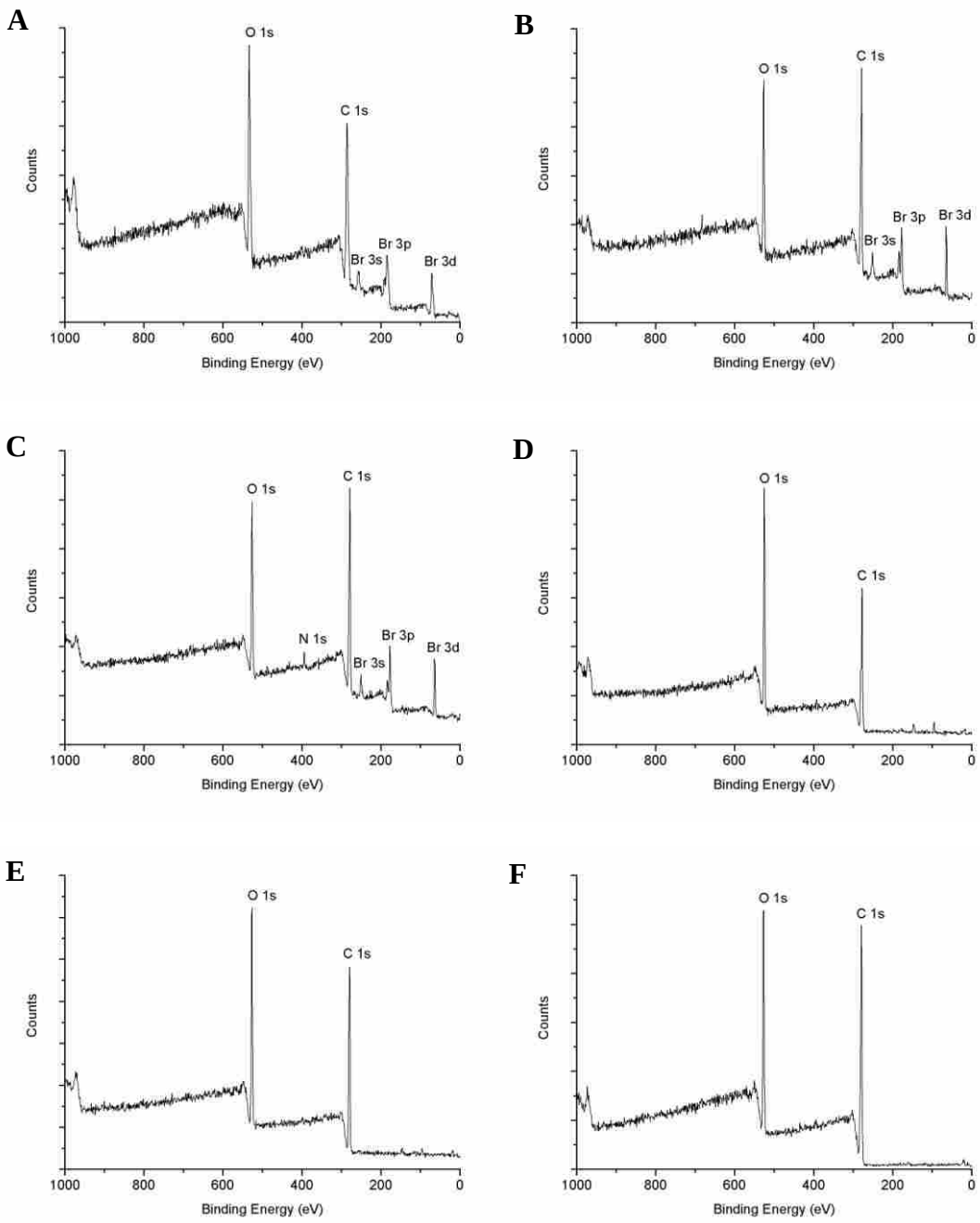

Figure 2.6. XPS survey spectra of (A) air plasma treated PGMAMMA with bonded ATRP initiator, (B) hydrolyzed PGMAMMA with bonded initiator, (C) aminolyzed PGMAMMA with bonded initiator, (D) air plasma treated PMMA with bonded initiator, (E) PEG grafted PGMAMMA using ATRP, and (F) untreated PGMAMMA. The binding energies of O 1s, N 1s, C 1s, Br 3s, Br 3p and Br 3d are 526.5 eV, 394.6 eV, 279.7 eV, 250.7 eV, 177.8 eV, and 64.9 eV, respectively.

scans, the bromine content (atom percentage) on each initiator-anchored surface was obtained (see Table 2.2). The bromine content was very small (0.19%) on the PMMA surface compared to the PGMAMMA surfaces (> 4.5%), although these surfaces were activated by different means. The hydrolyzed polymer surface had a bromine content similar to the aminolyzed surface. However, both were higher than the air plasma treated surface. This is because hydrolyzed and aminolyzed surfaces have relatively stable reactive groups, i.e., hydroxyl and amino groups. The reactive groups on the air plasma treated surface disappeared gradually due to hydrophobic recovery. For the PMMA surface, only a few reactive groups were generated after air plasma treatment. An aminolyzed PGMAMMA surface showed a nitrogen content of 3.03±0.26% based on three measurements at 95% confidence level.

After surface initiator bonding, ATRP was carried out to attach the polymer film to the surface. To render the microchip suitable for biomolecule separations, the microchannel surface should be resistant to biomolecule adsorption. PEG is useful for resisting adsorption of proteins and adhesion of platelets and other cells.[15] Recently, PEG has been used to passivate various surfaces, including metal, silicon and polymer surfaces.[3,16,17] In this work, I used PEGMEMA (MW ~475) as the ATRP monomer. Although the backbone of the grafted polymer is based on methacrylate, PEG side chains surround the backbone to provide a hydrophilic and neutral environment, which is nonadsorptive to biomolecules, such as proteins and peptides. Figure 2.7 shows the ATRP reaction. The thickness of the grafted layer can be adjusted by simply varying the polymerization time and monomer concentration. Compared with

Table 2.2. Atom percentages of Br on various polymer surfaces after bonding of the initiator as determined by XPS narrow scans.

	Plasma treated PGMAMMA	Hydrolyzed PGMAMMA	Aminolyzed PGMAMMA	Plasma treated PMMA
Br %	4.51±0.33 [a, b]	5.77±0.69 [a, b]	5.23±0.64 [a, b]	0.19

[a] Data were calculated from three measurements.

[b] CL% = 95%.

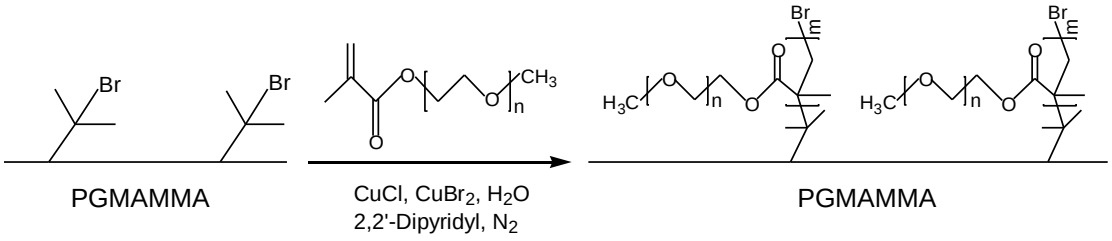

Figure 2.7. Surface-initiated atom transfer radical polymerization of PEGMEMA on a PGMAMMA surface.

modification of the PMMA surface, not only is the monomer concentration lower, but the polymerization time is also shorter. This is because of the greater density of initiator anchored on the PGMAMMA surface. In SI-ATRP, the polymerization rate is proportional to monomer and initiator concentrations.[11] When the initiator density is high, the monomer concentration should be reduced in order to carefully control the polymerization. In addition, the polymer graft density depends on the surface density of the initiator. It was observed, however, that the plate became opaque when the polymer density was too high, which not only destroyed the transparency of the plate, but also interfered with thermal bonding. To obtain suitably modified plates, I reduced the polymerization time to control the polymer molecular weight and the polymer graft density.

The contact angles of the PEG grafted surfaces are listed in Table 2.1. For the three activation methods, the final polymer surfaces have similar wettabilities. Their contact angles were approximately 39.4^{o}, which is in agreement with the results obtained from PEG films grafted on silicon (~41^{o})[16] and PMMA surfaces (~38.6^{o}).[3] Figure 2.6 E shows an XPS spectrum of a PEG grafted PGMAMMA surface, which was first hydrolyzed. Only carbon and oxygen peaks (C 1s and O 1s) appear in the spectrum. No bromine peak was found on the surface. Most likely, most of the chains were terminated and, therefore, no living chain-ends were left on the surface.[11]

2.3.4 Micro-CE of Biomolecules in Modified PGMAMMA Microchips

Electroosmotic flow. The electroosmotic (EO) mobility of an untreated PGMAMMA microchannel is (3.5±0.6)×10^{-4} cm^{2}/V·s (Table 2.3), and its direction is

from the anode to the cathode, which is opposite to the movement of negative analytes when a high voltage is applied. This EO mobility is larger than for a PMMA microchannel (~1.6×10^{-4} $cm^2/V\cdot s$) because of the presence of epoxy groups on the PGMAMMA surface. When a PEG film is generated on the polymer surface, the EO mobility reduces by one order of magnitude (Table 2.3). The EO mobility was approximately 3×10^{-5} $cm^2/V\cdot s$ when the polymer surface was activated using any of the three methods. This is because the EO mobility only depends on the surface characteristics.

CE separation of peptides. Figure 2.8 shows the CE separation of seven FITC labeled peptides using a PEG-grafted PGMAMMA microchip, which was first activated using an air plasma and then grafted with a PEG layer using the ATRP method. Seven peptides were completely separated in 30 s when the electric field strength was 500 V/cm (Figure 2.8 A). To achieve a faster separation, I applied a higher electric field strength (750 V/cm), and all peptides were totally separated in 18 s (Figure 2.8 B). The column efficiencies for each peak in Figure 2.8 are listed in Table 2.4. The efficiencies are all higher than 1.8×10^4 plates for a 3.5 cm separation channel.

CE separation of proteins. All PEG grafted PGMAMMA microchips gave good protein separations. Figure 2.9 A shows complete separation of four FITC labeled proteins in 20 s using a hydrolyzed and then grafted device. In addition to the main component (peak 4), HSA had three other minor components. The first two were located between peaks 1 and 2, and the third small peak was overlapped with peak 3

Table 2.3. Electroosmotic mobilities of untreated and PEG modified PGMAMMA microchips.[a,b]

	Untreated	Plasma treated	Hydrolyzed	Aminolyzed
EOF ($cm^2/V \cdot s$)	$(3.5\pm0.6)\times10^{-4}$	$(3.4\pm0.1)\times10^{-5}$	$(2.6\pm0.1)\times10^{-5}$	$(3.0\pm0.4)\times10^{-5}$

[a] Data were calculated from three consecutive measurements.

[b] CL% = 95%.

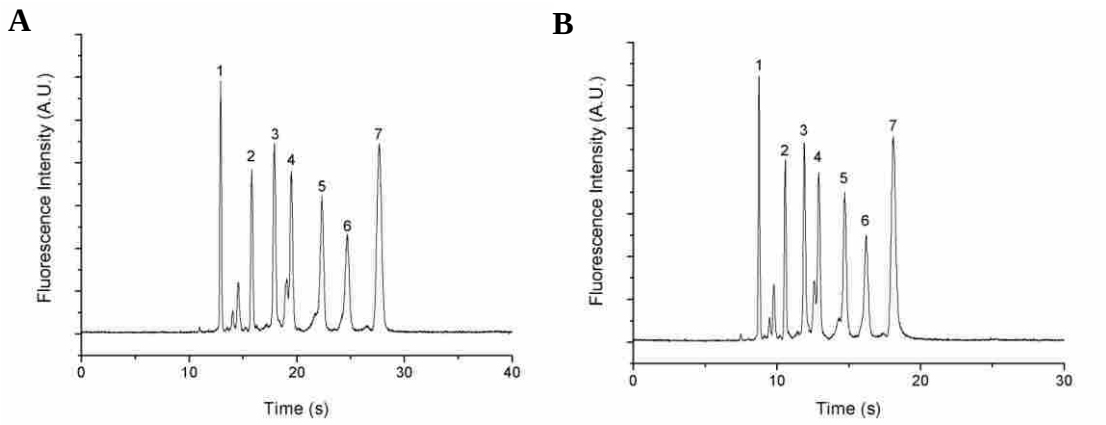

Figure 2.8. CE separations of seven FITC-labeled peptides using a PEG grafted PGMAMMA microchip, which was first treated by an air plasma. Injection voltage was 600 V, and separation voltage was (A) 2000 V and (B) 3000 V. Peak identifications: (1) FLEEI; (2) FA; (3) FGGF; (4) leu enkephalin; (5) angiotensin II, fragment 3-8; (6) angiotensin II and (7) FFYR.

Table 2.4. Column efficiencies for peaks separated in Figures 2.8 and 2.9.

Figure	Peak No.						
	1	2	3	4	5	6	7
Figure 2.8 A	3.6×10^4	3.1×10^4	2.8×10^4	2.7×10^4	2.3×10^4	1.9×10^4	1.8×10^4
Figure 2.8 B	3.5×10^4	3.2×10^4	2.7×10^4	2.3×10^4	2.1×10^4	2.0×10^4	1.8×10^4
Figure 2.9 A	4.4×10^4	3.4×10^4	3.5×10^4	3.6×10^4	--	--	--
Figure 2.9 B	1.5×10^4	--	--	--	--	--	--

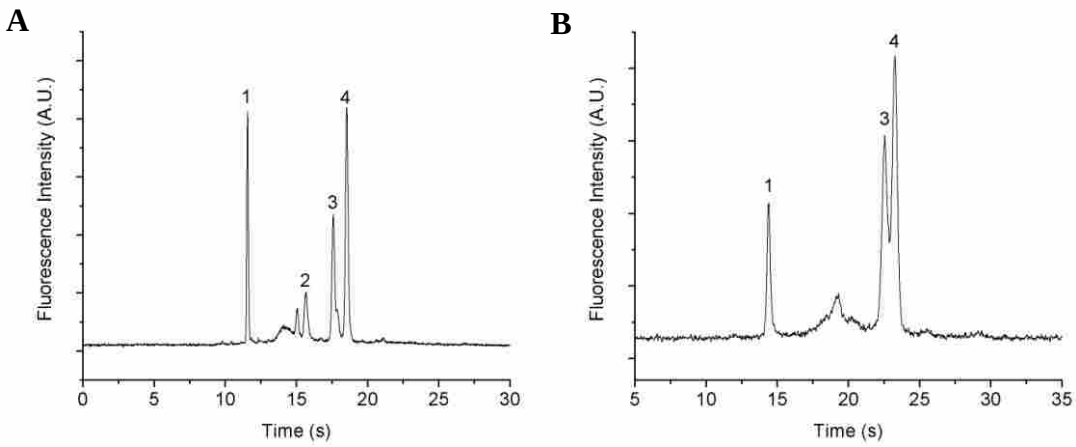

Figure 2.9. CE separations of FITC-labeled proteins using PEG grafted PGMAMMA microchips. (A) Hydrolyzed microchip. Peak identifications: (1) β-lactoglobulin A; (2) thyroglobulin; (3) myoglobin; and (4) human serum albumin (HSA). (B) Aminolyzed microchip. Peak identifications: same as for Figure 2.9 A. Injection voltage was 800 V and separation voltage was 3000 V.

(see Figure 2.10). The separation efficiencies are listed in Table 2.4; FITC-β-lactoglobulin A gave an efficiency of 4.4×10^4 plates. The other three peaks gave similar efficiencies. Figure 2.9 B shows the separation of three proteins using a PEG grafted PGMAMMA microdevice, which was first activated by aminolysis. Compared with Figure 2.9 A, this separation is not very good. The unlabeled small peaks belonging to HSA are not resolved, and peaks 2 and 3 are not completely separated. The column efficiency for the first peak was 1.5×10^4 plates, which was only one third of that achieved in Figure 2.9 A. The poor separation is most likely due to damage of the microchannel surface by ethylenediamine when performing the aminolysis treatment.

Reproducibility. A good microchip should provide good separation reproducibility. I used FITC-labeled HSA to examine the reproducibility of PEG-bound microchips. Figure 2.10 shows four independent electropherograms of HSA using a hydrolyzed and then PEG-grafted PGMAMMA microchip. One major peak and three minor peaks were resolved. The migration times and efficiencies of the major peak in the HSA sample are listed in Table 2.5. The relative standard deviations (RSD) for migration time and column efficiency were 1.3 and 2.7%, respectively. These results demonstrate that the PEG film grafted on the PGMAMMA surface using SI-ATRP is uniform and stable and, therefore, the resultant microchip demonstrates good reducibility for CE separation of biomolecules.

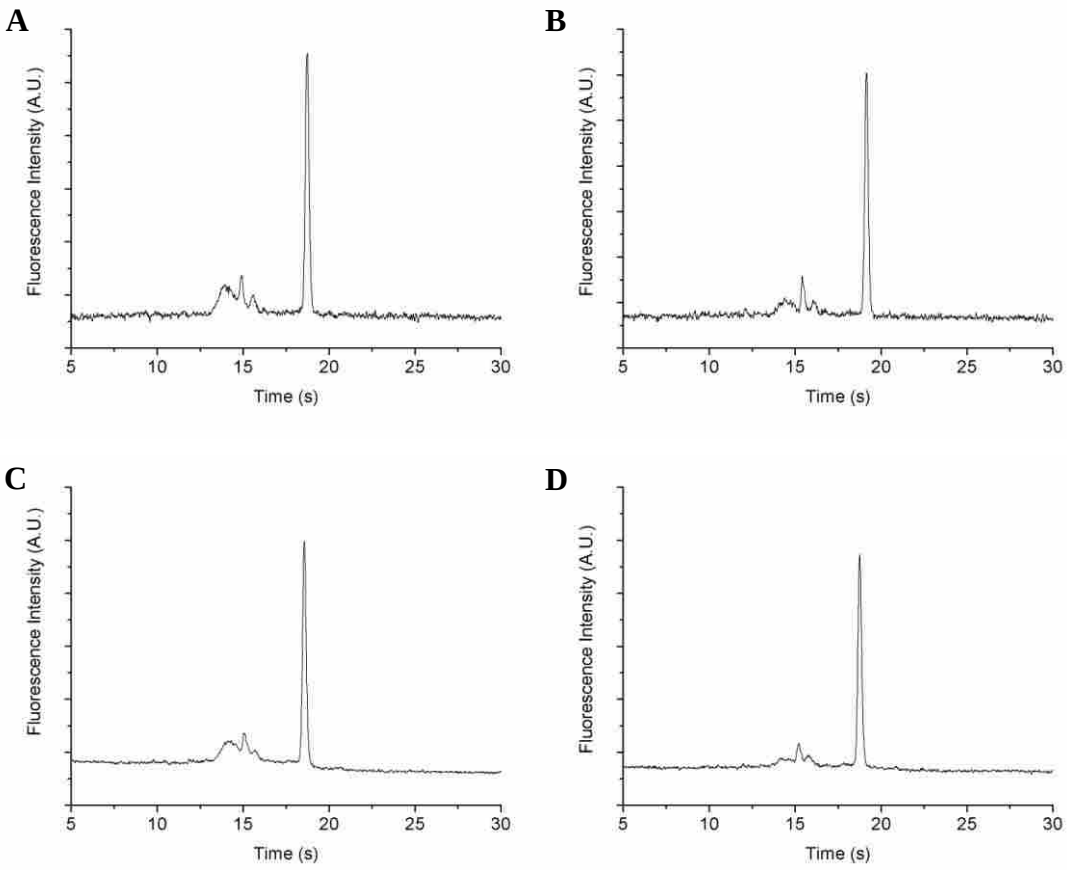

Figure 2.10. CE separations of FITC-HSA using PEG grafted PGMAMMA microchips, which were first hydrolyzed. Electropherograms were recorded for four different microchips. Injection voltage was 800 V and separation voltage was 3000 V.

Table 2.5. Migration time and column efficiency reproducibilities for the major HSA peak shown in Figure 2.10.

	Run				Mean	RSD (%)
	A	B	C	D		
t_m (s)	18.74	19.16	18.76	18.57	18.81	1.3
Total plates	3.4×10^4	3.5×10^4	3.3×10^4	3.4×10^4	3.4×10^4	2.7

2.4 Conclusions

The presence of epoxy functionalities on the PGMAMMA surface renders plastic plates made of this material easy to activate and modify. I successfully used three methods to activate this polymer surface. An air plasma oxidizes the polymer surface and, therefore, introduces oxygen-containing functionalities on the surface, such as hydroxyl groups. Compared with a PMMA surface, for which pure oxygen gas is required for plasma treatment, an air plasma at low power is sufficient to treat the PGMAMMA surface. In addition, the epoxy groups can be directly hydrolyzed under acidic conditions to generate diol groups on the surface. Also the epoxy rings can be opened when attacked by amine reagents. After surface activation, ATRP initiator groups can be anchored on the surface through reaction of the surface hydroxyl or amino groups with 2-bromoisobutyryl bromide. Plasma treated surfaces must be treated quickly in order to avoid hydrophobic recovery of the surface. Reagent activated surfaces are more stable. In the last step of surface modification, SI-ATRP was carried out to graft PEG groups on the surface. This grafted polymer film was uniform, hydrophilic, stable and resistant to protein adsorption. PGMAMMA microchips treated via this modification strategy showed excellent performance in separation of peptides and proteins. These devices provided high separation efficiency and good reproducibility.

2.5 References

1. Liu, J.; Sun, X.; Lee, M. L. *Anal. Chem.* **2005**, *77*, 6280-6287.

2. Liu, J.; Sun, X.; Farnsworth, P. B.; Lee, M. L. *Anal. Chem.* **2006**, *78*, 4654-4662.

3. Liu, J.; Pan, T.; Woolley, A. T.; Lee, M. L. *Anal. Chem.* **2004**, *76*, 6948-6955.

4. Svec, F.; Frechet, J. M. J. *Anal. Chem.* **1992**, *64*, 820-822.

5. Huang, X.; Gordon, M. J.; Zare, R. N. *Anal. Chem.* **1988**, *60*, 1837-1838.

6. Papra, A.; Bernard, A.; Juncker, D.; Larsen, N. B.; Michel, B.; Delamarche, E. *Langmuir* **2001**, *17*, 4090-4095.

7. Wang, Y.-C.; Choi, M. H.; Han, J. *Anal. Chem.* **2004**, *76*, 4426-4431.

8. Hillborg, H.; Ankner, J. F.; Gedde, U. W.; Smith, G. D.; Yasuda, H. K.; Wikstrom, K. *Polymer* **2000**, *41*, 6851-6863.

9. Chatelier, R. C.; Xie, X.; Gengenbach, T. R.; Griesser, H. J. *Langmuir* **1995**, *11*, 2576-2584.

10. Li, N.; Bai, R.; Liu, C. *Langmuir* **2005**, *21*, 11780-11787.

11. Tomlinson, M. R.; Genzer, J. *Macromolecules* **2003**, *36*, 3449-3451.

12. Carlmark, A.; Malmstrom, E. E. *Biomacromolecules* **2003**, *4*, 1740-1745.

13. Zhang, Z.; Chen, S.; Chang, Y.; Jiang, S. *J. Phy. Chem. B* **2006**, *110*, 10799-10804.

14. Cho, W. K.; Kong, B.; Choi, I. S. *Langmuir* **2007**, *23*, 5678-5682.

15. Liu, J.; Lee, M. L. *Electrophoresis* **2006**, *27*, 3533-3546.

16. Sharma, S.; Johnson, R. W.; Desai, T. A. *Langmuir* **2004**, *20*, 348-356.

17. Mougin, K.; Ham, A. S.; Lawrence, M. B.; Fernandez, E. J.; Hillier, A. C. *Langmuir* **2005**, *21*, 4809-4812.

3 SURFACE MODIFICATION OF POLYMER MICROFLUIDIC DEVICES USING IN-CHANNEL ATOM TRANSFER RADICAL POLYMERIZATION [*]

3.1 Introduction

As introduced in Chapter 2, I grafted PEG-functionalized layers on PGMAMMA microchannel surfaces using the SI-ATRP method.[1] During the ATRP modification process, the complete surfaces of both plates were grafted with a PEG layer, which affected the thermal bonding strength of the resultant microchips. Modification of only the microchannel surface would certainly improve the bonding strength.

Xiao et al.[2] carried out microchannel confined SI-ATRP to graft a thin polyacrylamide layer inside the PDMS microchannel. The patterned PDMS surface was oxidized using a UV/ozone plasma and then bound with ATRP initiator. Finally, an aqueous solution containing acrylamide, catalyst and ligand was introduced into the enclosed microchannel to perform ATRP. The resultant microchip was successfully used for electrophoretic separation of proteins with an efficiency of ~1.16×10^3 plates for a 3.5 cm-length microchannel.

Recently, Pan et al.[3] developed a new technique called in-channel ATRP to modify TPE microdevices, which were fabricated using a casting method. An ATRP initiator was first immobilized on the channel surface through the existing hydroxyl groups. Then a dilute PEG-functionalized monomer solution containing catalyst and

[*] This chapter is reproduced with permission from *Electrophoresis* **2008**, *29*, 2760-2767. Copyright 2008 Wiley-VCH.

ligand was introduced into the microchannel to perform ATRP. The resultant PEG-grafted TPE microchannel exhibited low, pH-stable EOF and low protein adsorption. Electrophoresis efficiencies of 4.5×10^3 plates for amino acids and 1.2×10^3 plates for peptides were obtained using the surface modified TPE microdevice with a 3.0-cm-long separation channel. This microdevice was used to separate phosducin-like protein and phosphorylated phosducin-like protein to evaluate the efficiency of phosphorylation.

In this study, I developed an in-channel ATRP method to graft a PEG-functionalized layer on a PGMAMMA microchannel surface, following ATRP initiator coupling and thermal bonding, for electrophoresis of peptides and proteins. I was hopeful that this approach would produce more stable and robust devices than previously reported ATRP methods.

3.2 Experimental Section

3.2.1 Materials and Preparation of Test Samples

GMA (97%), MMA, PEGMEMA (MW ~475), 2-bromoisobutyryl bromide (98%), 2,2'-azobisisobutyronitrile (AIBN, 98%), 2,2'-dipyridyl (99+%), copper(I) chloride (CuCl, 98+%), and copper(II) bromide ($CuBr_2$, 99%) were purchased from Aldrich (Milwaukee, WI). Pyridine (reagent grade), heptane (reagent grade), tetrahydrofuran (THF, reagent grade), sodium silicate solution (40^o-42^o Bé), urea (reagent grade), and dithiothreitol (molecular biology grade) were obtained from Fisher Scientific (Fair Lawn, NJ). Iodoacetamide was purchased from Amersham

Biosciences (Piscataway, NJ), isopropyl alcohol (IPA, USP grade) was obtained from AAPER Alcohol and Chemical (Shelbyville, KY), (heptadecafluoro-1,1,2,2-tetrahydrodecyl) trichlorosilane was from Gelest (Morrisville, PA), and DL-aspartic acid, DL-glutamic acid, DL-phenylalanine, DL-asparagine, and glycine were purchased from ICN Biomedicals (Aurora, OH). Fluorescein isothiocyanate (FITC), dimethyl sulfoxide (DMSO, 99.5%), tris(hydroxymethyl)aminomethane (TRIZMA, Tris), Gly-Tyr (GY), Phe-Gly-Gly-Phe (FGGF), Trp-Met-Asp-Phe (WMDG), Phe-Phe-Tyr-Arg (FFYR), angiotensin III (Ang III), myoglobin, porcine thyroglobulin, β-lactoglobulin A, β-casein, trypsin, FITC-conjugated human serum albumin (FITC-HSA), FITC-conjugated insulin, and FITC-conjugated β-casein were purchased from Sigma-Aldrich (St. Louis, MO). All monomers were directly used without further purification.

Amino acid, peptide and protein test samples were labeled with FITC for fluorescence detection. The labeling procedure was reported elsewhere.[4] In brief, each sample was dissolved in 10 mM carbonate solution (pH 9.2) to give 3 mM (amino acids), 2 mM (peptides), or 1 mg/mL (proteins) concentrations, respectively. The test solutions were filtered through 0.2 μm syringe filters (Pall Gelman Laboratory, Ann Arbor, MI) prior to use. FITC was dissolved in absolute DMSO to prepare a 6 mM solution. For amino acids, a 600 μL volume of sample solution was mixed with 200 μL of FITC solution; for peptides, a 200 μL volume of solution was combined with 50 μL of FITC solution; and for proteins, a 600 μL volume of solution was thoroughly mixed with 40 μL of FITC solution. All solutions were allowed to react in the dark for

at least 24 h at room temperature and then stored in a refrigerator (4 ^{o}C). Immediately prior to use, samples were diluted with 10 mM Tris-HCl buffer (pH 8.5).

β-Casein was digested using a protocol described in the literature.[5] In brief, 1 mg β-casein was sequentially treated with 6 M urea, dithiothreitol and iodoacetamide at 37 ^{o}C. Trypsin (20 mg) was then added, and the solution was left overnight at 37 ^{o}C and pH 8.0. The resulting digest was desalted using a cellulose ester dialysis membrane (MWCO 100, Spectrum Medical Industries, Houston, TX) for 24 h. Before CE analysis, the digest was diluted with 10 mM Tris-HCl (pH 8.5) buffer.

Deionized water (18.2 MΩ·cm) was prepared using a Milli-Q UF Plus water purification system (Millipore, Billerica, MA). All buffers used in FITC labeling, EOF measurements and μCE separations were filtered before use. Precleaned microscope slides with dimensions of 75 × 50 × 1 and 75 × 25 × 1 mm^3 were purchased from Fisher Scientific (Pittsburgh, PA) and Hardy Diagnostics (Santa Maria, CA), respectively.

3.2.2 Synthesis of PGMAMMA

PGMAMMA plates were synthesized using thermal-initiated free-radical polymerization of MMA and GMA in glass forms (75 × 50 × 1.5 mm^3) which had their surfaces passivated using (heptadecafluoro-1,1,2,2-tetrahydrodecyl) trichlorosilane to prevent polymer-glass adhesion.[1] The ingredients in the monomer solution included 50% (mol concentration) MMA, 50% GMA, and 0.1 % (weight percentage of total monomers) AIBN. Polymerization was carried out at 65°C for 24 h, after which the resulting polymer plates were released by immersing the glass forms

in a water bath. Finally, the plates were cleaned with IPA and deionized water.

3.2.3 Microchip Fabrication

The PGMAMMA plates were trimmed to dimensions of 50 × 20 mm^2 using a C-200 CO_2 laser engraving system (Universal Laser Systems, Scottsdale, AZ). The microfabrication procedure was followed as previously reported.[4] Briefly, a simple crosschannel design as shown in Figure 2.2 A on a silicon template was hot embossed into the PGMAMMA plates at 92 ^oC. Top plates containing four holes for reservoirs were fabricated using the laser engraving system. Top and bottom plates were assembled together, then clamped tightly and placed in an HP 5890 gas chromatograph oven to perform thermal bonding at 68 ^oC after immobilizing the ATRP initiator on the contacting surfaces as described in the next section.

3.2.4 Immobilization of ATRP Initiator

Before anchoring the ATRP initiator, the surfaces of the top and bottom plates were activated using an air plasma to produce oxygen-containing functionalities, such as hydroxyl and carboxyl groups. The activated plates were immediately immersed in a 5:1 (v/v) heptane/THF solution containing 25 mM 2-bromoisobutyryl bromide and 27.5 mM pyridine. An Erlenmeyer flask storing the reaction mixture was sealed with a rubber stopper and placed on a MaxQ 2000 shaker (Barnstead International, IA) at room temperature for 6 h. Then, the plates were removed, washed with IPA and deionized water, and dried with nitrogen gas.

3.2.5 In-Channel ATRP

After the top and bottom plates of a device were bonded together as described

in Section 3.2.3, the surface of the microchannel was grafted with a PEG-containing layer using an in-channel ATRP technique. The complete procedure was carried out in a nitrogen-filled glove box. Initially, a brown aqueous solution (10 mL) containing 20% PEGMEMA 475 (v/v), 18 mM CuCl, 5.4 mM $CuBr_2$, and 46.8 mM 2,2'-dipyridyl was prepared and mixed thoroughly using a magnetic stirrer. After all catalyst and ligand were dissolved, the solution was diluted five-fold by adding nitrogen-purged deionized water and then filtered through a 0.2 μm syringe filter. After the fittings and microchip were assembled, the final 4% PEGMEMA solution was withdrawn into a 3 mL syringe and pushed into the initiator-bound microchannel at room temperature from the end reservoir of the separation channel at 0.5 μL/min. Then the microchannel was flushed with deionized water to remove the unreacted monomer and residual catalyst and ligand.

3.2.6 Electroosmotic Flow Measurement

The current monitoring approach was employed to measure any EOF that could be generated by the PEG-grafted PGMAMMA microchannel.[5] Briefly, the separation microchannel and one reservoir were filled with 20 mM Tris-HCl buffer (pH 8.5), and the other reservoir was filled with 10 mM Tris-HCl buffer (pH 8.5) to the same level. A voltage (1000 V) was then immediately applied across the microchannel using a PS-350 high-voltage supply unit (Stanford Research Systems, Sunnyvale, CA). Current variation was recorded using a PCI-1200 data acquisition system (National Instruments, Austin, TX) and a LabView 6i software program (National Instruments).

3.2.7 X-ray Photoelectron Spectroscopy (XPS)

X-ray photoelectron spectroscopy (XPS) was employed to investigate the ATRP initiator-anchored PGMAMMA surface using an SSX-100 X-ray photoelectron spectrometer with a monochromatic Al Kα source and a hemispherical analyzer. An electron flood gun was utilized to perform a survey scan because the sample was an insulator. Data were recorded and processed using the instrument software (ESCA NT 3.0).

3.2.8 CE Separation of Amino Acids, Peptides and Proteins

The in-channel ATRP modified polymer microchips were employed to separate various mixtures of amino acids, peptides and proteins. The voltages applied to the reservoirs for both injection and separation are shown in Figures 2.2 B and C, respectively. The laser induced fluorescence (LIF) detection system and data acquisition system used in this study were described previously.[5] The sampling frequency was 100 Hz. Pinched injection was used for sample injection.

3.3 Results and Discussion

3.3.1 In-channel ATRP Modification

Surface-initiated ATRP has proven to be an effective method to modify PMMA and PGMAMMA microchannel surfaces.[1,5] PEG-functionalized groups were grafted using this technique to suppress electroosmotic flow and to resist protein adsorption. The resultant microchips provided highly efficient separations of peptides and proteins. During the fabrication of these microchips, ATRP grafting was

performed on the surfaces of top and bottom plates before thermally bonding them together to form the enclosed microchannels. Unfortunately, some of these bonded PEG-grafted microchips only survived several hours, delaminating spontaneously during use. This was due to the weak bonding strength of the PEG-functionalized surfaces. The grafted layer contained short PEG side chains (~8 ethylene glycol units) which could not interact or entangle sufficiently during thermal bonding to provide good adhesion. This problem is magnified by the fact that polymers of relatively low molecular weight are typically formed in aqueous solution using the ATRP method.[6] Furthermore, the underlying substrate surface polymers were prevented from interacting because of the more hydrophilic PEG-functionalized surface layer. It was found in this study that the PGMAMMA plates after immobilization of only the ATRP initiator bonded together strongly, similar to untreated PGMAMMA, producing much more robust devices than obtained in the previous study.

The modification procedure reported here is notably different from the reported TPE modification procedure.[3] I anchored the initiator on the total surfaces of both plates before bonding them together to form the enclosed microchannel, instead of bonding before introducing initiator into the channels. In this way, the reaction was faster and more efficient, which avoided swelling and deforming of the microchannel. Furthermore, clogging of the microchannel by precipitate generated in the reagent solution was avoided. Figure 3.1 shows an XPS spectrum of the initiator anchored polymer surface, in which the Br peaks are clearly visible. After thermal bonding of the plates, an aqueous solution containing monomer (PEGMEMA), catalyst and

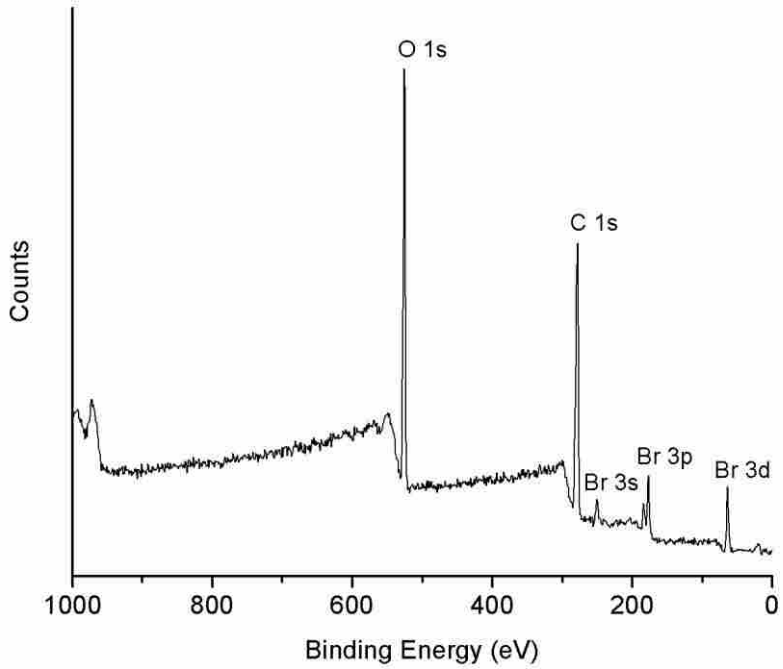

Figure 3.1. XPS survey scan spectrum of a PGMAMMA surface bound with ATRP initiator. The binding energies of O 1s, C 1s, Br 3s, Br 3p and Br 3d are 525.9 eV, 278.7 eV, 250.7 eV, 176.8 eV, and 63.9 eV, respectively.

ligand, prepared in an oxygen-free environment, was pumped into the microchannels to perform the in-channel ATRP modification. To avoid blocking of the channel, the monomer solution was diluted to approximately 4% PEGMEMA. In addition, the microchips were placed face down in order to drain solution out of the channels to prevent crystallization of the catalyst or excess polymerization in the microchannels around the reservoirs.

To evaluate the extent of in-channel ATRP modification, EOF measurements after modification were made as listed in Table 3.1. The grafted PEG layer not only resisted protein adsorption, but also reduced the EOF from 3.5×10^{-4} $cm^2/V\cdot s$ for untreated PGMAMMA microchips[1] to 6.6×10^{-5} $cm^2/V\cdot s$ after 24 h reaction time. This EOF was significantly lower than observed for untreated PMMA (1.6×10^{-4} $cm^2/V\cdot s$),[5] but was higher than measured for in-channel ATRP modified TPE microchannels (~1.0×10^{-5} $cm^2/V\cdot s$),[3] as well as for PGMAMMA (~2.6×10^{-5} $cm^2/V\cdot s$),[1] and PMMA (~1.0×10^{-5} $cm^2/V\cdot s$)[5] microchannels modified using the ATRP method before bonding the cover plates to the microfluidic devices. Even though the EOF is higher, the in-channel ATRP method is preferred over ATRP reaction before bonding because the microfluidic chips are more robust.

3.3.2 CE Separations of Amino Acids, Peptides and Proteins

Figure 3.2 shows a CE separation of five FITC-labeled amino acids using an in-channel ATRP modified PGMAMMA microchip. The column efficiency of the completely resolved glycine peak was ~1.8×10^4 plates for the 3.5 cm separation channel, which was approximately four times that obtained with PEG-grafted TPE

Table 3.1. Electroosmotic flow measurements for PGMAMMA microchannels modified by in-channel ATRP for different times. [a, b]

Modification time (h)	EO mobility ($cm^2/V \cdot s$)
6	$(1.9 \pm 0.3) \times 10^{-4}$
12	$(9.4 \pm 0.7) \times 10^{-5}$
24	$(6.6 \pm 1.7) \times 10^{-5}$

[a] Data were calculated from three consecutive measurements.

[b] CL% = 95%.

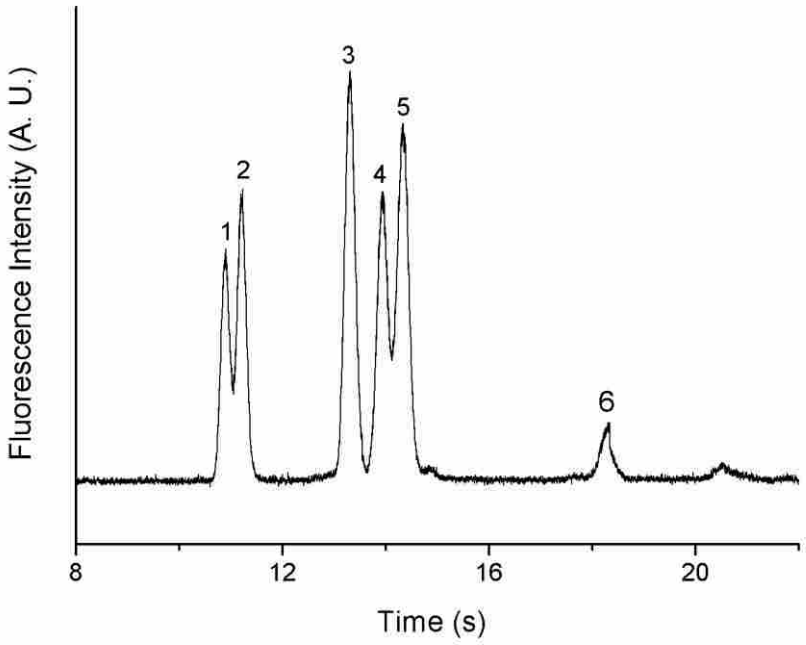

Figure 3.2. CE separation of five FITC-labeled amino acids. Injection voltage was 600 V and separation voltage was 2000 V. Peak identifications: (1) aspartic acid, (2) glutamic acid, (3) glycine, (4) asparagine, (5) phenylalanine, and (6) FITC.

microdevices.[3] Figure 3.3 A shows CE separations of four FITC-labeled peptides using an in-channel PEG-grafted PGMAMMA microchip for different applied electric field strengths. With an increase in electric field strength from 375 to 1000 V/cm, the separation time decreased from 75 to 22 s. Figure 3.3 B shows a plot of total theoretical plates as a function of field strength for each peak in Figure 3.3 A. In general, column efficiencies increased with an increase in electric field strength. Approximately 4.0×10^4 plates for the 3.5 cm separation channel were obtained for GY at 1000 V/cm electric field. A high electric field resulted in fast separation as well as a gain in efficiency. Figure 3.4 shows a separation of five FITC-labeled peptides. Theoretical plate measurements of four of the peaks are listed in Table 3.2, which were all over 1.4×10^4 plates for the 3.5 cm separation channel, or one order of magnitude greater than that obtained with PEG-grafted TPE microdevices.[3]

Figure 3.5 A is an electropherogram of FITC-labeled HSA using an in-channel ATRP modified microdevice. In addition to the main component, three other minor components were resolved, which is consistent with previous results.[1] The main peak gave an efficiency of 1.9×10^4 plates. An electropherogram of FITC-labeled insulin (Figure 3.5 B) shows five peaks, which again agrees with a previously reported separation.[5] These peaks most likely result from the FITC labeling reaction, producing multiple FITC tags or labeled peptide decomposition products. The theoretical plate measurements of the three major peaks are listed in Table 3.2. The first two peaks gave efficiencies over 1.0×10^4 plates. Figure 3.5 C shows a separation of four standard proteins. A high efficiency of 7.1×10^4 plates was obtained for

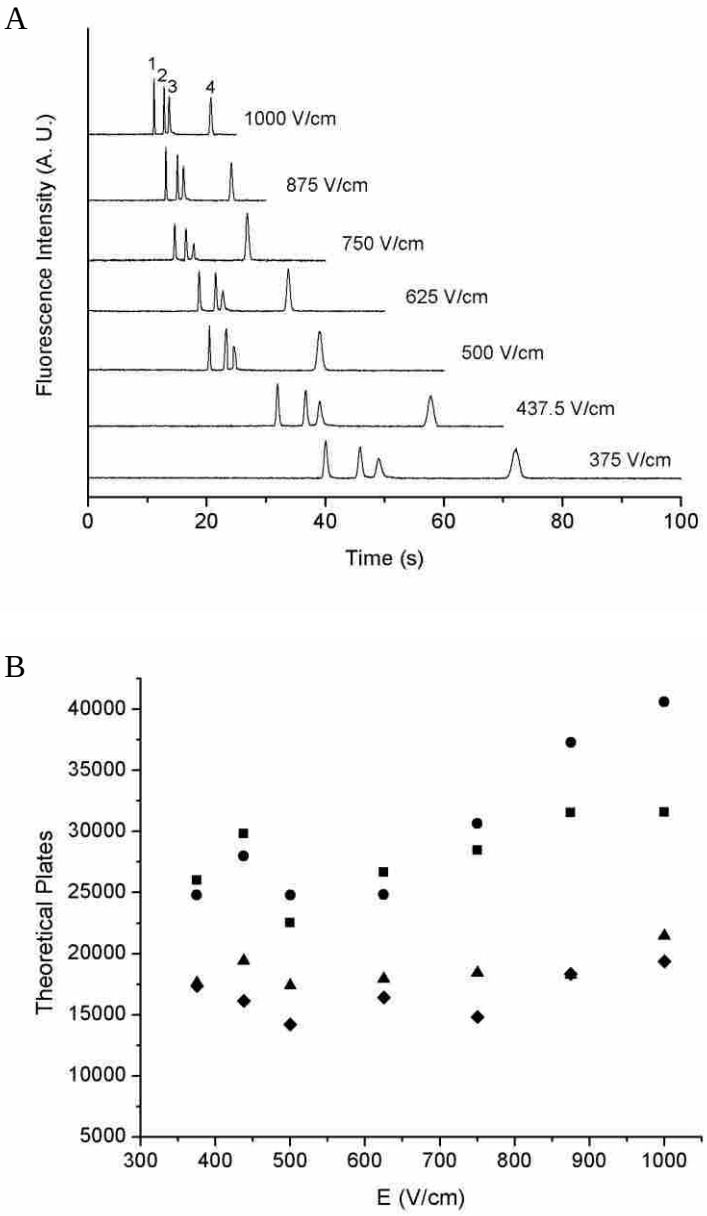

Figure 3.3. (A) CE separation of four FITC-labeled peptides at different applied electric field strengths (given in figure) and (B) theoretical plates versus applied electric field strength for the peptide separations shown in Figure 3.3 A. Legend: 1. GY (●), 2. FGGF (■), 3. WMDG (▲), 4. FFYR (◆).

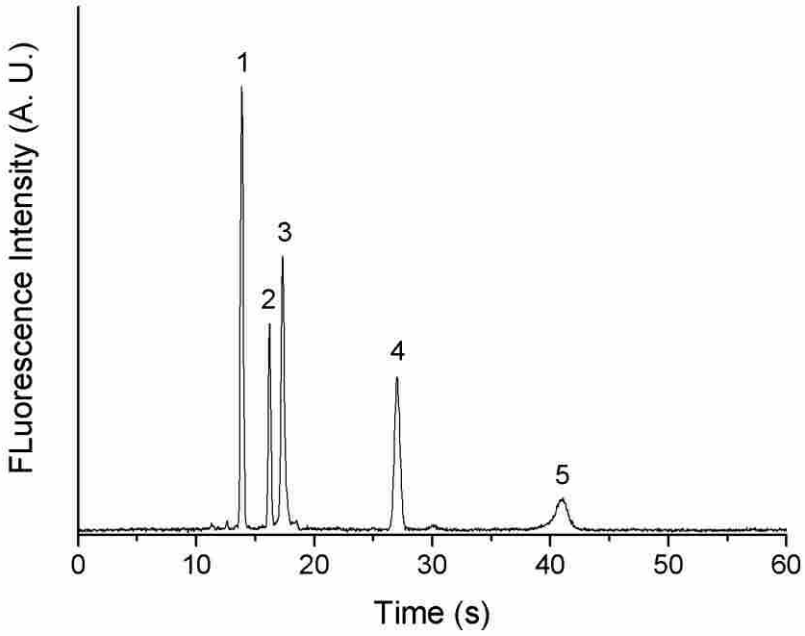

Figure 3.4. CE separation of five FITC-labeled peptides. Injection voltage was 600 V and separation voltage was 3000 V. Peak identifications: (1) GY; (2) FGGF; (3) WMDG; (4) FFYR; (5) Ang III.

Table 3.2. Theoretical plate measurements of peaks numbered in Figures 3.4, 3.5 B and 3.5 C.

Figure	Peak No.			
	1	2	3	4
3.4	1.5×10^4	2.4×10^4	1.7×10^4	1.5×10^4
3.5 B	1.2×10^4	1.0×10^4	5.8×10^3	--
3.5 C	3.9×10^4	7.1×10^4	2.3×10^4	9.8×10^3

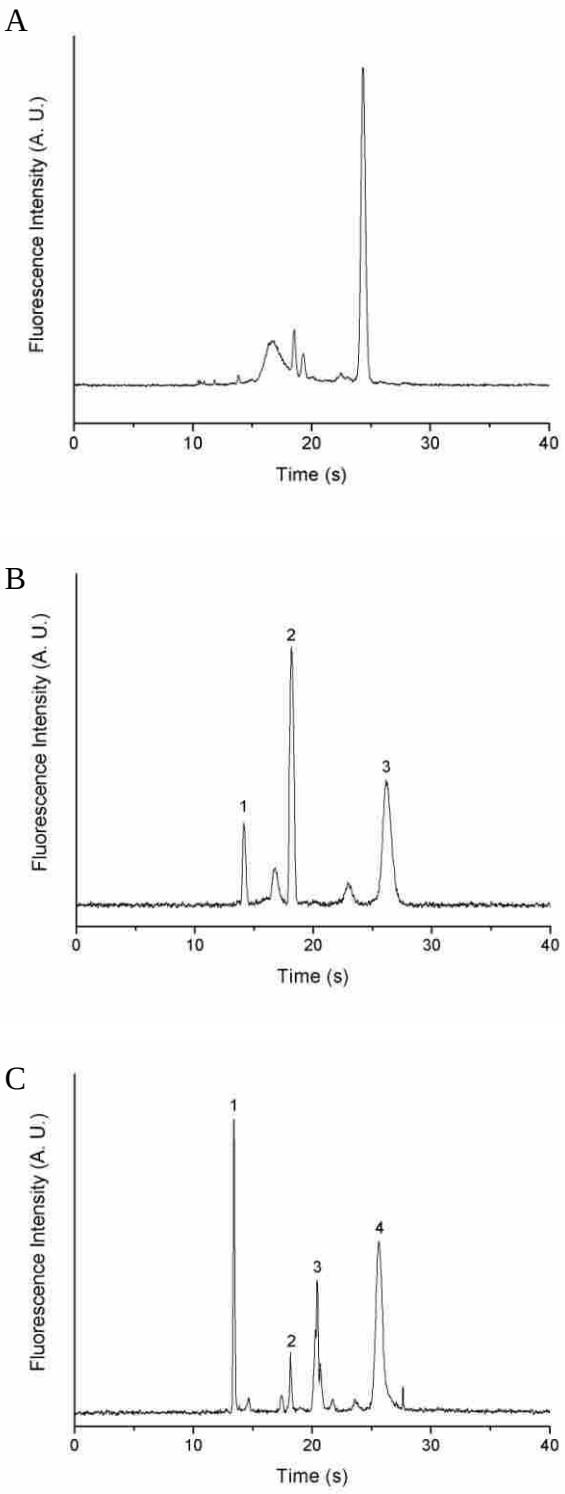

Figure 3.5. CE separations of (A) FITC-HSA, (B) FITC-insulin, and (C) FITC-labeled protein mixture. Injection voltage was 800 V and separation voltage was 3000 V. Peak identifications in electrophoregram C: (1) β-lactoglobulin A; (2) thyroglobulin; (3) myoglobin; and (4) β-casein.

thyroglobulin. All of these protein separations gave efficiencies approximately one order of magnitude higher than polyacrylamide grafted PDMS microchips modified using the ATRP technique.[2] Moreover, most of the peaks were symmetrical, which indicates that there was little protein adsorption on the microchannel surface. Figure 3.6 shows a separation of FITC-labeled β-casein tryptic digest.

FITC-labeled β-lactoglobulin A was used to evaluate the repeatability and stability of the PEG grafted microchip devices. Figure 3.7 shows four electropherograms of β-lactoglobulin A chosen randomly from more than 200 sequential CE runs over a 2-wk period using a single PEG-grafted PGMAMMA microchip. No degradation of performance was observed over this 2-wk period. The migration times and efficiencies of the peaks are given in Table 3.3. The relative standard deviations (RSD) for migration time and efficiency were 1.4 and 3.3%, respectively. These results demonstrate that the PEG layer grafted on the PGMAMMA microchannel surface using in-channel ATRP is homogeneous and stable. Furthermore, microchips modified using in-channel ATRP have bonding strength similar to untreated microchips, and can last for at least several hundred CE runs and several weeks.

3.4 Conclusions

In-channel ATRP was successfully employed to graft a PEG-functionalized layer on a PGMAMMA microchannel surface without compromising the bonding strength. The resultant microchips had low EOF and resisted protein adsorption.

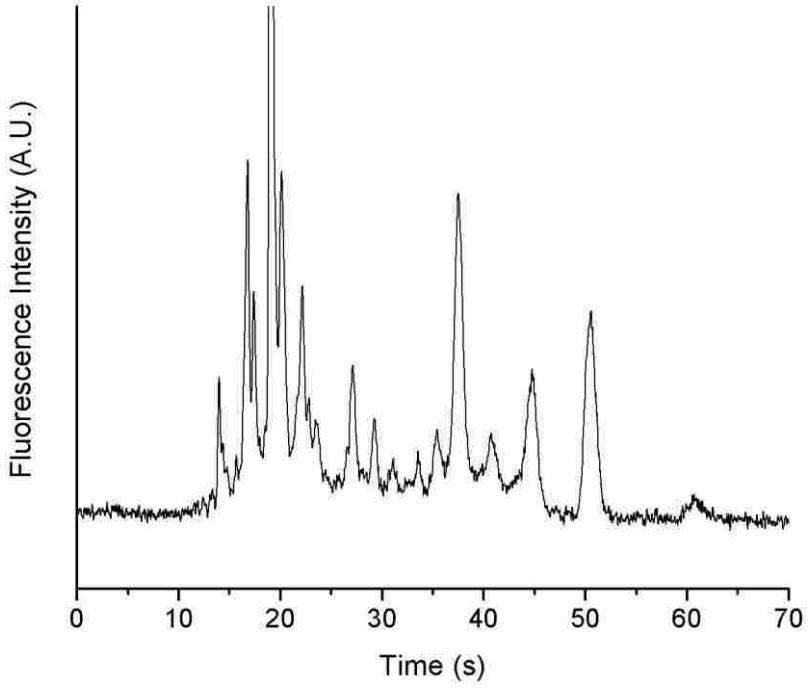

Figure 3.6. CE separations of FITC-labeled β-casein tryptic digest. Injection voltage was 800 V and separation voltage was 3000 V.

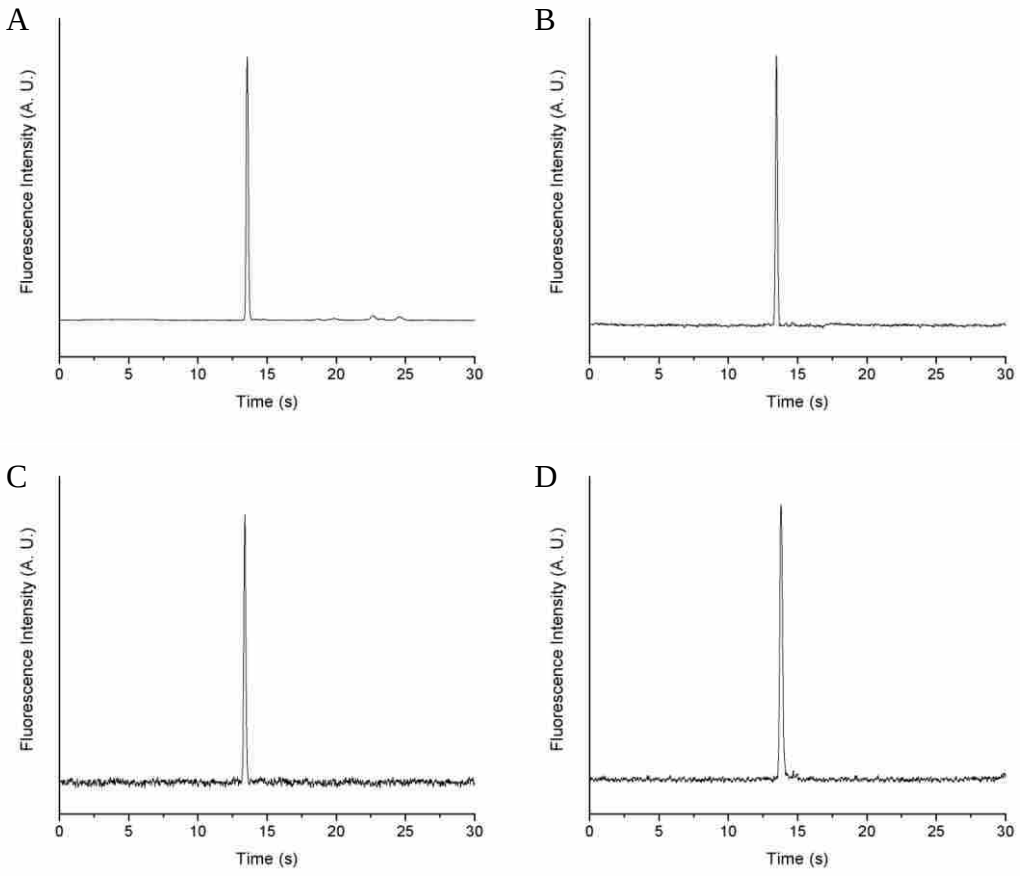

Figure 3.7. CE separation of FITC-labeled β-lactoglobulin A. Electropherograms were recorded for four different runs. Injection and separation voltages were 800 V and 3000 V, respectively.

Table 3.3. Repeatabilities of migration times and theoretical plate measurements of β-lactoglobulin A from electropherograms in Figure 3.7.

	Electropherograms				Mean	RSD (%)
	A	B	C	D		
t_m (s)	13.57	13.50	13.40	13.83	13.58	1.4
Total plates	3.5×10^4	3.5×10^4	3.4×10^4	3.3×10^4	3.4×10^4	3.3

Rapid CE separations of amino acids, peptides and proteins with good reproducibility were obtained. Compared with previously reported in-channel ATRP modified TPE and PDMS microchips, PGMAMMA microchips gave higher efficiencies in CE separations, indicating that the in-channel grafted PEG-functionalized layer on the PGMAMMA surface was more dense and uniform. Compared with PGMAMMA microchips modified using the previously reported ATRP method, microchips modified using the in-channel ATRP technique showed better long-term stability. This technique should be applicable to PMMA and other commercial polymer microchips.

3.5 References

1. Sun, X.; Liu, J.; Lee, M. L. *Anal. Chem.* **2008**, *80*, 856-863.
2. Xiao, D.; Le, T. V.; Wirth, M. J. *Anal. Chem.* **2004**, *76*, 2055-2061.
3. Pan, T.; Fiorini, G. S.; Chiu, D. T.; Woolley, A. T. *Electrophoresis* **2007**, *28*, 2904-2911.
4. Liu, J.; Sun, X.; Lee, M. L. *Anal. Chem.* **2005**, *77*, 6280-6287.
5. Liu, J.; Pan, T.; Woolley, A. T.; Lee, M. L. *Anal. Chem.* **2004**, *76*, 6948-6955.
6. Oh, J. K.; Min, K.; Matyjaszewski, K. *Macromolecules* **2006**, *39*, 3161-3167.

4 INHERENTLY INERT POLY(ETHYLENE GLYCOL)-FUNCTIONALIZED POLYMERIC MICROCHIPS FOR CAPILLARY ELECTROPHORESIS

4.1 Introduction

Among the surface modification techniques, dynamic adsorption is usually not reproducible or durable. Dynamic surface modifiers can also interfere with mass spectrometric detection. On the other hand, permanent surface modification often involves multi-step physical/chemical processing. Obviously, the solution to all problems encountered in surface modification is to prepare new polymeric materials with inherent analyte resistance and good physical properties that are desirable for microfabrication. Microfluidic devices made from such materials could be directly used for separation without any surface modification.

Recently, Kim et al.[1] fabricated PEG micro/nanochannels using UV light induced photopolymerization of PEG-functionalized crosslinkers. The microfluidic devices were non-biofouling and irreversibly bonded. Liu et al.[2] used a similar method to fabricate PEG-functionalized polymer microchips. A monomer mixture containing poly(ethylene glycol) diacrylate (PEGDA), poly(ethylene glycol) methyl ether methacrylate (PEGMEMA) and MMA was introduced into a microchip form constructed from a silica template and a glass slide. Exposure to UV light for a specific period of time initiated polymerization and imprinting of a patterned prepolymer plate. Another plate with reservoirs was prepared using the same procedure. The two plates were assembled together and exposed to UV light again to

complete the polymerization and chemical bonding of the plates together. The resulting microchips were directly used for separation of peptides and proteins without surface modification.

In this work, I investigated the effect of monomer composition on microchip CE performance, including the purity of the PEGDA crosslinker and the addition of MMA as a co-monomer. CE separations of various small molecules, peptides and proteins were evaluated using the improved microchips. Chiral separation was also explored by introducing β-cyclodextrin (β-CD) into the running buffer as a chiral selector.

4.2 Experimental Section

4.2.1 Materials

Poly(ethylene glycol) diacrylate (PEGDA, MW~258), poly(ethylene glycol) methyl ether methacrylate (PEGMEMA, MW~1100), methyl methacrylate (MMA, 99%), 2,2'-dimethoxy-2-phenylacetophenone (DMPA), and β-cyclodextrin hydrate (β-CD) were purchased from Aldrich (Milwaukee, WI, USA). Sodium carbonate (Na_2CO_3) and anhydrous Na_2SO_4 were obtained from Fisher Scientific (Fair Lawn, NJ, USA). Dichloromethane was purchased from Mallinckrodt (Hazelwood, MO), fluorescein was purchased from Fluka (Buchs, Switzerland), and fluorescein isothiocyanate (FITC) was purchased from Invitrogen (Carlsbad, CA, USA). D,L-aspartic acid (D,L-Asp), D,L-glutamic acid (D,L-Glu), D,L-phenylalanine (D,L-Phe), D,L-asparagine (D,L-Asn), D,L-serine (D,L-Ser), D,L-leucine (D,L-Leu)

and glycine were purchased from ICN Biomedicals (Aurora, OH). D,L-tryptophan (D,L-Trp) was obtained from Matheson, Coleman & Bell (Norwood, OH). Dimethyl sulfoxide (DMSO, 99.5%), phenylmethanesulfonyl fluoride, tris(hydroxymethyl)aminomethane (TRIZMA, Tris), D-Asp, D-Glu, D-Asn, D-Gln, D-Phe, D-histidine (D-His), D-arginine (D-Arg), D-proline (D-Pro), L-Asp, L-Glu, L-Asn, L-Gln, L-Phe, L-His, L-Arg, L-Pro, Glu-Val-Phe, D-Leu-Gly, Phe-Phe, β-lactoglobulin A, and lysozyme were purchased from Sigma (St. Louis, MO, USA).

A protein mixture was extracted from *Escherichia coli (E. coli)*. The *E. coli* DH5 α cells were cultivated in Luria-Bertani medium at 37 ^{o}C until the optical density at 600 nm reached 1.0. The cells were harvested by centrifugation at 4000 rpm and then washed with 50 mL prechilled PBS buffer (10 mM, pH 8.5) twice. After the cells were suspended in PBS buffer, lysozyme and phenylmethanesulfonyl fluoride were added to a final concentration of 1 mg/mL and 1 mM, respectively. The cell suspension was sonicated for 20 min. Then the cell debris was removed by centrifugation at 12,000 rpm to obtain a cell-free protein mixture. All processes were conducted at 4 ^{o}C. The total protein concentration in the mixture was approximately 1.0 mg/mL as measured by the Bradford assay.

Deionized water (18.2 MΩ·cm) was prepared using a Milli-Q UF Plus water purification system (Millipore, Billerica, MA, USA). Buffer solutions included 10 mM Tris-HCl (pH 8.3), 10 mM carbonate buffers (pH 9.2, pH 10 and pH 11), and 10 mM Tris-HCl buffer containing 1 mM β-CD (pH 8.3), which were filtered using 0.2 μm syringe filters (Pall Gelman Laboratory, Ann Arbor, MI, USA) before use.

Pre-cleaned microscope slides with dimensions of 75 × 50 × 1 mm^3 and 75 × 25 × 1 mm^3 were obtained from Fisher Scientific (Pittsburgh, PA, USA) and Hardy Diagnostics (Santa Maria, CA, USA), respectively. Unless specifically noted, all chemicals were used as purchased without further purification.

4.2.2 FITC Labeling of Amino Acids, Peptides and Proteins

All amino acid, peptide and protein samples were labeled with FITC for laser induced fluorescence detection (LIF).[3] Each sample was dissolved in 10 mM carbonate buffer solution (pH 9.2) to form 3 mM (amino acids), 2 mM (peptides), or 1 mg/mL (proteins) concentrations. A 6 mM FITC solution was prepared in DMSO. For amino acids, a 600 μL volume of sample solution was thoroughly mixed with 200 μL of FITC solution; for peptides, a 200 μL volume of solution was mixed with 50 μL of FITC solution; and for proteins, a 600 μL volume of solution was mixed with 40 μL of FITC solution. All solutions were allowed to react in the dark for at least 24 h at room temperature and then stored at 4 ^oC. All FITC-tagged samples were diluted with 10 mM Tris-HCl buffer (pH 8.3) before use.

4.2.3 Purification of PEGDA 258

Typically, monomers should be purified before polymerization in order to remove impurities and any inhibitors. In this work, only the crosslinker, PEGDA 258, was purified before use because it was the major monomer. The purification procedure was reported previously.[2] In brief, PEGDA (50 mL) was washed with aqueous saturated Na_2CO_3 solution (30 mL) three times to remove the acidic impurities and inhibitor. Then the Na_2CO_3 residue was removed by thoroughly rinsing

with deionized water (50 mL). Dichloromethane (50 mL) was used to extract PEGDA 258 from the aqueous phase twice. The dichloromethane extracts were combined together and desiccated with anhydrous Na_2SO_4. Finally, the dichloromethane solvent was removed using a rotary evaporator after filtering through a filter paper (0.2-μm pore size).

4.2.4 Fabrication of Microchips

The PEG-functionalized microchips were fabricated by casting as reported previously.[2] In brief, two plate glass forms were assembled. One was used to fabricate the top plate, for which four PDMS posts served as reservoir molds. The other was used to fabricate the bottom plate. A silicon wafer containing a typical cross pattern was used as template to form the microchannels. The thickness of the final polymer plates depended on the PDMS spacers. Monomer solution was introduced into the forms and the assemblies were placed under a Dymax 5000AS UV curing lamp (Torrington, CT) for 10-15 s for photopolymerization. The ingredients in the monomer solution included PEGDA 258, PEGMEMA 1100 and MMA (Table 4.1). The resultant incompletely polymerized plates were assembled together and placed again under the UV light for 5 s to complete the polymerization and covalently bond the plates together. Careful control of the polymerization times was necessary to avoid blocking the enclosed microchannels. After bonding, the microchips were immediately pressed under a weight for 10 min to release stress and heat, and flatten the microchips.

Table 4.1. Ingredients of monomer solutions for fabrication of three different microchips.

Microchip	PEGDA 258	PEGMEMA 1100	MMA	DMPA*
A	85% (purified)	15%	0%	0.1%
B	85% (purified)	12%	3%	0.1%
C	85% (impure)	12%	3%	0.1%

*DMPA content is given as a weight percentage of the total amount of monomers.

4.2.5 Scanning Electron Microscopy (SEM)

The microchannel cross sectional shape was observed using SEM. To avoid damaging the microchannel when exposing it for SEM analysis, a CO_2 laser (Universal Laser Systems, Scottsdale, AZ) was used to cut the polymeric plates on both sides of the channel, but not into the channel. This was followed by breaking the microchip by hand to make a smooth cross section. SEM images were taken using an FEI Philips XL30 ESEM FEG (Hillsboro, OR).

4.2.6 CE Separations

Microchips were used to separate fluorescent dyes, amino acids, peptides and proteins. Laser induced fluorescence (LIF) detection and data acquisition system were used as previously reported.[4] The voltage scheme for injection and separation is illustrated in Figure 2.2. During injection (Figure 2.2 B), reservoirs 1, 3, and 4 were grounded, and +0.6 kV were applied at reservoir 2. During separation (Figure 2.2 C), reservoirs 1 and 2 were maintained at +0.6 kV, reservoir 3 was grounded, and reservoir 4 was set at +2.0 kV.

4.3 Results and Discussion

4.3.1 Fabrication of PEG-Functionalized Microchips

The PEG-functionalized microchips were fabricated by casting. The procedure was simple and easy, and the fabrication was fast. The top and bottom plates were photopolymerized in two molds.[2] The thickness of the plates depended on the mold dimensions. In this work, approximately 400 μm thick plates were fabricated, and

they possessed excellent mechanical strength. During fabrication, the most important concern was to control the extent of polymerization. Usually, only 15 s were required to polymerize a fresh monomer solution to form plates with the desired degree of polymerization. It was important to stop the initial polymerization step before the plates were completely polymerized so that they could be covalently bonded together by subsequent UV light exposure. If the UV exposure time was too long, the plates over-polymerized and deformed. If the reaction time was too short, the plates were soft and difficult to handle. In addition, unsolidified monomer solution on the surfaces could flow into the microchannels during bonding of the plates together, causing blockage. A major advantage of this method is the ease and strength of covalent bonding of the plates, which was effected by reaction between the partially polymerized liquid layers on the top and bottom plate surfaces. Figure 4.1 shows SEM images of two final microchannel cross-sections. In Figure 4.1 A, the two plates were bonded together very well and the microchannel had a good shape. However, in Figure 4.1 B, the partially polymerized top plate was a little too hard, which left a small groove between the two plates after bonding. Obviously, such a groove would impact the separation performance. In both cases the plates were seamlessly bonded together.

PEG-funtionalized acrylates were used as the major components in the monomer solutions to provide protein adsorption resistant characteristics. In the previous work,[2] a small amount of MMA was added to increase the material mechanical strength (microchip B listed in Table 4.1). However, it was suspected that

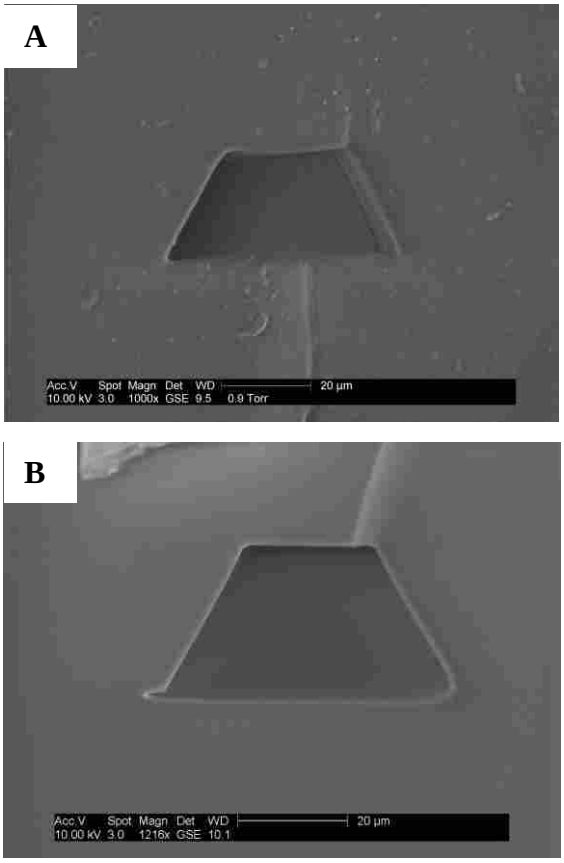

Figure 4.1. SEM images of microchannel cross sections. (A) Microchannel with a good shape, and (B) microchannel with a groove defect.

the presence of MMA could affect the performance of the microchips. In this study, I fabricated a microchip without MMA (microchip A), with ingredients as listed in Table 4.1. Polymerization of this microchip only required ~10 s to achieve the desired prepolymerized plates. The PEG-functionalized acrylate monomers were more reactive than MMA. Another microchip made with impure PEGDA (microchip C in Table 4.1) was also fabricated to study the influence of crosslinker purity on separation performance.

4.3.2 CE Separation of Fluorescent Dyes

The PEG-functionalized microchips were able to separate both small molecules and macromolecules. Figure 4.2 shows the separation of fluorescein and FITC at different pH values using microchip B. With an increase in pH, the migration times decreased. This is expected since fluorescein and FITC are weak acids. Fluorescein has a pK_a of 6.3[5] and FITC is a fluorescein derivative (pK_a 6.9),[6] with an isothiocyanate group replacing a hydrogen atom on a benzene ring. Therefore, in a basic environment, both are negatively charged. Separation efficiency measurements of each peak in Figure 4.2 are listed in Table 4.2. While all efficiency measurements were higher than 1.0×10^4 plates for the 3.5 cm long microchannel, they were higher at higher pH values. At pH 11, the efficiency of fluorescein reached 2.6×10^4 plates.

4.3.3 CE Separation of Amino Acids

Figure 4.3 shows separations of 6 amino acids using three different microchips under the same conditions. With microchip A made from purified PEGDA and PEGMEMA, all of the amino acids were almost completely resolved (Figure 4.3 A).

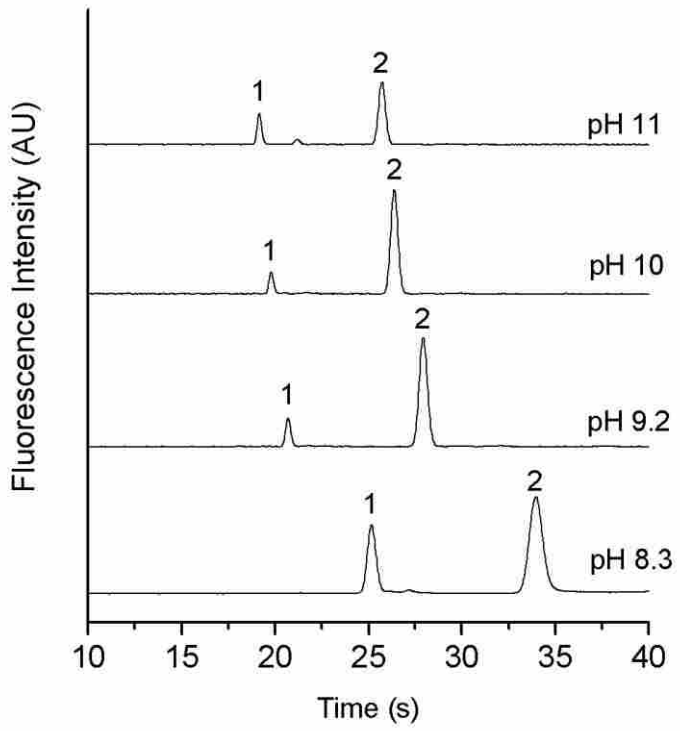

Figure 4.2. CE separations of fluorescein (peak 1) and FITC (peak 2) at different pH values using microchip B (Table 4.1). Injection voltage was 600 V and separation voltage was 2000 V.

Table 4.2. Efficiencies of fluorescein and FITC peaks in Figure 4.2.

		pH 8.3	pH 9.2	pH 10	pH 11
Fluorescein	Total plates*	1.4×10^4	2.5×10^4	2.6×10^4	2.6×10^4
	RSD*	8.3%	0.5%	0.8%	11%
FITC	Total plates*	1.1×10^4	1.7×10^4	1.9×10^4	1.9×10^4
	RSD*	7.3%	5.8%	4.8%	2.9%

*Data were calculated from three consecutive runs.

In addition, this microchip provided the highest efficiency. The theoretical plates measured for each peak in Figure 4.3 A are listed in Table 4.3. The efficiency of FITC-Asp was 4.2×10^4 plates for the 3.5 cm long microchannel.

Figure 4.3 B shows the separation of amino acids using microchip B, which was synthesized with 3% MMA. Compared with Figure 4.3 A, the migration times of the corresponding amino acids are similar, however, all peak widths are broader and the first 5 peaks are not well resolved. When impure PEGDA is used in the fabrication of microchips (microchip C in Table 4.1), not only are the efficiency and resolution lower, but also analytes migrate slower in the microchannel (Figure 4.3 C). The migration times and efficiencies of the sixth peak (FITC-Arg) for the three microchips are listed in Table 4.4. The migration times for microchips A and B are almost the same, however, the efficiency for microchip A is nearly 4 times that of microchip B. On the other hand, the efficiencies of microchips B and C are similar, but the migration times for microchip C are longer than microchip B. These results demonstrate that MMA mainly impacts separation efficiency, while PEGDA purity affects migration time. Both MMA and impurities in PEGDA change the polymer surface properties. Addition of a small amount of MMA in the polymer increases analyte adsorption on the surface and, therefore, decreases separation efficiency and resolution. Impurities present in the original PEGDA (such as carboxylic acids) greatly increase electroosmotic flow (EOF), which is in the opposite direction to electrophoresis migration and, therefore, reduces analyte migration speed in the channel.

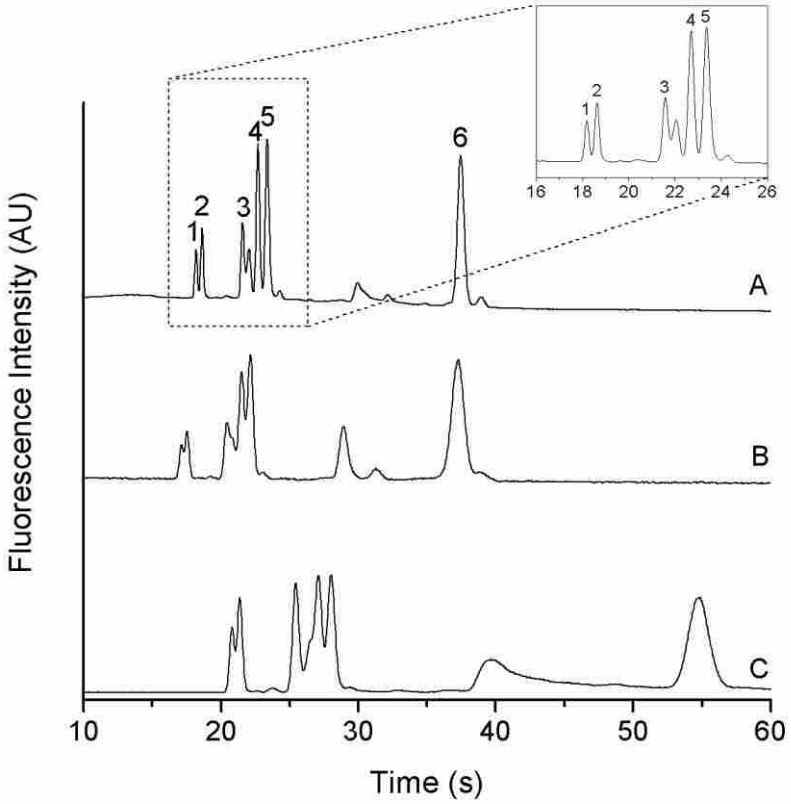

Figure 4.3. CE separations of 6 amino acids using three different microchips (Table 4.1). Injection voltage was 600 V and separation voltage was 2000 V. Peak identifications: (1) FITC-Asp, (2) FITC-Glu, (3) FITC-Gly, (4) FITC-Asn, (5) FITC-Phe, and (6) FITC-Arg.

Table 4.3. Efficiencies of amino acid peaks in Figure 4.3 A.

	1	2	3	4	5	6
Total plates*	4.2×10^4	4.1×10^4	3.5×10^4	3.4×10^4	3.3×10^4	2.4×10^4
RSD*	2.5%	4.2%	4.9%	11%	10%	6.2%

*Data were calculated from three consecutive runs.

Table 4.4. Migration times and efficiencies of peak 6 in Figure 4.3.

		Microchip		
		A	B	C
t_m (s)	Mean*	37.8	37.6	55.2
	RSD*	3.2%	0.8%	0.8%
Total plates	Mean*	2.4×10^4	6.3×10^3	5.8×10^3
	RSD*	6.2%	4.4%	0.8%

*Data were calculated from three consecutive runs.

4.3.4 CE Separation of Peptides and Proteins

Peptides were also used to evaluate the separation performance of these different microchips. Table 4.5 lists the migration times and efficiencies of 3 peptide peaks separated using the different microchips under the same separation conditions. Similar to the separation of amino acids, microchip A provided the best separation efficiency (see Figure 4.4). The analytes migrated in microchip B at similar rates to those in microchip A, however, the peak efficiencies were lower. For example, the efficiency of the first peak (FITC-Glu-Val-Phe) for microchip A was approximately 5 times that for microchip B. For microchip C, the peptide samples migrated slower than in the other two microchips. However, the peak efficiencies were similar to those measured for microchip B.

Electropherograms of FITC-β-lactoglobulin A separated using microchips A and B are illustrated in Figure 4.5. Migration times and theoretical plates for both peaks are listed in Table 4.6. Although this protein migrates at similar velocities, the efficiency obtained using microchip A is nearly 4 times that achieved using microchip B (i.e., 3.2×10^4 plates for a 3.5 cm long channel). When the performance of microchip C was evaluated for this protein, the peak was very broad and tailing, the signal was low and the baseline drifted. Figure 4.6 shows a separation of many *E. coli* proteins using microchip A.

Table 4.5. Migration times and efficiencies of 3 peptide peaks separated using three different microchips (Table 4.1) under the same conditions as described in Figure 4.4.

Peak No.		Microchip		
		A	B	C
1	t_m (s)	22.4	21.6	29.0
	Total plates	3.8×10^4	7.6×10^3	7.9×10^3
2	t_m (s)	24.8	24.6	34.4
	Total plates	3.3×10^4	7.6×10^3	7.4×10^3
3	t_m (s)	26.2	26.1	37.1
	Total plates	1.7×10^3	7.1×10^3	6.9×10^3

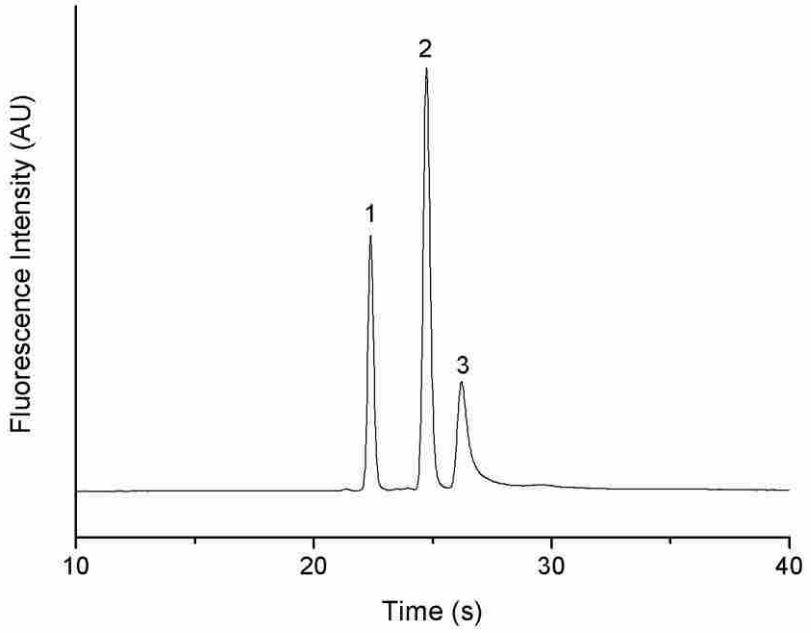

Figure 4.4. CE separation of 3 peptides using microchip A (Table 4.1). Injection voltage was 600 V and separation voltage was 2000 V. Peak identifications: (1) FITC-Glu-Val-Phe, (2) FITC-D-Leu-Gly, (3) FITC-Phe-Phe.

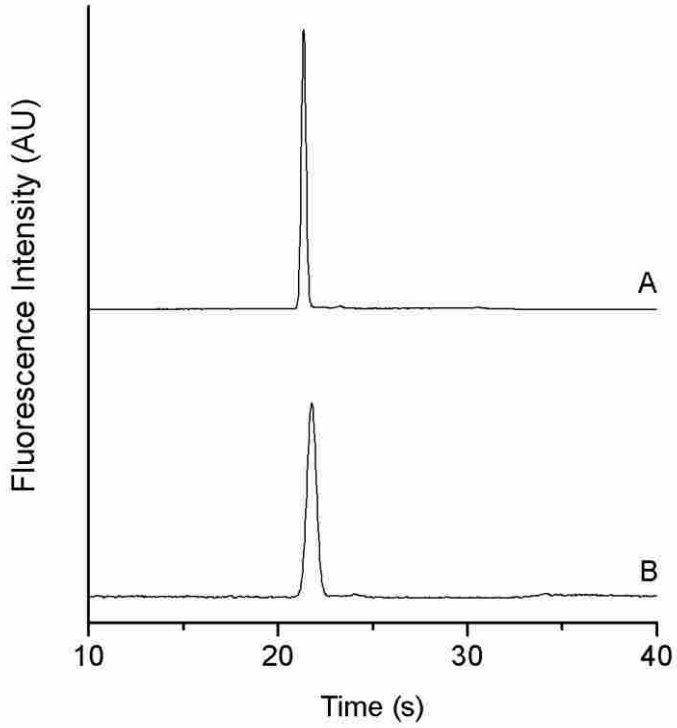

Figure 4.5. CE of FITC-β-lactoglobulin A using two different microchips (Table 4.1). Injection voltage was 600 V and separation voltage was 2000 V.

Table 4.6. Migration times and efficiencies of peaks in Figure 4.5.

Peak	Figure 4.5 A	Figure 4.5 B
t_m (s)	21.4	21.8
Total plates	3.2×10^4	8.3×10^3

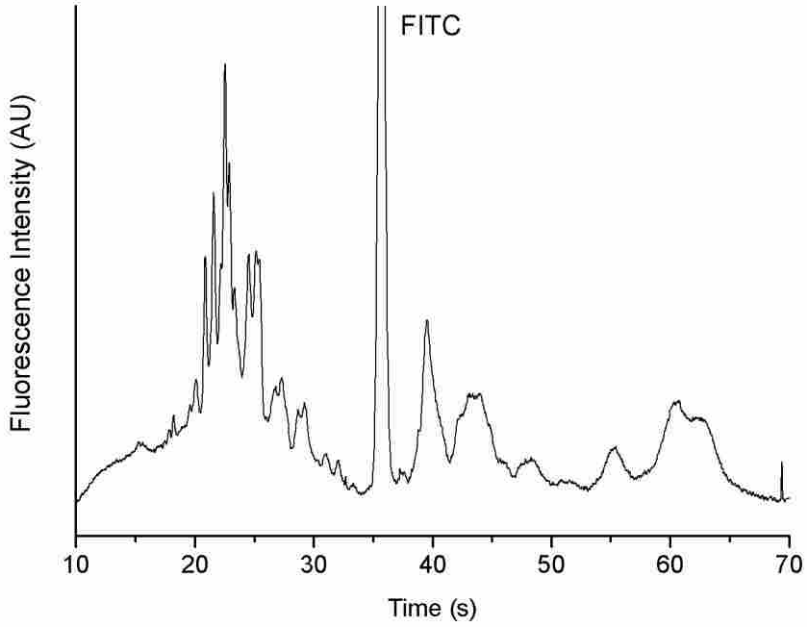

Figure 4.6. CE separation of FITC labeled *E. coli* proteins using microchip A (Table 4.1). Injection voltage was 600 V and separation voltage was 2000 V.

4.3.5 CE Chiral Separation of Amino Acids

During the past decade, microchip CE was studied for enantiomer separations by addition of a chiral selector in the operating buffer.[7-10] Cyclodextrins (CDs) are the most frequently used chiral selectors in CE.[11] CDs are cyclic oligosaccharides, which contain six (α-CD), seven (β-CD), or eight (γ-CD) glucopyranose units. CDs possess a hydrophilic surface with hydroxyl groups and a truncated cone with a hydrophobic cavity. Chiral recognition is based on inclusion of the bulky hydrophobic group of an analyte in the hydrophobic cavity of the CD.

In this study, β-CD was added as a chiral selector to the Tris-HCl buffer. First, I studied the influence of this additive on separation performance. Figure 4.7 shows CE elution of FITC-D-Asp using microchip A in 10 mM Tris-HCl (pH 8.3) buffer containing 1 mM β-CD (Figure 4.7 A) and buffer without β-CD (Figure 4.7 B). The migration times and efficiencies of the first peaks (FITC-D-Asp) are listed in Table 4.7. The addition of β-CD resulted in slow migration in the channel and broad peaks. When an analyte interacts with β-CD, the mobility of the analyte decreases because β-CD is a large neutral molecule. It was reported that γ-CD is a better selector because the cavity diameter of γ-CD is suitable for FITC-tagged amino acids.[7] The β-CD cavity is so small that the interaction between the analyte and β-CD is weak. Therefore, the whole β-CD-analyte complex is not sufficiently stable, which definitely leads to broad peaks and low separation efficiency. CE elution performed in buffer without β-CD gave 6 times higher efficiency.

I evaluated the chiral separation performance of 10 different D,L-amino acids.

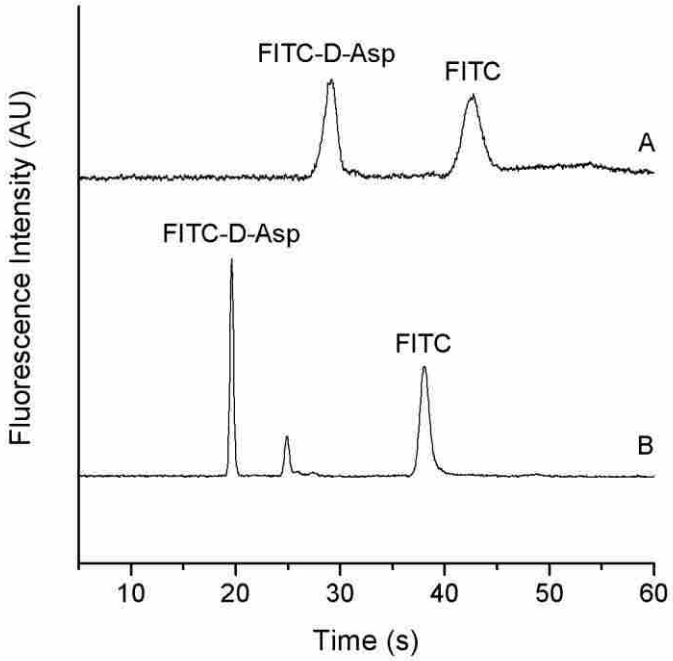

Figure 4.7. CE elution of FITC-D-Asp using microchip A (Table 4.1). (A) 10 mM Tris buffer (pH 8.3) containing 1 mM β-CD and (B) 10 mM Tris buffer (pH 8.3). Injection voltage was 600 V and separation voltage was 2000 V.

Table 4.7. Migration times and efficiencies of D-Asp peaks in Figure 4.7.

Peak	Figure 4.7 A	Figure 4.7 B
t_m (s)	29.21	19.66
Total plates	2.3×10^3	1.4×10^4

Figure 4.8 shows CE separations of FITC-labeled D,L-Asn (Figure 4.8 A) and Leu (Figure 4.8 B). The separation selectivities (α) for Asn and Leu enantiomers were 1.08 and 1.16, respectively, where α is defined as the ratio of electrophoretic mobilities (μ). When EOF is negligible (such as in PEG-functionalized microchips), α approximately equals the ratio of migration times. The resolution values for Asn and Leu enantiomer peaks were 1.13 and 1.64, respectively. Because the composition ratio of the enantiomeric mixture was 1:1, both peaks have approximately equal peak areas. The selectivities and resolution values of the other amino acids are listed in Table 4.8. Except for proline, all other amino acids had selectivities larger than 1.06, however, most resolution values were low due to low peak efficiencies. FITC labeled proline enantiomers were not separated using our system. The large steric hindrance after FITC labeling inhibited the interaction between the β-CD and analyte to form a stable host-guest complex. When the R groups of amino acids contain a benzene ring, such as phenylalanine and tryptophan, the resolution of enantiomers is too low to be precisely measured.

In this work, I aimed only to demonstrate the feasibility of chiral separation of FITC-tagged amino acids using the PEG-functionalized microchips. The separations were not optimized. γ-CD and other CD derivatives may provide better chiral separation performance as a result of higher selectivity, resolution and efficiency. In addition, chiral separation depends on other conditions, such as concentration of CD, type and concentration of operating buffer, addition of surfactant in the buffer solution, pH, applied voltage, and operating temperature.

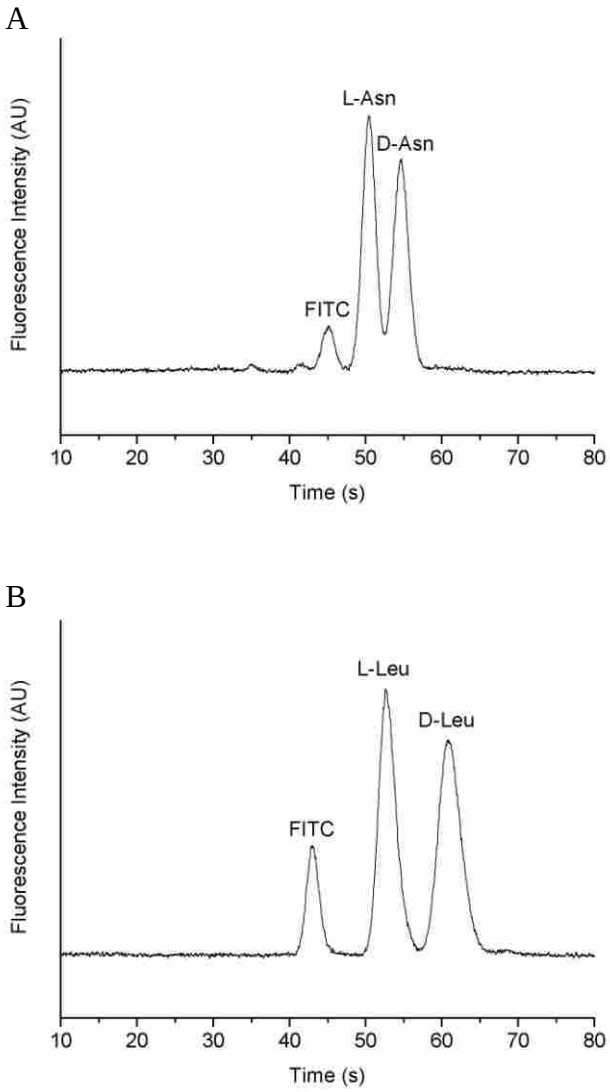

Figure 4.8. CE chiral separations of (A) D,L-Asn and (B) D,L-Leu using microchip A (Table 4.1) in 10 mM Tris buffer (pH 8.3) containing 1 mM β-CD. Injection voltage was 600 V and separation voltage was 2000 V.

Table 4.8. Selectivity (α) and resolution (R_s) for chiral separation of D,L-amino acids using PEG-functionalized microchips with addition of 1 mM β-CD in 10 mM Tris buffer (pH 8.3).

	α		R_S	
	Mean	RSD	Mean	RSD
D,L – Asp	1.11	0.4%	1.05	6.5%
D,L – Glu	1.11	0.2%	0.89	5.4%
D,L – Asn	1.08	0.2%	1.13	3.4%
D,L – Gln	1.10	0.2%	0.87	3.1%
D,L – Leu	1.16	0.3%	1.64	0.8%
D,L – His	1.07	0.1%	0.77	5.0%
D,L – Ser	1.06	0.3%	0.89	4.2%
D,L – Phe	1.06	0.4%	--	--
D,L – Trp	1.06	0.7%	--	--
D,L – Pro	1.00	--	--	--

4.4 Conclusions

A PEG-functionalized microchip was fabricated to separate small molecules (fluorescent dyes and amino acids), peptides and proteins without surface modification. I studied the influence of monomer type and purity on CE separation performance. Impurities in the PEGDA monomer induced undesirable EOF, which increased analyte migration time. Addition of a small amount of MMA increased the analyte adsorption on the surface, which decreased separation efficiency. Chiral separations of FITC-labeled amino acids were demonstrated by adding β-CD to the running buffer as a chiral selector. Chiral selectivity and enantiomer resolution were reported. Although most enantiomers studied were separated, the conditions could be optimized to improve the separation performance, such as using γ-CD or other CD derivatives as chiral selectors, optimizing the concentrations of chiral selector and buffer solution, and utilizing other additives.

4.5 References

1. Kim, P.; Jeong, H. E.; Khademhosseini, A.; Suh, K. Y. *Lab Chip* **2006**, *6*, 1432-1437.
2. Liu, J.; Sun, X.; Lee, M. L. *Anal. Chem.* **2007**, *79*, 1926-1931.
3. Sun, X.; Liu, J.; Lee, M. L. *Electrophoresis* **2008**, *29*, 2760-2767.
4. Sun, X.; Farnsworth, P. B.; Woolley, A. T.; Tolley, H. D.; Warnick, K. F.; Lee, M. L. *Anal. Chem.* **2008**, *80*, 451-460.
5. Lavis, L. D.; Rutkoski, T. J.; Raines, R. T. *Anal. Chem.* **2007**, *79*, 6775-6782.

6. Rodriguez, I.; Jin, L. J.; Li, S. F. Y. *Electrophoresis* **2000**, *21*, 211-219.

7. Hutt, L. D.; Glavin, D. P.; Bada, J. L.; Mathies, R. A. *Anal. Chem.* **1999**, *71*, 4000-4006.

8. Ludwig, M.; Belder, D. *Electrophoresis* **2003**, *24*, 2481-2486.

9. Gao, Y.; Luo, Y.; Qin, j.; Lin, B. *Electrophoresis* **2008**, *29*, 1918-1923.

10. Belder, D.; Ludwig, M. *Electrophoresis* **2003**, *24*, 2422-2430.

11. Scriba, G. K. E. *J. Sep. Sci.* **2008**, *31*, 1991-2011.

5 POLY(ETHYLENE GLYCOL)-FUNCTIONALIZED DEVICES FOR ELECTRIC FIELD GRADIENT FOCUSING [*]

5.1 Introduction

Electric field gradient focusing (EFGF), a member of the family of equilibrium gradient focusing techniques,[1] depends on an electric field gradient and a counter-flow to focus, concentrate and separate charged analytes, such as peptides and proteins.[2-6] The constant counter flow is opposite to the electrophoretic force that drives the analytes. When the electrophoretic velocity of a particular analyte is equal and opposite to the velocity of the counter flow, the analyte is focused in a narrow band because at this position its net force is zero. This technique avoids protein precipitation that often occurs in IEF when proteins reach their isoelectric points. A major challenge in EFGF is establishment of the desired electric field gradient. Currently, several methods have been reported to create an electric field gradient, including the use of a conductive changing cross-sectional area around a separation channel,[2,7-10] a buffer conductivity gradient in a column,[11-14] electrodes along a channel for digital field gradient focusing,[15-17] and a temperature gradient along a column filled with a buffer that has a temperature-dependent conductivity.[18-23]

Humble et al.[8] prepared capillary-based planar devices for analytical scale EFGF based on the changing cross-sectional area design. The separation channel was created using a small diameter wire as template to form a channel surrounded by an ionically conductive acrylic copolymer that freely allowed passage of small ions but

[*] This chapter is reproduced with permission from *Anal. Chem.* **2008**, *80*, 451-460. Copyright 2008 American Chemical Society.

restricted migration of biomacromolecules into the gel. This nanoporous copolymer was shaped to form a linear electric field gradient by changing the cross-sectional area. Although the fabrication of these devices was easy and reproducible, limitations included low peak capacity and low resolution, primarily due to flow dispersion in the open channel, which was due to (a) the parabolic laminar counterflow profile, (b) variable ζ potential along the channel in the changing electric field, and (c) protein adsorption on the channel wall. Furthermore, the hydrogel could not be chemically bonded to the PMMA substrate surface.

Recently, Kelly et al.[9] miniaturized this capillary-based EFGF device into a PMMA microchip format, in which a microchannel was imprinted on the bottom plate and a shaped cavity of changing cross-sectional area was cut into the top plate. The same ionically conductive copolymer was polymerized in the shaped cavity using phase-changing sacrificial layers to protect the microchannel. Liu et al.[10] used a different approach to fabricate a micro electric field gradient focusing (μEFGF) device out of poly(glycidyl methacrylate-co-methyl methacrylate). A weir structure was fabricated between the separation channel and changing cross-section electric field gradient generating channel. A buffer ion-permeable membrane made from a poly(ethylene glycol) (PEG)-functionalized copolymer was positioned on the weir to separate the two microchannels.

In this work, I fabricated changing cross-sectional EFGF devices using PEG-functionalized polymers. These materials were used to resist protein adsorption and suppress electroosmotic flow. Another considerable advantage of this approach

was the ability to covalently bond the hydrogel to the substrate without prior surface modification. I also incorporated a PEG-functionalized monolith in the EFGF channel to reduce analyte band dispersion.

5.2 Experimental Section

5.2.1 Materials and Sample Preparation

Methyl methacrylate (MMA, 99%), 2-hydroxyethyl methacylate (HEMA, 99%+), poly(ethylene glycol) methyl ether methacrylate (PEGMEMA 1100, MW~1100), poly(ethylene glycol) diacrylate (PEGDA 258, MW ~258), 3-(trimethoxysilyl)propyl methacrylate (98%), 2,2'-dimethoxy-2-phenylacetophenone (DMPA), and poly(vinyl alcohol) (PVA, 99%+ hydrolyzed, MW ~89,000 – 98,000) were purchased from Aldrich (Milwaukee, WI). Ethoxylated trimethylolpropane triacrylate (SR 9035) was obtained from Sartomer (Warrington, PA). Anhydrous methyl alcohol (MeOH) and hydrochloric acid (HCl, 37%) were purchased from Mallinckrodt Chemicals (Phillipsburg, NJ). Anhydrous ethyl ether was purchased from Fisher Scientific (Fair Lawn, NJ). Sodium hydroxide (NaOH) was purchased from Columbus Chemical Industries (Columbus, WI). Fluorescein isothiocyanate (FITC), tris(hydroxymethyl)-aminomethane (Trizma, Tris), β-lactoglobulin A, and myoglobin were ordered from Sigma (St. Louis, MO). R-phycoerythrin (R-PE) was obtained from Polysciences (Warrington, PA). Recombinant, enhanced green fluorescent protein was purchased from Clontech (Palo Alto, CA). All chemicals were used as received without further purification.

Deionized water (18.2 MΩ·cm) was prepared using a Milli-Q UF Plus water purification system (Millipore, Billerica, MA). Tris-HCl buffers (50 mM and 100 mM, pH 8.5) were filtered using 0.2-μm syringe filters (Pall, East Hills, NY) before experiments. Precleaned microscope slides with dimensions of 70 × 50 × 1 mm^3 and 70 × 25 × 1 mm^3 were obtained from Fisher Scientific (Pittsburgh, PA) and Hardy Diagnostics (Santa Maria, CA), respectively.

To label β-lactoglobulin A and myoglobin, the protein samples were dissolved in filtered 10 mM sodium bicarbonate buffer (pH 9.2) with a concentration of 1 mg/mL. FITC was dissolved in absolute dimethyl sulfoxide (DMSO) to make a 6 mM solution. Then the protein solutions (600 μL) were thoroughly mixed with 40 μL FITC solution and placed in the dark for at least 2 days at room temperature.[24] All protein samples were diluted with 10 mM Tris (pH 8.5) before use.

5.2.2 Capillary Treatment

Polyimide coated fused silica capillary tubing with 150-μm i.d. and 365-μm o.d. was supplied by Polymicro Technologies (Phoenix, AZ). To resist protein adsorption on the capillary wall and suppress electroosmotic flow, PVA was used to coat the inner wall surface using an established protocol.[25] Briefly, a PVA aqueous solution (6.5%, w/w) in a vial was pushed through the capillary using pressurized nitrogen gas for 3 h, after which the vial was removed and the PVA solution still inside the capillary was slowly pushed out under pressure. The capillary was then placed in an HP 5890 gas chromatograph oven and heated to 145 ^oC for 5 h while being purged with nitrogen gas. Then the above procedure was repeated from the

other capillary end. After this treatment, PVA became insoluble in water and formed a smooth coating on the capillary inner surface.

After PVA coating, the polyimide coating outside the capillary near the ends was removed carefully using a micro-torch or razor blade. The length of the uncoated capillary ends was 1 cm, and the distance between the two was approximately 16 cm. The two ends of the capillary were sealed with a rubber septum, and the coiled capillary was immersed sequentially into acetone, water, 0.2 M NaOH, water, 0.2 M HCl, water and acetone for 30 min each to clean and activate the uncoated ends. After being dried in an oven at 120 ^{o}C for 1 h, the capillary was placed in a 30% 3-(trimethoxysilyl)propyl methacrylate/acetone solution and put in the dark for 24 h.[26] Thus, double bonds were introduced on the uncoated sections so that the hydrogel could be covalently bonded to the outside surface of the capillary. After reaction, the capillary was washed with acetone and dried using a stream of nitrogen. Finally, the treated capillary was cut at the middle of the uncoated and coated parts to make 8 cm long capillaries, each with one 5 mm end that was covered with bonded acrylic groups.

5.2.3 Fabrication of EFGF Devices

Based on the changing cross-sectional area design,[8] new EFGF devices were fabricated with PEG-functionalized materials using a casting method.[27] The fabrication procedure is outlined in Figure 5.1. In step A1, a glass form was assembled from two glass slides and two PDMS spacers. Two small PDMS sheets of the same height as the PDMS spacers, which would become the reservoir molds, were

placed at their proper positions and also sandwiched in the form. Then the PEG-functionalized monomer solution for device synthesis, with the formulation shown in Table 5.1, was introduced into the form. The assembly was then placed 60 cm below a UV lamp (8 mW/cm^2) to initiate polymerization. After UV exposure of 16 s, the assembly was cooled to room temperature immediately. The glass slides were carefully removed using a razor blade yielding a cover plate with two reservoirs (Figure 5.1 B1). Because the reaction time was short, the cover plate was only semi-cured and a thin film of unreacted monomer solution remained on the plate surface. To fabricate the bottom plate with shaped channel, a glass form was built as shown in Figure 5.1 A2, which contained a PDMS mold with changing cross-sectional area in the center of the form. However, the thickness of the spacers was larger than the shaped mold, which resulted in a space between the top glass slide and the shaped mold. After introducing the monomer solution into the form, the assembly was exposed to UV light for 16 s to partially polymerize the solution. A diagram of the semi-cured bottom plate with shaped channel is shown in Figure 5.1 B2. Following this synthesis, two PVA coated capillaries threaded together with a Nichrome wire (120-μm i.d.) were placed on the bottom plate at the ends of the shaped channel. The wire was pulled taut, and the two capillaries were centered at the ends of the shaped channel with the treated ends positioned in contact with the plastic device (Figure 5.1 A3). The semi-cured cover plate was then placed on top of the shaped plate (Figure 5.1 B3). Any bubbles generated between the two plates were removed with silicon wafer-handling tweezers. Then the temporarily bonded device was placed 15 cm

below a UV lamp (50 mW/cm^2) and exposed to UV radiation for 5 s. During exposure, the methacryl and acryl residues on the contacting plate surfaces formed covalent bonds, which permanently linked them together (Figure 5.1 A4). Because the reaction was very fast, a stress force usually developed in the bonded copolymer substrate, which made it deform slightly. To avoid this, the device was sandwiched between two glass slides immediately after UV exposure and placed under a weight (2.4 kg) for 8 min.

After removing the weight from the top, a hydrogel solution containing 85 wt % SR 9035, 15 wt % 100 mM Tris-HCl buffer (pH 8.5) and DMPA (0.5 wt % of SR 9035) was carefully introduced into the shaped channel from one reservoir. Care was taken to avoid bubble generation and to leave the reservoirs empty. Then the device was exposed to UV light for 1 min to polymerize the PEG-functionalized hydrogel. After reaction, the wire was withdrawn from the device to form a separation channel that was surrounded by hydrogel (Figure 5.1 B4). The capillaries were attached to the separation channel and covalently bonded with hydrogel. The channel between the two capillaries was 4 cm long.

If no monolith was incorporated in the channel, the device was flushed with 50 mM Tris-HCl buffer (pH 8.5) until focusing experiments were performed. The two reservoirs were filled with buffer and sealed with flat pieces of PDMS to avoid drying of the hydrogel.

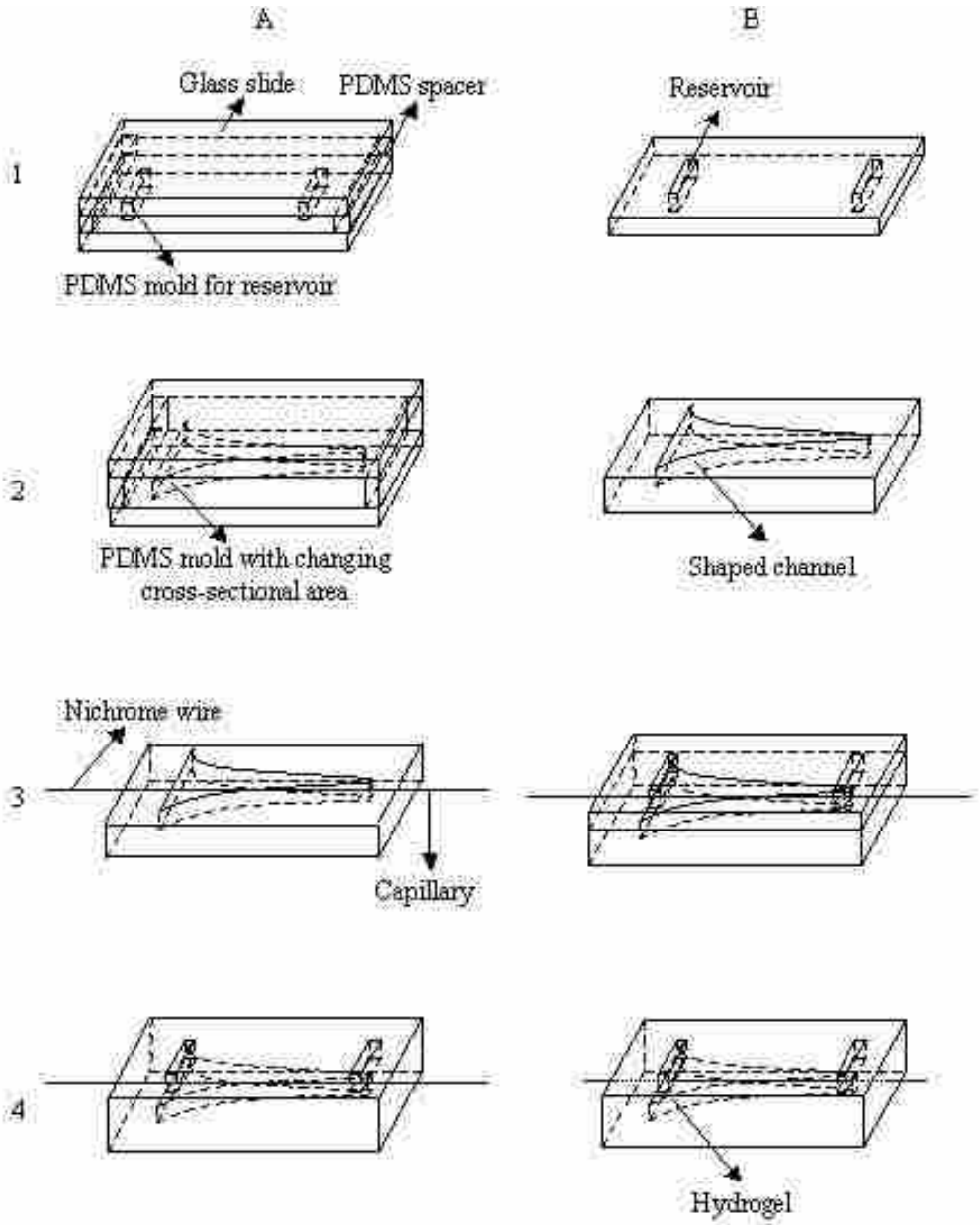

Figure 5.1. Fabrication of the PEG-functionalized EFGF device. A1: glass-PDMS form for fabrication of top plate; B2: pre-polymerized top plate with two reservoirs; A2: glass-PDMS form for fabrication of bottom plate; B2: pre-polymerized bottom plate with shaped-channel; A3: assembly of wire-capillary on top of the bottom plate; B3: assembly of the top plate with the bottom plate; A4: bonding the two plates; B4: incorporation of hydrogel in the shaped-channel and formation of EFGF channel by withdrawing the wire.

5.2.4 Synthesis of a Monolith in the EFGF Channel

A monomer mixture with formulation given in Table 5.1 was prepared by introducing the photoinitiator, monomer, crosslinker and porogens into a glass vial, shaking by hand to dissolve the initiator and ultrasonicating for 10 s. Because the ethyl ether porogen is easy to evaporate, the ultrasonication time was short and the mixture was prepared before each use. After the EFGF channel was formed, fresh monolith solution was introduced into the channel using a syringe. After the solution filled the channel and no bubbles were seen under a microscope, the device was placed for 8 min perpendicular to a UV dichroic mirror (Navitar, Newport Beach, CA), which was positioned at 45^{o} directly under the UV curing lamp. The device was then connected to an HPLC micro pump (Eksigent, Dublin, CA) and flushed with methanol for 5 h at 0.4 μL/min to remove unreacted monomers and porogens, followed by flushing with 50 mM Tris buffer (pH 8.5) until focusing experiments were performed.

5.2.5 Scanning Electron Microscopy (SEM) and Pore Size Measurement

The morphologies of the EFGF channels and monoliths were studied using SEM. Samples were prepared using a CO_2 laser (Universal Laser Systems, Scottsdale, AZ). To avoid melting and deforming the channel and monolith, the device was cut by the laser from both sides up to the channel, followed by breaking the channel by hand to make samples that were 5×5 mm^2 in size. SEM images were taken using an FEI Philips XL30 ESEM FEG (Hillsboro, OR).

The pore size distribution of the monolith was investigated using a PMI

Table 5.1. Ingredients of the PEG-functionalized EFGF substrate, hydrogel and monolith.

Substrate	PEGDA 258 (85 wt %)	PEGMEMA 1100 (12 wt %)	MMA (3 wt %)	DMPA [a] (0.1 wt %)	--
Hydrogel	SR9035 (85 wt %)	100 mM Tris, pH 8.5 (15 wt %)	DMPA [a] (0.5 wt %)	--	--
Monolith	PEGDA 258 (22.5 wt %)	HEMA (7.5 wt %)	Methanol (25 wt %)	Ethyl ether (45 wt %)	DMPA [a] (1 wt %)

[a] The content of photoinitiator, DMPA, is given as a weight percentage of the total amount of monomers.

capillary flow porometer (Porous Materials, Ithaca, NY). In order for the sample to fit in the porometer sample chamber, it was prepared in a UV transparent capillary (75-μm i.d., 360-μm o.d., Polymicro Technologies, Phoenix, AZ) after the inner surface was modified with 3-(trimethoxysilyl)propyl methacrylate to immobilize double bonds for covalently bonding the monolith to the inner wall.[26] The polymerization conditions were the same as in the EFGF channel. After reaction, the monolith was washed with methanol for 4 h at 1 μL/min. Then a wetting liquid, Galwick, with a surface tension of 15.9 dynes/cm was introduced to fill the monolith void volume. The sample was placed in the chamber and nitrogen pressure was used to remove the liquid from the monolith pores. The maximum test pressure was 200 psi.

5.2.6 Operation of the EFGF Devices

Figure 5.2 shows a schematic of the EFGF setup. The buffer used in the focusing and separation experiments was 50 mM Tris-HCl (pH 8.5), and the test protein samples were either fluorescently labeled or natively fluorescent when excited at 488 nm. The sample was introduced into the EFGF separation channel using an electrokinetic injection method.[8] At the beginning of an analysis, the cathode was placed in a buffer reservoir. During injection, this buffer reservoir was replaced with a reservoir containing the sample, followed by applying 800 V for 5-30 s. After injection, the sample reservoir was replaced with the buffer reservoir and voltage was applied to electrophoretic migration of the analytes. Once the sample was observed entering the separation channel, the syringe pump was activated to create a

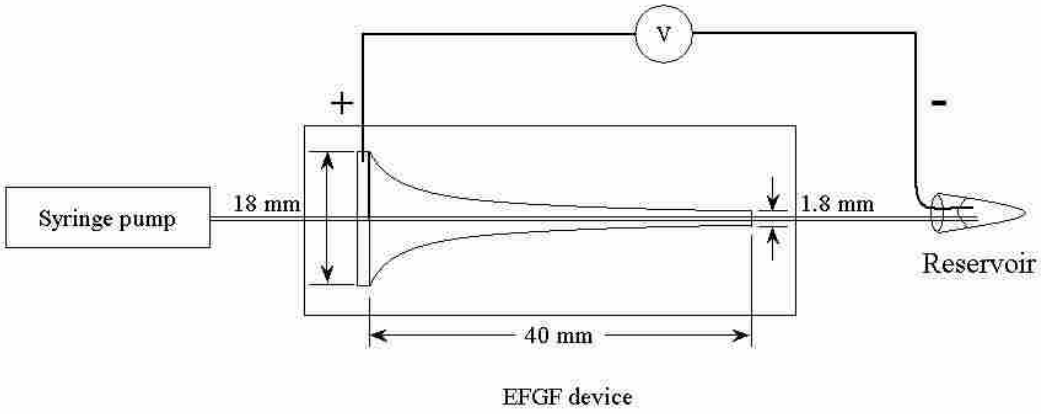

Figure 5.2. Operational set-up of the EFGF device.

hydrodynamic counter flow.

When the proper counter flow and voltage were applied to the device, proteins could be focused in the separation channel. Changing the counter flow rate or the applied voltage caused the sample bands to move to new equilibrium positions.

5.2.7 Detection System

The microscope system used for detection and imaging was described elsewhere.[10] In brief, the 488 nm line generated from an Ar ion laser source (Melles Griot, Carlsbad, CA) was introduced into a TE 2000-U inverted microscope (Nikon, Tokyo, Japan) through an optical path, which consisted of different optical parts for imaging or detection. The imaging fluorescence passed through a Z488LP long-pass filter set (Chroma) and was recorded with a digital camera (Nikon). To carry out point detection, a beam expander (Special Optics, Wharton, NJ) was used to expand the laser beam, which was finally focused into a beam spot. Laser-induced fluorescence was detected using a photomultiplier tube (Bridgewater, NJ) after passing through the long-pass filter. The signals were amplified and recorded using LabView (National Instruments, Austin, TX) software. To scan the separation channel, a servomotor was installed to drive the microscope stage, and the movement was controlled by a home-built microstepping controller.

5.3 Results and Discussion

5.3.1 EFGF Device Fabrication

Among the previously reported EFGF devices, the capillary-based device with

changing cross-sectional area has several advantages, such as ease of fabrication and operation, and good reproducibility.[8] In this work, I still used the wire template casting method to form the separation channel, and the shaped channel design to produce a linear electric field gradient. However, different materials were used to fabricate the EFGF device, including the hydrogel. In addition, devices with reservoirs and shaped channel were prepared using the casting method (shown in Figure 5.1).

The body of the device was made from a PEG-functionalized copolymer. PEG and its derivatives are now widely used as biomaterials because of their hydrophilicity, biocompatibility, low toxicity and resistance to protein adsorption. The formulation of the body of the device is listed in Table 5.1 and the structures of the monomers used in the synthesis are shown in Figure 5.3. The main monomers were PEG-functionalized acrylate or methacrylate. PEGDA was the crosslinker and PEGMEMA enhanced the resistance to protein adsorption. A small amount of MMA was used to increase the mechanical strength. This copolymer was successfully applied in the fabrication of microchips, which were used for micro capillary electrophoresis separations of peptides and proteins without further surface modification due to their natural resistance to protein adsorption.[27]

Photopolymerization of the copolymer was very fast, usually requiring only approximately 16 s to prepare the semicured copolymer, which was soft, but solidified. A thin liquid film remained on the surface, which contained unreacted monomers that allowed the top and bottom plates to covalently bond together when exposed to UV

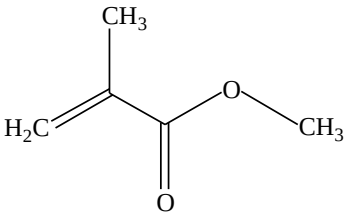

MMA

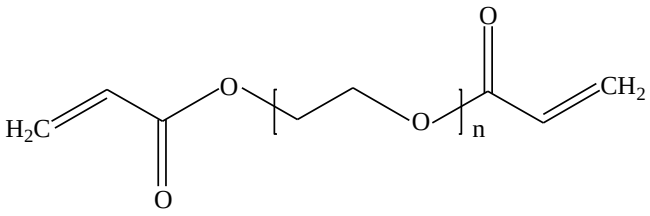

PEGDA

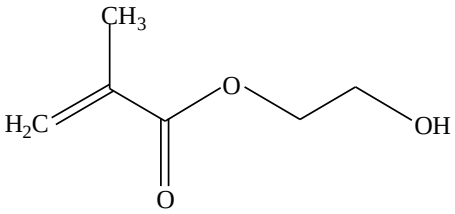

HEMA

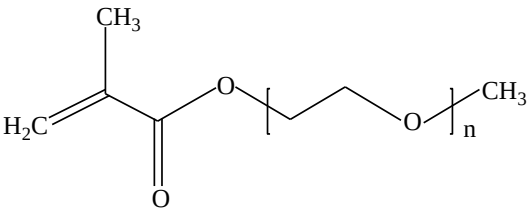

PEGMEMA

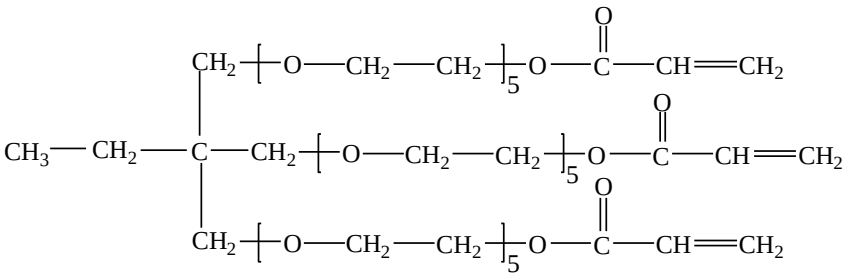

SR 9035

Figure 5.3. Monomers used in the syntheses of PEG-functionalized devices, hydrogels and monoliths.

radiation. After bonding, the copolymer was hard, and possessed a variety of attractive characteristics, including transparency to UV light above 300 nm and resistance to various organic solvents.[27] An advantage of the fabrication method is that various channel shapes can be made to generate different electric field gradients.

A major fabrication challenge was how to make an ideal conductive membrane, which was permeable to small buffer ions, but able to retain large biomolecules. Simultaneously, the membrane should be resistant to protein adsorption and have no electroosmotic flow (EOF). In a previous device, a considerable amount of MMA (23 wt %) was used for synthesis of the conductive membrane to increase its strength and bond it well to the PMMA substrate.[8] However, the use of MMA affects the channel surface characteristics, making it possible to adsorb proteins and induce unwanted EOF, which disturbs the operation. In this work, I utilized only one monomer (SR 9035) to prepare the conductive hydrogel. The ingredients listed in Table 5.1 are fewer compared with those used to synthesize the acrylic copolymer.[8] The molecular structure of SR 9035 is shown in Figure 5.3, which indicates that it has three acrylic groups and a total of 15 ethylene glycol (EG) units. As a result, the polymerized hydrogel is highly crosslinked, hydrophilic, and resistant to protein adsorption. During the focusing experiments, no protein adsorption on the channel surface was observed even when the protein was retained in the channel for more than 8 h. Tris buffer (100 mM, pH 8.5) was added to render the hydrogel conductive. Its conductivity was measured using a method reported elsewhere.[10] Briefly, the hydrogel monomer solution was introduced into a channel with dimensions of 45 (length) × 5

(width) × 1.5 (thickness) mm^3, which was prepared from the PEG-functionalized copolymer using the method described above, and then photopolymerized in situ. A 50 mM Tris buffer (pH 8.5) was added to the reservoirs at both ends of the channel. A voltage of 1000 V was applied along the channel via two electrodes in contact with the electrolyte solution. The current was recorded using LabView software. The conductivity of the hydrogel was calculated using the equation

$$C = LI/AV \tag{5.1}$$

where C is the conductivity, I is the current, V is the applied voltage, L is the channel length, and A is the cross-sectional area of the channel. The hydrogel conductivity was 2.1×10^{-4} S/m. Because the buffer was more dilute than the buffer in the hydrogel, the current initially decreased with time. When equilibrium was reached, the conductivity was approximately 5.3×10^{-5} S/m, which was close to the hydrogel conductivity made from 50 mM Tris buffer (4.1×10^{-5} S/m).

Similar to the bonding of the microfluidic device pieces, the hydrogel was also covalently bonded to the surface of the cavity. Detachment of hydrogel from the device was never observed during operation. The hydrogel slab assumed the same shape as the shaped channel with changing cross-sectional area normal to the separation channel. The hydrogel was 1.5 mm thick, 18 mm wide at the low field end, and 1.8 mm wide at the high field end. The separation channel was centered in the hydrogel from high field side to low field side. Figure 5.4 shows an SEM image of the open EFGF channel. Its diameter was approximately 120 μm, which is consistent with the diameter of the Ni wire. The inner surface of the channel appeared smooth. These

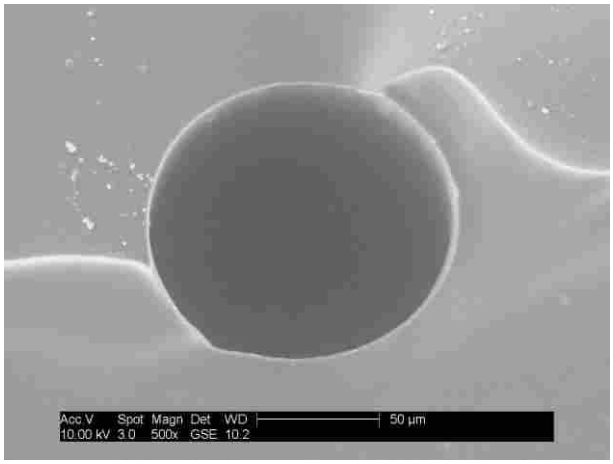

Figure 5.4. SEM image of the EFGF open channel.

observations indicated that no damage occurred to the inner surface of the separation channel when withdrawing the wire out of the hydrogel. Due to treatment of the outside capillary surface, the hydrogel also covalently bonded with the capillary. No gaps or fluid leaks at this location were observed during operation.

5.3.2 Protein Focusing in the Open EFGF Channel

The concentration of all protein samples was 10 μg/mL. I used electrokinetic injection to introduce the sample into the EFGF channel. Before focusing, a broad band was observed entering the channel. When the counter flow was applied to balance the electrophoretic force, the broad band moved to its equilibrium point and gradually became narrow. Panels A and B in Figure 5.5 show focused R-PE and GFP bands, respectively, in the open EFGF channel.

In the experiments, I found that the focused band position and bandwidth changed when altering the applied counter flow rate or voltage. Usually, it required approximately 30 min to reach equilibrium after changing the focusing conditions. Figure 5.6 A shows focused R-PE peaks for different counter flow rates and constant voltage (500 V), which were recorded by scanning along the open separation channel. With an increase in counter flow rate, the focused band moved toward the high electric field end, and the band broadened significantly. Table 5.2 lists the peak widths at half height for different conditions. When the counter flow rate increased 5-fold, from 6 nL/min (0.53 mm/min linear velocity) to 30 nL/min (2.65 mm/min), the peak width at half height changed more than 10-fold, from 0.53 mm to 5.99 mm. It is evident that the bulk flow had significant impact on the focused bandwidth. Peaks for

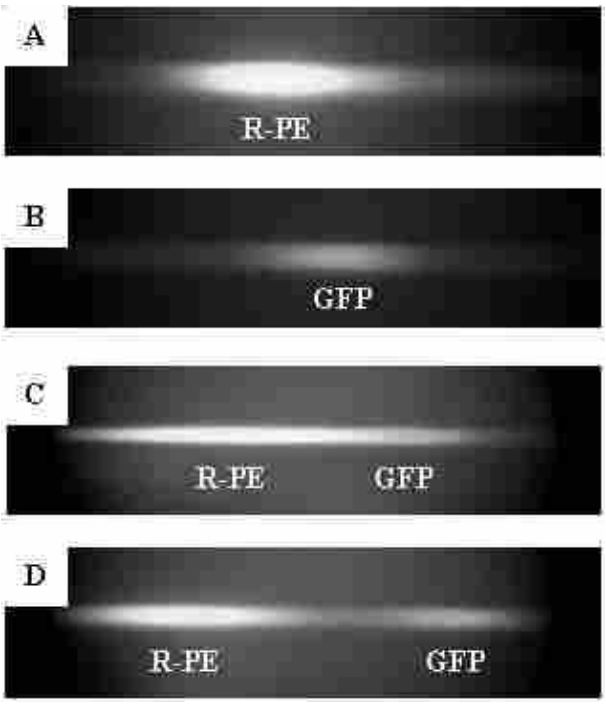

Figure 5.5. Fluorescence images of focused proteins in an EFGF open channel. (A) R-PE focused at 500 V and 20 nL/min; (B) GFP focused at 500 V and 10 nL/min; (C) and (D) R-PE and GFP focused at 500 V, 5 nL/min and 8 nL/min, respectively.

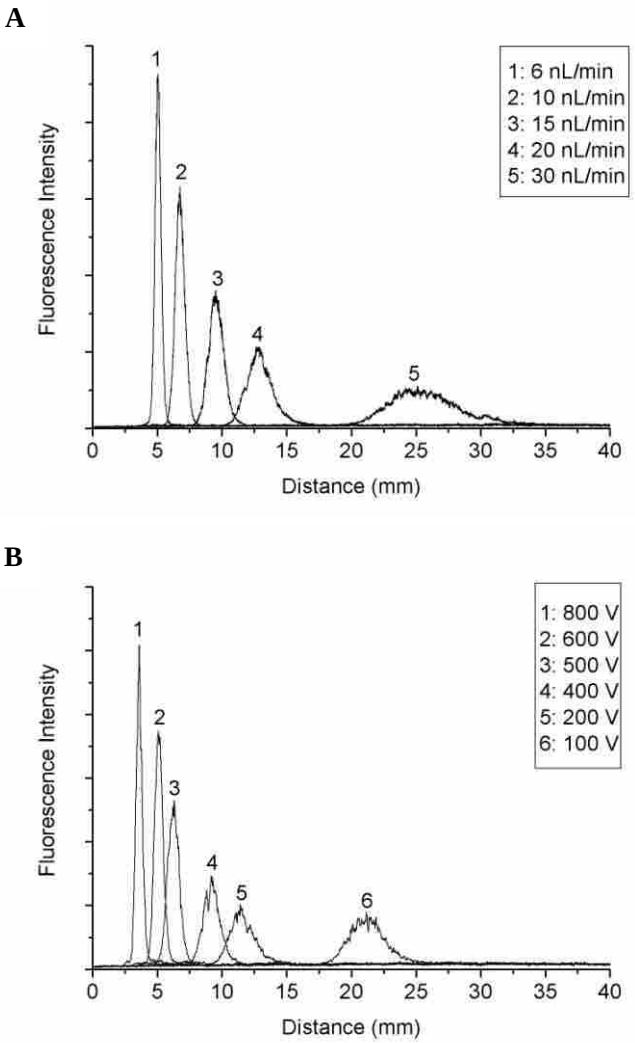

Figure 5.6. Focusing of R-PE in an EFGF open channel for (A) different counter flow rates and constant applied voltage of 500 V, and (B) different applied voltages and constant counter flow rate of 10 nL/min.

Table 5.2. Peak width (mm) at half height of peaks in Figures 5.6 and 5.8.

Figure No.	Peak number					
	1	2	3	4	5	6
5.6 A	0.53	0.82	1.32	1.96	5.99	--
5.6 B	0.53	0.75	1.05	1.42	2.27	3.09
5.8 A	0.28	0.45	0.68	0.80	1.08	--
5.8 B	0.31	0.39	0.54	0.70	0.82	--

R-PE focused at different voltages and constant counter flow rate (10 nL/min) are shown in Figure 5.6 B. With an increase in applied voltage, the focused band moved toward the low electric field region, and the band became narrower (Table 5.2). When the voltage increased from 100 V to 800 V, the peak width at half height decreased from 3.09 mm to 0.53 mm.

These results are consistent with the EFGF theory developed by Tolley et al.[4] When an analyte is in its focused equilibrium state, the standard deviation (σ) of the bandwidth can be described by the equation

$$\sigma = \sqrt{D_T / \mu q(x_0)} \tag{5.2}$$

where μ is the analyte electrophoretic mobility, $q(x_o)$ is the electric field gradient at point x_o, and D_T is the dispersion coefficient that represents the sum of the molecular diffusion (D_M) and dispersion induced by the counter laminar flow (D_u) in the channel

$$D_T = D_M + D_u \tag{5.3}$$

In my device, the PEG-functionalized hydrogel was assumed to have negligible protein adsorption. With this assumption, the dispersion coefficient in the open channel can be represented by

$$D_T = D_M + \frac{u^2 d^2}{192 D_M} \tag{5.4}$$

where u is the laminar flow rate and d is the diameter of the separation channel. The electric field gradient at any point, $q(x_o)$, was assumed to be invariable when a constant voltage was applied since our device was designed to provide a linear electric field gradient. Therefore, when u increases, D_T increases significantly,

which results in an increase in σ.

The device was designed to create a linear electric field gradient. With high field and low field cross-sectional areas given by A_h and A_l, the gradient can be expressed by the equation

$$q = \frac{I}{CL}\left(\frac{1}{A_h} - \frac{1}{A_l}\right) \tag{5.5}$$

where I is the current, C is the conductivity, and L is the length of the separation channel. Equation 5.5 was derived from the equations

$$E(x) = \frac{I}{CA(x)} \tag{5.6}$$

$$E(x) = qx + E_0 \tag{5.7}$$

where E_0 is the electric field strength at the low field end ($x = 0$). When increasing the applied voltage, the current through the device increases, which leads to an increase in the electric field gradient. Therefore, the bandwidth decreases because the standard deviation of the focused band is inversely proportional to the square root of the electric field gradient.

Panels C and D in Figure 5.5 show images of R-PE and GFP, which were focused and separated in the open EFGF channel at different counter flow rates. When the flow rate was low, the two protein bands were located next to each other (Figure 5.5 C). When the flow rate increased, the two protein bands separated (Figure 5.5 D). Based on the theory,[5] the resolution R_s of two analytes can be expressed as

$$R_s = \frac{\Delta x}{4\sigma} = \frac{|u|}{4}\cdot\left(\frac{\bar{\mu}}{q(x_0)D_T}\right)^{1/2}\cdot\frac{\Delta\mu}{\bar{\mu}^2} = \frac{1}{4}\cdot\left(\frac{\bar{\mu}}{q(x_0)\cdot\left(\frac{D_M}{u^2} + \frac{d^2}{192D_M}\right)}\right)^{1/2}\cdot\frac{\Delta\mu}{\bar{\mu}^2} \tag{5.8}$$

where $\bar{\mu}$ is the average electrophoretic mobility, and $\Delta\mu$ is the electrophoretic mobility difference of two analytes. When the applied voltage is fixed (i.e., the electric field gradient $q(x_o)$ remains constant), the resolution increases when increasing the counter flow rate. On the other hand, if the counter flow rate is kept constant, an increase in the applied voltage leads to a reduction in resolution because the resolution is inversely proportional to the square root of the electric field gradient. Figure 5.7 shows the results of scanning along the separation channel, which was in qualitative agreement with the theoretical predictions. For example, the resolution increased from 0.76 to 3.23 when the counter flow rate changed from 5 nL/min to 10 nL/min at constant applied voltage (500V). The resolution decreased from 3.23 to 1.64 when the applied voltage increased from 500 V to 800 V at constant counter flow rate (10 nL/min).

5.3.3 Monolith Synthesis

The focused bands in the EFGF experiments described above were broad, which is a result of the large dispersion coefficient for laminar flow. A narrower focused band could be obtained by increasing $q(x_o)$ or decreasing D_T based on equation 5.2. For a fixed applied voltage and linear gradient, $q(x_o)$ does not change. Therefore, the dispersion coefficient must be reduced to achieve narrower bands. This can be done by packing the channel with particles[11] or incorporating a monolith in the channel.[17] In an open channel, the parabolic laminar flow profile broadens the sample zone. In a packed or monolithic column, the laminar flow profile is disrupted into a large number of much smaller laminar flow profiles formed in the interparticle spaces

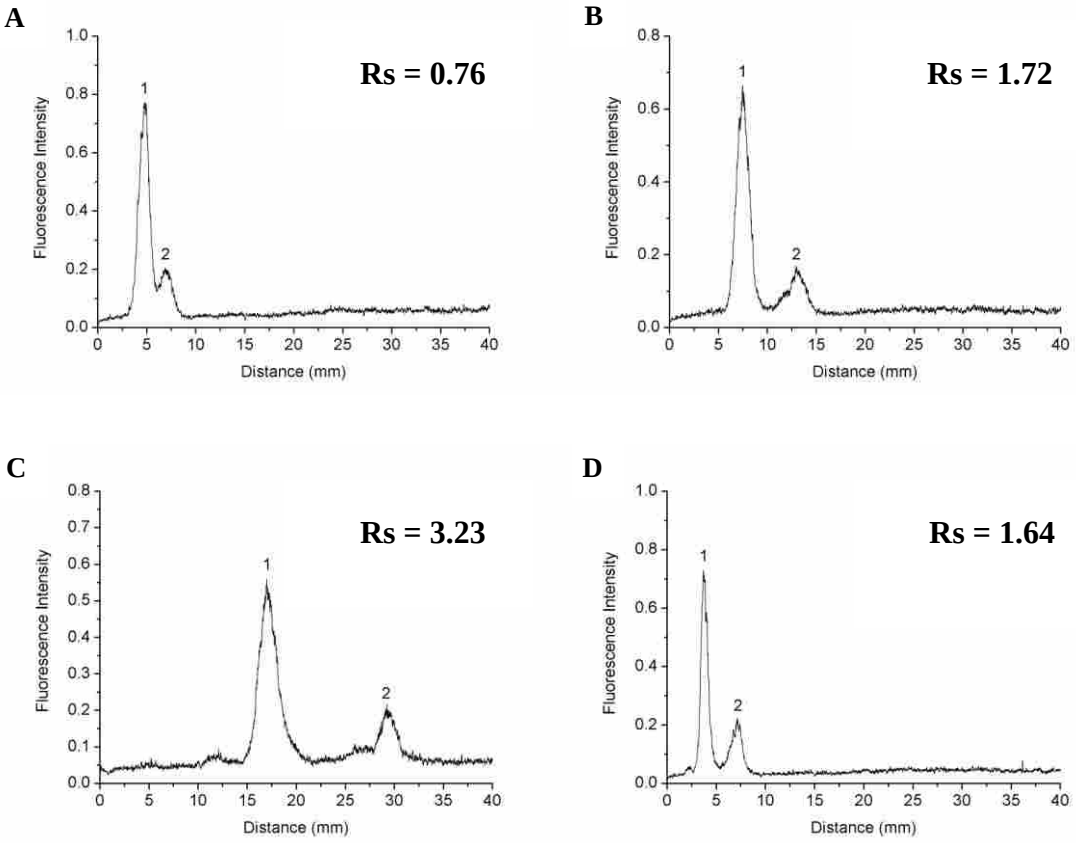

Figure 5.7. Focusing and separation of (1) R-PE and (2) GFP in an EFGF open channel under different conditions: (A) 5 nL/min flow rate, 500 V; (B) 8 nL/min flow rate, 500 V; (C) 10 nL/min flow rate, 500 V; (D) 10 nL/min flow rate, 800 V.

or throughpores. These individual profiles overlap to generate an overall pluglike flow profile, which reduces the dispersion considerably.

Koegler[2,7] and Greenlee[11] successfully packed a size exclusion resin in a dialysis tube to improve the performance of their preparative scale EFGF devices. However, in our device, the separation channel is very small, which makes it difficult to obtain uniform packing with small particles. Also, it is necessary to make a frit to prevent the particles from moving out of the channel during packing and operation. Incorporation of a monolith in the channel is the most reasonable approach to reducing laminar flow in the channel. Polymer monoliths were developed as chromatographic stationary phases over 15 years ago.[28,29] Recently, they have received increased attention due to advantages compared to packed columns, including ease of fabrication and low back pressure. Polymer monoliths have been applied in various chromatographic modes, such as reversed phase chromatography,[30] affinity chromatography,[31] and ion exchange chromatography.[32] Recently, Gu et al. developed a novel polymer monolith, which was prepared with PEG-functionalized methacrylate/acrylate monomers.[33] PEGDA 258 functioned as a biocompatible crosslinker. Negligible interaction was observed between the monolith and proteins.

In my work, a similar PEG-functionalized monolith was introduced into the EFGF channel. The ingredients are listed in Table 5.1; HEMA is the monomer, PEGDA 258 is the crosslinker, and methanol and ethyl ether are porogens. The monolith was formed using photopolymerization. SEM images of the monolith in the EFGF channel are shown in Figures 5.8 A and B. The monolith was bonded well to

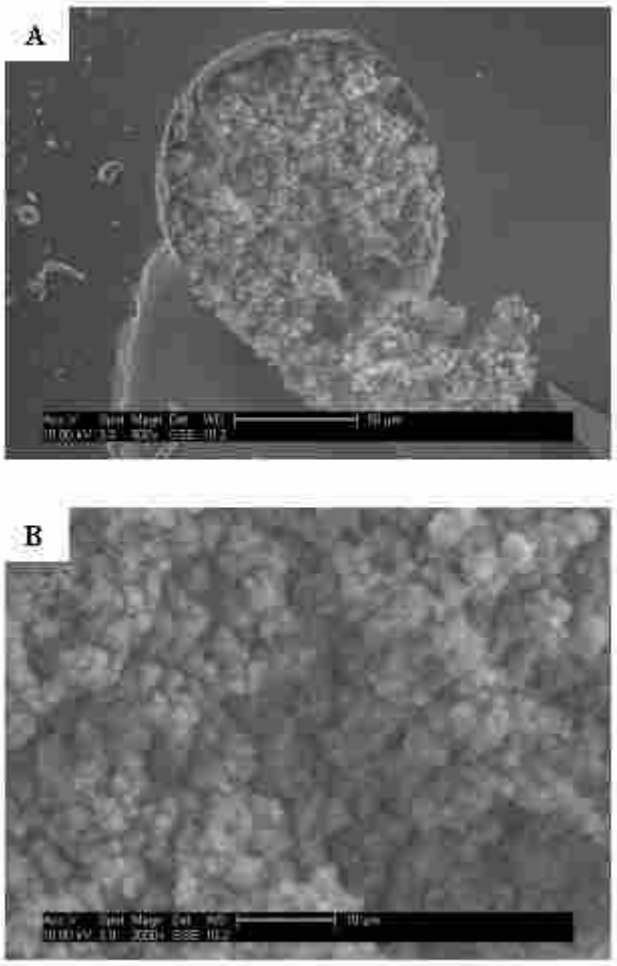

Figure 5.8. SEM images of the PEGDA/HEMA monolith incorporated in an EFGF channel. (A) 500× and (B) 2000× magnification of the monolith-filled EFGF channel.

the channel surface and had a typical monolith structure. The back pressure was approximately 200 psi when methanol was pumped through a 4 cm long monolith filled channel at 0.4 μL/min flow rate. The mean flow pore diameter (constricted pore diameter) was approximately 64 nm as measured using a capillary flow porometer.

5.3.4 Focusing of Proteins in Monolith Filled EFGF Channels

Figure 5.9 A shows focusing of R-PE in a monolith filled channel at different counter flow rates. The shifting and broadening of peaks followed the same trend as for the open channel. With an increase in flow rate, the peak moved to a higher electric field region and increased in width. However, the increase in peak width in the monolith filled channel was less than in an open channel. In the monolith filled channel, when the bulk flow rate changed 20-fold, from 2 nL/min (0.25 mm/min linear velocity) to 40 nL/min (5.05 mm/min), the peak width at half height increased less than 4-fold, from 0.28 mm to 1.08 mm (Table 5.2). This result indicates that the incorporated monolith reduced the flow dispersion and narrowed the protein bands. Compared with focusing in an open channel, the monolith filled channel produced significantly narrower peaks, even at high counter flow rate. However, when the counter flow rate was low, the peak focused in the open channel was as narrow as that in the monolith filled channel. From equation 5.2, the standard deviation of the focused band only depends on the dispersion coefficient when the electric field gradient is constant. When the counter flow rate is low, the total dispersion (D_T) is dominated by molecular diffusivity (D_M), which should be minimally affected by adding a monolith to the channel. Therefore, the peak widths should be similar. When

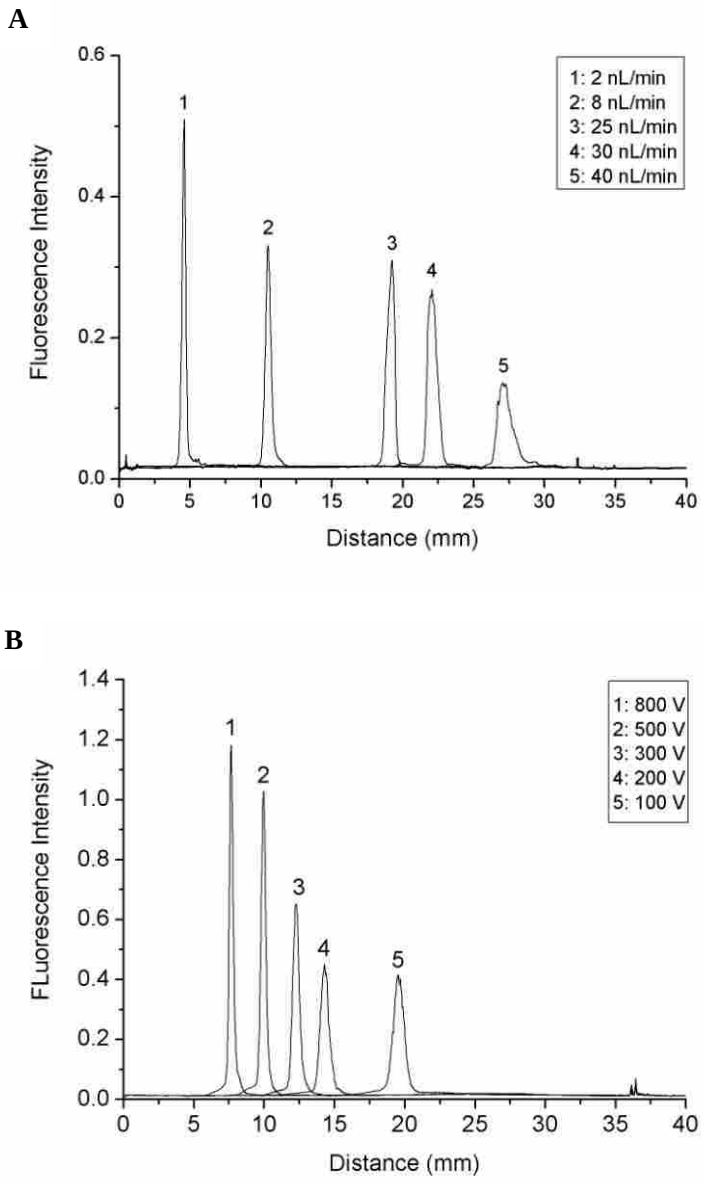

Figure 5.9. Focusing of R-PE in a monolith-filled EFGF channel for (A) different counter flow rates and constant applied voltage of 800 V, and (B) different applied voltages and constant counter flow rate of 5 nL/min.

the counter flow rate is high, D_u dominates in the total dispersion, which can be reduced by incorporation of a monolith in the channel to change the flow profile. In this case, the effect of the monolith is significant.

Figure 5.9 B shows focusing of R-PE in the monolith filled channel at different applied voltages and constant counter flow rate. With a decrease in the voltage from 100 V to 800 V, the protein band moved to the low electric field end of the channel. However, the peak width at half height decreased from 0.82 mm to 0.31 mm (Table 5.2). This change was less than that measured for an open channel, which again shows that the monolith helps to reduce the bandwidth in the EFGF channel.

Figure 5.10 shows the separation and focusing of three proteins in a monolith-filled EFGF channel. Even though the three proteins were not separated completely, their peak widths were narrower. In this case, the peak capacity of this channel increased. In EFGF, the resolution depends not only on the individual protein characteristics, such as electrophoretic mobility and size, but also on the hydrogel shape and focusing conditions. The hydrogel shape can be designed to provide shallow electric field gradient, which can improve the resolution. From the results described above for an open EFGF channel, resolution increases with an increase in counter flow rate or decrease in applied voltage.

The performance of the EFGF device described in this work, compared with the device described by Humble et al.,[8] was superior in several ways: the focused bands were more symmetrical due to less protein adsorption, focusing was easier to control because disturbances from electroosmotic flow were eliminated, and

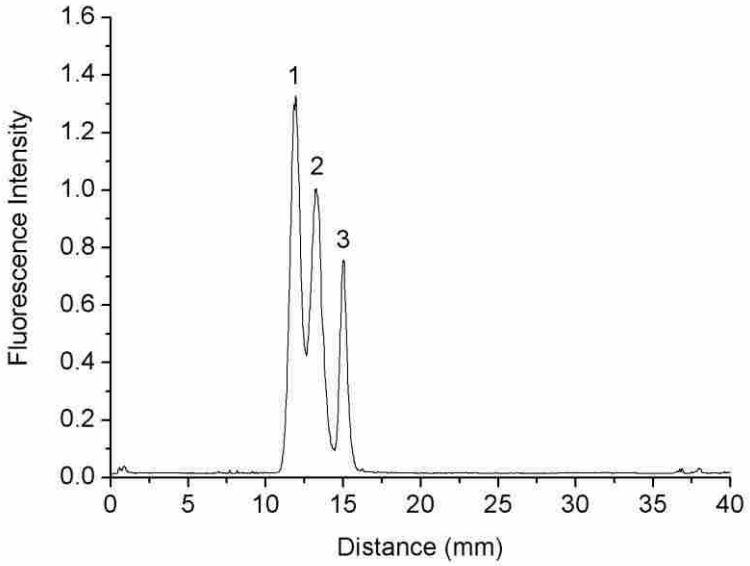

Figure 5.10 Focusing and separation of three proteins in a monolith-filled EFGF channel. The counter flow rate was 10 nL/min and the applied voltage was 800 V. Peaks: (1) FITC-β-lactoglobulin A, (2) FITC-myoglobin, and (3) GFP.

incorporation of a monolith in the focusing channel eliminated the dispersion resulting from laminar flow in an open channel. Since the focused bands were narrower, the peak capacity increased. Attempts to immobilize a stable monolith in the separation channel of the previous Humble et al. device were unsuccessful.

5.4 Conclusions

EFGF devices were cast out of a PEG-functionalized copolymer. The separation channel was formed in the hydrogel portion of the device using a wire. An electric field gradient was obtained by changing the cross-sectional dimension of the PEG-functionalized hydrogel normal to the separation channel. This type of device was successfully used to focus and separate proteins. The position of the focused band in the channel and the bandwidth depend on the electric field and the opposing hydrodynamic flow. High counter flow rate caused broad bands, but high resolution. High voltage led to narrow bands and low resolution. Incorporation of a PEG-functionalized monolith in the EFGF channel reduced dispersion induced by the laminar flow and narrowed the focused band. Both open channel and monolith-filled devices showed negligible EOF because the device body, hydrogel and monolith were all PEG functionalized materials, and the end capillaries were coated with PVA. Another approach to obtain narrow bands is to change the hydrogel shape to produce a nonlinear electric field gradient.[4] For example, a bilinear electric field gradient, which contains a steep gradient region and a shallow gradient region, should produce sharp peaks in the steep region and high resolution in the shallow region, leading to

high peak capacity.

5.5 References

1. Giddings, J. C.; Dahlgren, K. *Sep. Sci.* **1971**, *6*, 345-356.
2. Koegler, W. S.; Ivory, C. F. *J. Chromatogr. A* **1996**, *726*, 229-236.
3. Ivory, C. F. *Sep. Sci. Technol.* **2000**, *35*, 1777-1793.
4. Tolley, H. D.; Wang, Q.; LeFebre, D. A.; Lee, M. L. *Anal. Chem.* **2002**, *74*, 4456-4463.
5. Wang, Q.; Tolley, H. D.; LeFebre, D. A.; Lee, M. L. *Anal. Bioanal. Chem.* **2002**, *373*, 125-135.
6. Kelly, R. T.; Woolley, A. T. *J. Sep. Sci.* **2005**, *28*, 1985-1993.
7. Koegler, W. S.; Ivory, C. F. *Biotechnol. Prog.* **1996**, *12*, 822-836.
8. Humble, P. H.; Kelly, R. T.; Woolley, A. T.; Tolley, H. D.; Lee, M. L. *Anal. Chem.* **2004**, *76*, 5641-5648.
9. Kelly, R. T.; Li, Y.; Woolley, A. T. *Anal. Chem.* **2006**, *78*, 2565-2570.
10. Liu, J.; Sun, X.; Farnsworth, P. B.; Lee, M. L. *Anal. Chem.* **2006**, *78*, 4654-4662.
11. Greenlee, R. D.; Ivory, C. F. *Biotechnol. Prog.* **1998**, *14*, 300-309.
12. Wang, Q.; Lin, S.-L.; Warnick, K. F.; Tolley, H. D.; Lee, M. L. *J. Chromatogr. A* **2003**, *985*, 455-462.
13. Lin, S.-L.; Tolley, H. D.; Lee, M. L. *Chromatographia* **2005**, *62*, 277-281.
14. Lin, S.-L.; Li, Y.; Tolley, H. D.; Humble, P. H.; Lee, M. L. *J. Chromatogr. A*

2006, *1125*, 254-262.

15. Huang, Z.; Ivory, C. F. *Anal. Chem.* **1999**, *71*, 1628-1632.
16. Petsev, D. N.; Lopez, G. P.; Ivory, C. F.; Sibbett, S. S. *Lab Chip* **2005**, *5*, 587-597.
17. Myers, P.; Bartle, K. D. *J. Chromatogr. A* **2004**, *1044*, 253-258.
18. Ross, D.; Locascio, L. E. *Anal. Chem.* **2002**, *74*, 2556-2564.
19. Kim, S. M.; Sommer, G. J.; Burns, M. A.; Hasselbrink, E. F. *Anal. Chem.* **2006**, *78*, 8028-8035.
20. Balss, K. M.; Ross, D.; Begley, H. C.; Olsen, K. G.; Tarlov, M. J. *J. Am. Chem. Soc.* **2004**, *126*, 13474-13479.
21. Balss, K. M.; Vreeland, W. N.; Phinney, K. W.; Ross, D. *Anal. Chem.* **2004**, *76*, 7243-7249.
22. Hoebel, S. J.; Balss, K. M.; Jones, B. J.; Malliaris, C. D.; Munson, M. S.; Vreeland, W. N.; Ross, D. *Anal. Chem.* **2006**, *78*, 7186-7190.
23. Shackman, J. G.; Munson, M. S.; Ross, D. *Anal. Bioanal. Chem.* **2007**, *387*, 155-158.
24. Liu, J.; Sun, X.; Lee, M. L. *Anal. Chem.* **2005**, *77*, 6280-6287.
25. Clarke, N. J.; Tomlinson, A. J.; Schomburg, G.; Naylor, S. *Anal. Chem.* **1997**, *69*, 2786-2792.
26. Yu, C.; Davey, M. H.; Svec, F.; Frechet, J. M. J. *Anal. Chem.* **2001**, *73*, 5088-5096.
27. Liu, J.; Sun, X.; Lee, M. L. *Anal. Chem.* **2007**, *79*, 1926-1931.

28. Hjerten, S.; Liao, J.-L.; Zhang, R. *J. Chromatogr. A* **1989**, *473*, 273-275.

29. Svec, F.; Frechet, J. M. J. *Anal. Chem.* **1992**, *64*, 820-822.

30. Wang, Q. C.; Svec, F.; Frechet, J. M. J. *Anal. Chem.* **1993**, *65*, 2243-2248.

31. Petro, M.; Svec, F.; Frechet, J. M. J. *Biotechnol. Bioeng.* **1996**, *49*, 355-363.

32. Gu, B.; Chen, Z.; Thulin, C. D.; Lee, M. L. *Anal. Chem.* **2006**, *78*, 3509-3518.

33. Gu, B.; Armenta, J. M.; Lee, M. L. *J. Chromatogr. A* **2005**, *1079*, 382-391.

6 PERFORMANCE OPTIMIZATION IN ELECTRIC FIELD GRADIENT FOCUSING [*]

6.1 Introduction

As described in Chapter 5, I fabricated an EFGF device completely from PEG-functionalized copolymers, including the substrate, buffer ion-permeable but protein-excluding conductive hydrogel, and flow dispersion-minimizing monolith, which all contributed to the high resistance to adsorption of proteins.[1] The electric field gradient was generated by applying a voltage across the changing cross-sectional area filled with the conductive hydrogel. However, I observed that the actual electric field gradient along the channel was not the predicted linear gradient from the shaped region design and the current was not stable over time.

In this work, I replaced the hydrogel containing Tris buffer with hydrogel containing phosphate buffer and a salt (KCl) to improve the performance. In addition, I investigated the influence of separation channel diameter on the focused sample bandwidth and the concentrating ability of the new device.

6.2 Experimental Section

6.2.1 Materials and Sample Preparation

Methyl methacrylate (MMA, 99%), poly(ethylene glycol) methyl ether methacrylate (PEGMEMA 1100, MW~1100), poly(ethylene glycol) diacrylate (PEGDA 258, MW ~258), and 2,2'-dimethoxy-2-phenylacetophenone (DMPA) were

[*] This chapter is reproduced with permission from *J. Chromatogr. A* **2009**, *1216*, 159-164. Copyright 2009 Elsevier B.V.

purchased from Aldrich (Milwaukee, WI). Ethoxylated trimethylolpropane triacrylate (SR 9035) was obtained from Sartomer (Warrington, PA). Potassium chloride (KCl) and potassium phosphate monobasic (KH_2PO_4) were purchased from EM Science (Gibbstown, NJ). Potassium phosphate dibasic (anhydrous) (K_2HPO_4) was purchased from Mallinckrodt Specialty Chemicals (Paris, KY). Fluorescein isothiocyanate (FITC) was purchased from Invitrogen (Carlsbad, CA). β-Lactoglobulin A and dimethyl sulfoxide (DMSO) were ordered from Sigma (St. Louis, MO). R-Phycoerythrin (R-PE) was obtained from Polysciences (Warrington, PA). Recombinant, enhanced green fluorescent protein (GFP) was purchased from Clontech (Palo Alto, CA). All chemicals were used as received without further purification.

Deionized water (18.2 MΩ·cm) was prepared using a Milli-Q UF Plus water purification system (Millipore, Billerica, MA). Phosphate buffer (5 mM, pH 8.0) containing KCl (5 mM) was filtered using 0.2-μm syringe filters (Pall, East Hills, NY) before use.

To label β-lactoglobulin A, the protein was dissolved in filtered 10 mM sodium bicarbonate buffer (pH 9.2) with a concentration of 1 mg/mL. FITC was dissolved in absolute DMSO to make a 6 mM solution. Then, 600 μL protein solution was thoroughly mixed with 40 μL FITC solution and placed in the dark for at least 2 days at room temperature. Before use, the FITC-labeled protein sample was diluted to 20 μg/ mL with the running buffer.

6.2.2 Fabrication of EFGF Devices

All EFGF devices were fabricated using the previously reported casting method.[1] In brief, two small prepolymerized slab plates (65 × 25 × 1.5 mm^3 and 65 × 25 × 2.5 mm^3), one containing two reservoirs and the other containing a conical shaped cavity, were first fabricated using a monomer solution containing PEGDA (85%), PEGMEMA (12%), MMA (3%) and DMPA (0.1% of the total monomer weight). The concave cone shape of the cavity was designed to generate a linear electric field gradient. Two PVA inner-coated fused silica capillaries (150 μm i.d.) were threaded with a metal wire and mounted as inlet and outlet capillaries on top of the bottom plate containing the cavity, followed by placing the cover plate containing the two reservoirs over the bottom plate. The assembly was chemically bonded together by exposure to UV radiation. After bonding, a hydrogel monomer solution containing SR9035 (85%), buffer solution (15%) and DMPA (0.5% of the monomer weight) was introduced into the conical shaped cavity through the reservoir at the wide end of the cavity and photo-polymerized under a UV light. The previously used Tris buffer (100 mM, pH 8.5) in the hydrogel was replaced with phosphate buffer (5 mM, pH 8.0) containing KCl (5 mM). Finally the metal wire was pulled out of the fused silica capillaries, leaving a small channel through the hydrogel. Three different metal wires were used to form channels, including two nickel wires (50 and 120 μm diameter, MWS Wire Industries, Westlake Village, CA) and nitinol wire (70 μm diameter, Fort Wayne Metals, Fort Wayne, IN). The schematic of the final EFGF device is shown in Figure 5.2. The separation channel was 40 mm long, and the

widths of the hydrogel at the low and high field ends and the thickness of the hydrogel were 18 mm, 1.8 mm, and 1.5 mm, respectively.

6.2.3 EFGF Operation

The general operating procedure for EFGF using these changing cross-sectional devices was reported previously.[1] As shown in Figure 5.2, the sample was introduced into the EFGF separation channel through the high field end capillary using electrokinetic injection. A hydrodynamic counter flow was created by a syringe pump (Harvard Apparatus, Holliston, MA, USA) from the low field end as soon as the sample was observed to enter the separation channel. A voltage was applied along the channel from the reservoir at the low field end of the device (+) to a buffer-filled vial connected to the capillary at the high field end of the device (-). The detection system was a laser induced fluorescence (LIF) inverted microscope (488 nm) described previously.[1] The focused protein bands were detected by scanning along the channel. The fluorescence signal was detected using a photomultiplier (Hamamatsu, Bridgewater, NJ) and recorded using LabView (National Instruments, Austin, TX) software.

6.3 Results and Discussion

When an analyte is focused in an EFGF channel, the magnitude of the electrophoretic velocity of the analyte equals the hydrodynamic counter flow velocity,

$$u = \frac{F}{S} = \mu E \tag{6.1}$$

but their directions are opposite.[2] Where u is the linear velocity of the counter flow,

F is the bulk counter flow rate, S is the cross-sectional area of the EFGF separation channel, μ is the analyte electrophoretic mobility, and E is the electric field strength. By differentiating both sides of equation 6.1, assuming that the electrophoretic mobility and channel cross-sectional area are constant, I obtain

$$\frac{dF}{dx} = \mu S \frac{dE}{dx} = \mu S q(x) \tag{6.2}$$

where $q(x)$ is the electric field gradient at the equilibrium position, x, which is defined as the distance along the channel from the start of the low field end of the channel to the position of the focused peak maximum. Therefore, I can determine the electric field gradient, $q(x)$, in an EFGF channel by measuring the focusing positions of an analyte of known mobility for different hydrodynamic flow velocities. For a linear electric field gradient under a constant applied voltage, $q(x)$ and dF/dx are constant along the channel, which means that there is a linear relationship between the bulk counter flow rate and the corresponding analyte equilibrium position, with a slope that is proportional to the analyte electrophoretic mobility and the channel cross-sectional area.

I plotted the counter flow rate versus equilibrium position using data measured from Figure 5.6 A, which was obtained using an earlier device containing a hydrogel with 100 mM Tris-HCl buffer. When the counter flow rate was low, the sample was focused close to the low field end of the channel, and the relationship between F and x was approximately linear. However, when the counter flow rate was increased, the relationship between F and x deviated more from linearity, which meant that the electric field gradient along the whole channel length was not linear. The variation

in current with time for devices prepared with hydrogels containing Tris-HCl buffer and phosphate buffer (plus KCl) were measured and plotted as shown in Figure 6.1. The applied potential was 500 V. For the hydrogel containing Tris-HCl (upper curve), the current decreased with time and became stable in approximately 3 h. Similar current decrease was also observed for the EFGF device reported by Humble.[3] However, the explanation that buffer solution evaporation was the cause is not appropriate here because the hydrogel was enclosed in the channel with a top plate. The most reasonable cause is ion transport in the hydrogel. The hydrogel was designed to have nano-scale pores for small ion permeability, but not for larger molecules such as proteins. Proteins remained in the separation channel. Tris ion ($Tris^+$) is larger than other ions, such as K^+, Cl^-, OH^- and H^+, and its migration in the hydrogel was hindered. Because the buffer in the anode reservoir was frequently refilled to offset evaporation and the buffer in the channel was refreshed by the continuous counter-flow, it is clear that slow transport of $Tris^+$ ions resulted in build-up or depletion of buffer ions in the hydrogel, which impacted the electrical current and electric field distribution along the channel.

To eliminate this undesirable phenomenon, a phosphate buffer containing a strong electrolyte (KCl) comprised of small ions was doped in the hydrogel in place of the Tris-HCl buffer. The variation in current with time for a device containing this new hydrogel formulation is shown in Figure 6.1 (lower curve). The current was much more stable than the previous device over the 3-h period. In addition, even though the Tris-HCl buffer concentration was much higher, the current through the

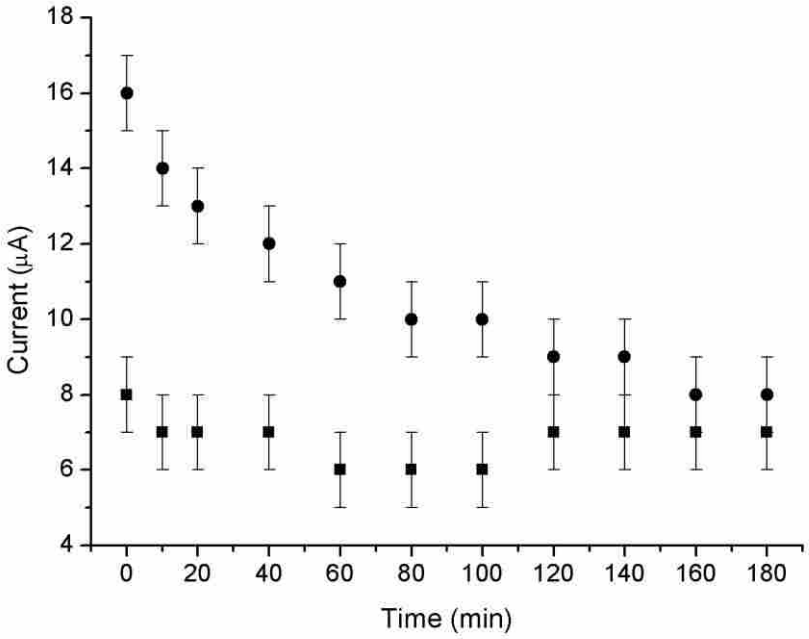

Figure 6.1. Current variation as a function of time for EFGF devices made from different hydrogels. The applied voltage was 500 V; (●) hydrogel containing 100 mM Tris-HCl (pH 8.5) buffer; (■) hydrogel containing 5 mM KCl and 5 mM phosphate buffer (pH 8.0). Error bar breadth was taken from the typical current display accuracy of the power supply (Stanford Research Systems, Sunnyvale, CA), ±1 μA.

new device was close to that observed with the previous one. These observations indicate that the large ions ($Tris^+$) migrate in the hydrogel much more slowly than smaller inorganic ions (such as K^+), which results in a decrease in conductivity and, therefore, less disturbance of the electric field distribution. This new hydrogel conductivity is approximately 2.2×10^{-5} S/m, which was measured as previously reported.[1] Although the new buffer concentration (~10 mM) was one fifth that in the former hydrogel containing 50 mM Tris-HCl buffer, its conductivity was approximately half that of the former (4.1×10^{-5} S/m).[1]

EFGF with the improved hydrogel was utilized to focus R-PE at different hydrodynamic flow rates and constant voltage (500 V) to determine the electric field distribution. Figure 6.2 A shows the focused R-PE peaks for the flow rates tested. With an increase in hydrodynamic flow rate, the focused sample band moved toward the high field end of the channel and broadened gradually. Compared with results obtained using previous devices, the band broadening was not as pronounced for this new device, even for high flow rates. The equilibrium position was plotted versus flow rate as shown in Figure 6.2 B. A good linear relationship was obtained, indicating that a linear electric field gradient was established in this new EFGF device. I also repeated these experiments using GFP as a test solute, and the same linear relationship was observed (Figure 6.2 C). The slopes were measured to be 0.90 and 0.50 for R-PE and GFP, respectively. The electrophoretic mobilities of R-PE and GFP in pH 9 buffer were 2.4×10^{-4} cm^2 V^{-1} s^{-1} and 1.9×10^{-4} cm^2 V^{-1} s^{-1}, respectively.[4] Although analyte mobility depends on pH and other buffer conditions, in this study, I

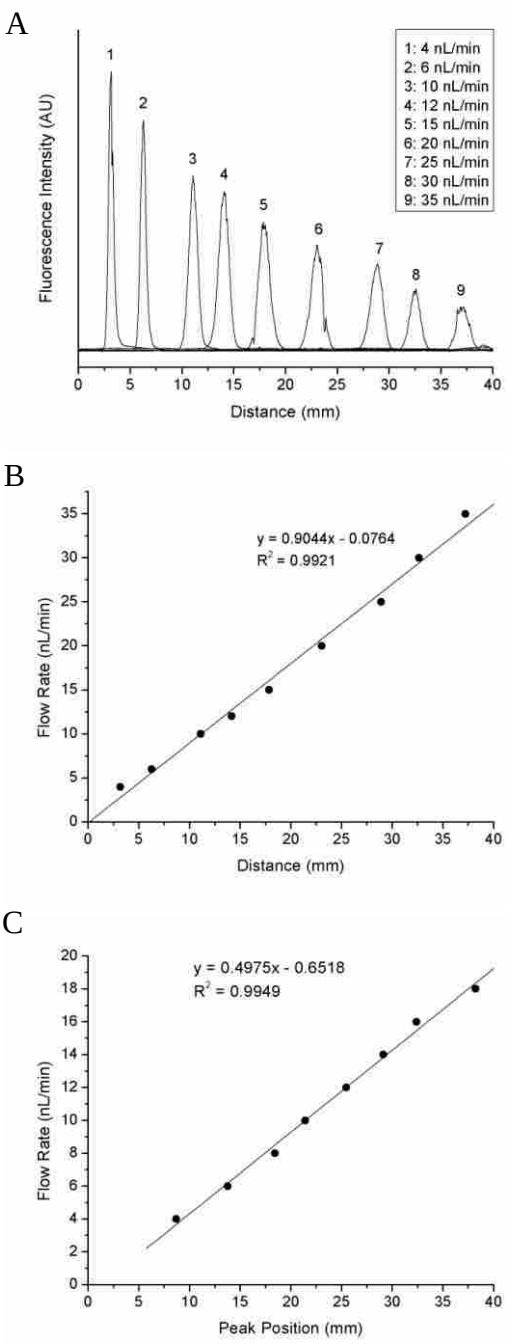

Figure 6.2. (A) Focusing of R-PE along an EFGF channel for different hydrodynamic flow rates using a hydrogel containing KCl. The channel i.d. was 120 μm and the applied voltage was 500 V. (B) Flow rate versus focused peak position for R-PE as shown in A. (C) Flow rate versus focused peak position for GFP at an applied voltage of 500 V.

used literature values for approximate mobilities of R-PE and GFP to calculate the electric field gradient in my EFGF device. The values of 5.55 V/cm^2 and 3.86 V/cm^2 for R-PE and GFP, respectively, were calculated using equation 6.2. Theoretically, the gradients calculated for different proteins should be identical at constant applied voltage; the lack of agreement here is a result of the approximate mobilities used in the calculations.

Figure 6.3 compares focusing experiments using three different EFGF devices under the same conditions. The peak positions and peak widths at half height are listed in Table 6.1. The GFP bands were focused at approximately 10 mm from the low field end of the channels. The relative standard deviation (RSD) for peak position was 1.4%. The peak widths at half height were approximately 1 mm and the RSD for peak width was 6.2%. The standard deviations were calculated based on equation $\sigma_{\exp} = W_{1/2} / 2.354$, and are similar (see Table 6.2) to the theoretical value (0.43 mm) obtained based on the known diffusion coefficient of GFP (~8.5 × 10^{-7} cm^2/s).[4] These results demonstrate the best device-to-device reproducibility produced by me to date.

From equation 6.2, the slopes of the lines in Figures 6.3 B and 6.3 C should be directly proportional to the separation channel cross-sectional area as well as to the analyte mobility. Therefore, I investigated the focusing performance in EFGF channels of different diameters. For example, the slope of the linear fit line is 0.331 for focusing of R-PE in a 70 μm i.d. separation channel for an applied voltage of 500 V. According to equation 6.2, the electric field gradient was calculated to be 5.97 V/cm^2, which is close to the value obtained for a 120 μm i.d. EFGF channel with

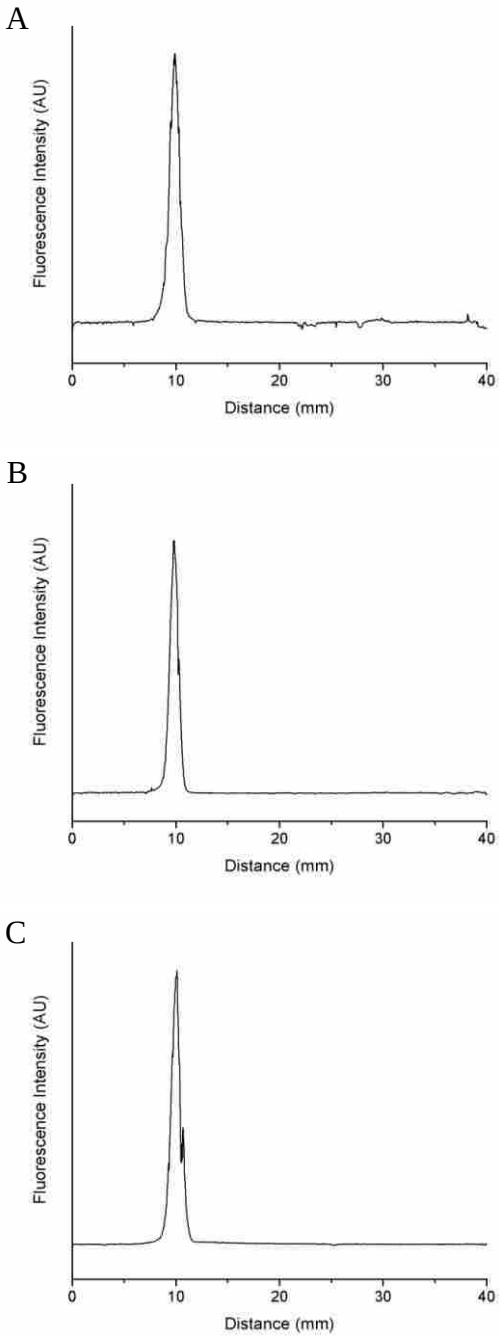

Figure 6.3. Comparison of GFP focusing experiments under the same conditions using three different EFGF devices containing hydrogel with 5 mM KCl. The channel i.d. was 120 μm, the counter flow rate was 5 nL/min, the applied voltage was 500 V, and the current was 6~7 μA.

Table 6.1. Reproducibility measurements from the focusing of GFP in three different EFGF devices containing KCl in the hydrogel (see Figure 6.3).

	A	B	C	Mean (CL=95%)	RSD
Peak position (mm)	9.90	9.83	10.10	9.94 ± 0.35	1.4%
$W_{1/2}$ (mm)	1.03	0.96	0.91	0.97 ± 0.15	6.2%

Table 6.2. Calculated and experimental values of standard deviations in Figures 6.3 and 6.4.

Figure	6.3 A	6.3 B	6.3 C	6.4 A	6.4 B	6.4 C
σ_{theory} (mm) [1]	0.43	0.43	0.43	0.31 [2]	0.40	0.69
σ_{exp} (mm) [3]	0.44	0.41	0.38	0.21	0.27	0.53

[1] $\sigma_{theory} = \sqrt{D_M / \mu q + u^2 d^2 / 192 D_M \mu q}$

[2] For the calculation, q = 5.76, which was the average of the two gradients obtained for the 70 μm and 120 μm i.d. channels.

[3] $\sigma_{exp} = W_{1/2} / 2.354$

R-PE as analyte (5.55 V/cm^2). This indicates that the field gradient is not affected by the separation channel and only depends on the shaped hydrogel.

Figure 6.4 shows the focusing of R-PE in three different diameter EFGF channels. The channel diameters (d) were 50, 70 and 120 μm, respectively. For comparison, the voltage (500 V) was applied over the two reservoirs molded in the top plate instead of from the inlet reservoir to the exit vial. The counter flow rates for each are listed in Table 6.3. Although the bulk flow rates were different, the linear flow velocities were adjusted to be similar (~1 mm/min). Therefore, the peaks were focused at similar positions in the channels. As can be seen, the peak widths at half height broadened with an increase in channel diameter. This is because the Taylor dispersion is less in smaller channels.[2] Standard deviations (σ) including theoretical and experimental values are listed in Table 6.2. The diffusion coefficient of R-PE is 4 × 10^{-7} cm^2/s.[4] For the 50 μm i.d. channel, the gradient (5.76 V/cm^2) was taken as the average of the values obtained for the 70 μm and 120 μm i.d. channels. The two sets of values are close, and the experimental values are slightly smaller than the theoretical values because the actual gradients are larger due to the fact that the voltage was applied over the two reservoirs on top of the device instead of using the end vial. According to EFGF theory,[1] σ^2 is linearly related to d^2 for the same analyte and field gradient when the counter flow velocity is similar. A linear relationship does exist between σ_{exp}^2 and d^2 based on the experimental results shown in Figure 6.4.

Figure 6.5 shows a separation of three proteins in a 120 μm i.d. EFGF channel. When the applied voltage was higher or the counter flow was slower, the peaks were

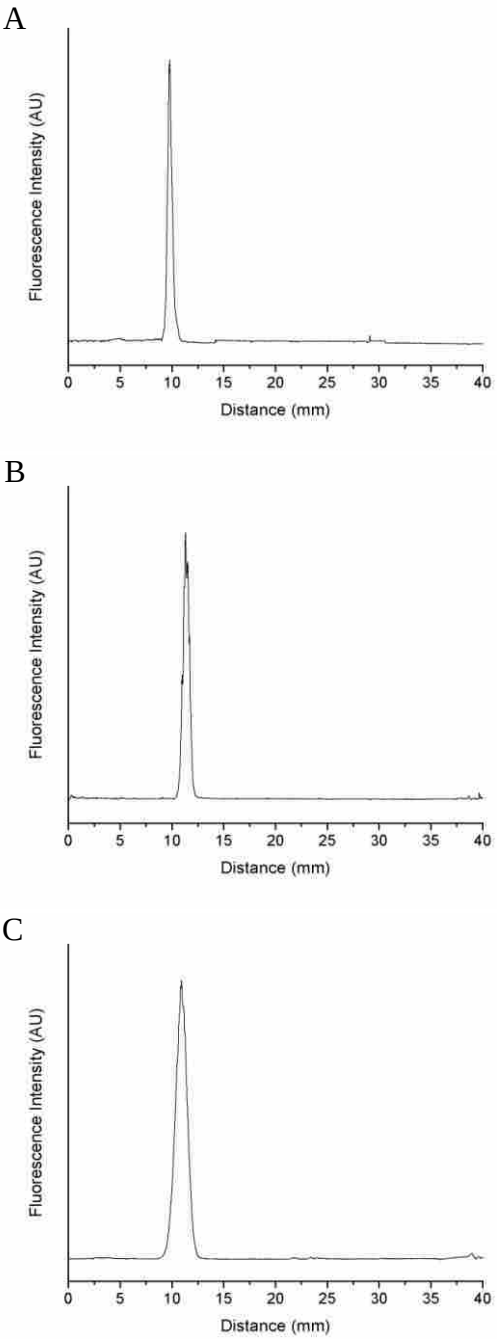

Figure 6.4. Focusing of R-PE in three EFGF channels of different diameter. (A) 50 μm i.d., (B) 70 μm i.d., and (C) 120 μm i.d. Voltage (500 V) was applied across the two reservoirs of each device. The counter flow rates are listed in Table 6.2.

Table 6.3. Measurements from the focusing of R-PE in three EFGF channels with different diameters (see Figure 6.4).

Figure	Channel i.d. (μm)	Bulk flow rate (nL/min)	Linear velocity (mm/min)	Peak position (mm)	$W_{1/2}$ (mm)
6.4 A	50	2	1.02	9.77	0.49
6.4 B	70	4	1.04	11.32	0.64
6.4 C	120	12	1.06	10.94	1.25

narrow but stacked together. When the voltage was lower or the counter flow was faster, the peaks were resolved, but broad. Therefore, the operating conditions were optimized to provide narrow, resolved peaks in a reasonably short time. In Figure 6.5, the three peaks are almost completely resolved, although the FITC-β-lactoglobulin A peak is quite broad and a shoulder is observed, which is likely due to FITC labeling.

Currently, the most useful application of a linear gradient EFGF device is to preconcentrate target analytes and order them according to electrophoretic mobility. The EFGF device reported by Humble et al. and the micro EFGF device reported by Liu et al. were shown to concentrate GFP by 10,000- and 4,000-fold, respectively.[5, 6] To determine the concentrating ability of this new EFGF device, a calibration curve was first constructed based on five R-PE solutions of known concentrations ranging from 10 μg/mL to 100 μg/mL. To measure the fluorescence intensity of each of these standard R-PE solutions, the EFGF channel was first filled with the solution. Then the laser was focused on the channel and the corresponding fluorescence intensity was recorded. Three values were measured at different positions along the channel for each standard solution, and the average fluorescence intensity was used to construct the calibration curve (Figure 6.6). A sample solution containing 2 ng/mL R-PE was injected into the EFGF channel electrokinetically with a voltage of 500 V for 60 min. Then a counter flow (5 nL/min) was applied to focus the analyte in the channel. The fluorescence intensity of the focused R-PE band was compared to the calibration curve, and the concentration of the focused R-PE band was found to be 27 μg/mL, corresponding to a concentration factor of approximately 14,000.

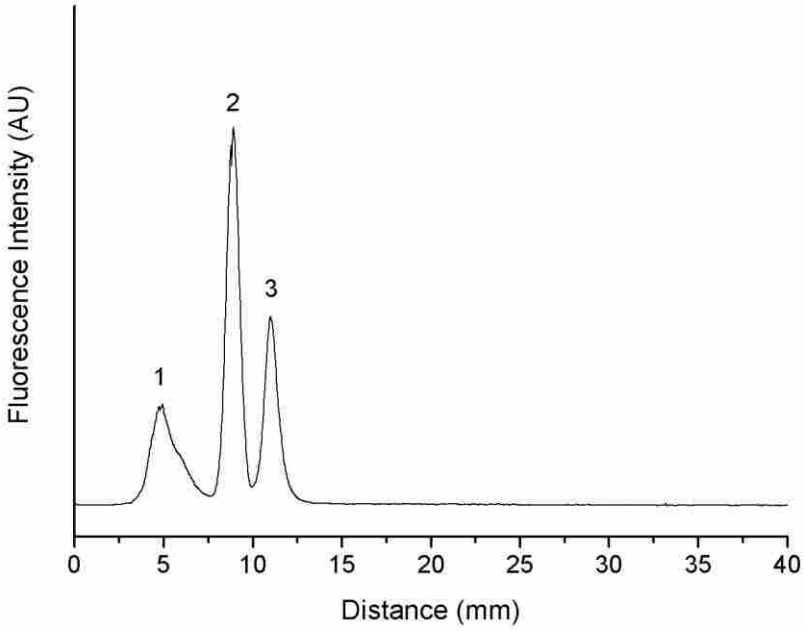

Figure 6.5. Separation of three proteins in a 120 μm i.d. EFGF channel. The counter flow rate was 10 nL/min and the applied voltage was 800 V. Peak identifications: (1) FITC-β-lactoglobulin A, (2) R-PE, and (3) GFP.

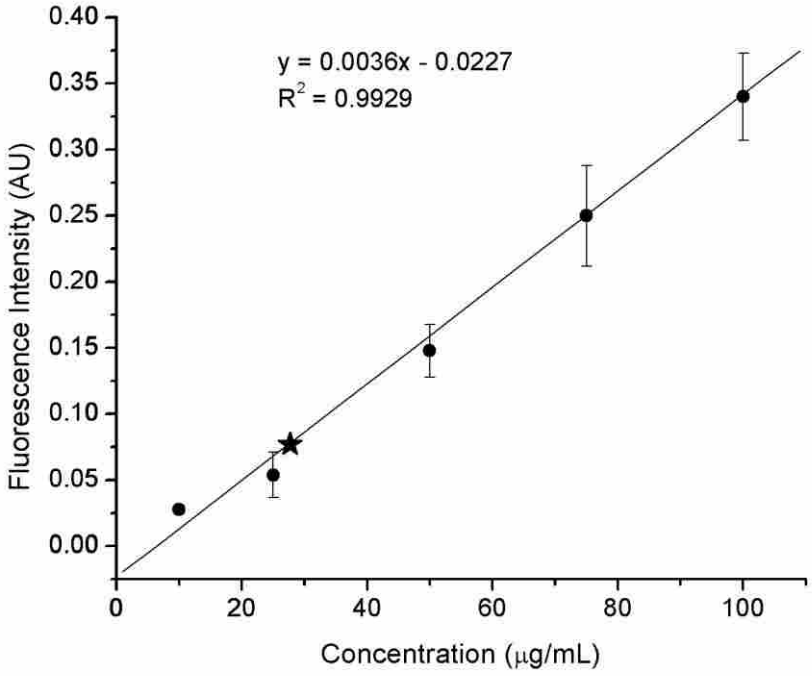

Figure 6.6. Calibration curve used to determine the concentration factor for R-PE. Each data point used to construct the curve was averaged from three measurements (CL% = 95%). The star (★) denotes the fluorescence intensity of the concentrated R-PE band in the channel.

6.4 Conclusions

A phosphate buffer containing an electrolyte with small ions (i.e., KCl) was employed in place of the previously used Tris-HCl buffer to improve ion transport through the hydrogel surrounding the separation channel in EFGF. The current through the new hydrogel was stable. The electric field distribution was indirectly determined by measuring the focused band positions of standard proteins at constant voltage for different hydrodynamic flow rates. The expected linear electric field gradient was achieved, in good agreement with theoretical prediction based on device design. When the applied voltage was 500 V, the field gradients generated in a 120 μm i.d. EFGF channel for R-PE and GFP were 5.55 V/cm^2 and 3.86 V/cm^2, respectively. The performance of separation channels of different diameters was also investigated. Narrower bands were obtained in smaller diameter channels due to reduced Taylor dispersion. The gradient established in a 70 μm i.d. channel for R-PE was 5.97 V/cm^2 when the applied voltage was 500 V. Three proteins were successfully separated in the EFGF channel. The EFGF device was able to concentrate a 2 ng/mL R-PE sample by 14,000 fold.

6.5 References

1. Sun, X.; Farnsworth, P. B.; Woolley, A. T.; Tolley, H. D.; Warnick, K. F.; Lee, M. L. *Anal. Chem.* **2008**, *80*, 451-460.
2. Tolley, H. D.; Wang, Q.; LeFebre, D. A.; Lee, M. L. *Anal. Chem.* **2002**, *74*, 4456-4463.

3. Humble, P. H.; Harb, J. N.; Tolley, H. D.; Woolley, A. T.; Farnsworth, P. B.; Lee, M. L. *J. Chromatogr. A* **2007**, *1160*, 311-319.

4. St'astna, M.; Radko, S. P.; Chrambach, A. *Electrophoresis* **2000**, *21*, 985-992.

5. Humble, P. H.; Kelly, R. T.; Woolley, A. T.; Tolley, H. D.; Lee, M. L. *Anal. Chem.* **2004**, *76*, 5641-5648.

6. Liu, J.; Sun, X.; Farnsworth, P. B.; Lee, M. L. *Anal. Chem.* **2006**, *78*, 4654-4662.

7 NON-LINEAR ELECTRIC FIELD GRADIENT FOCUSING

7.1 Introduction

So far, only a linear gradient (line 1 in Figure 7.1) has been reported in EFGF devices based on changing cross-sectional area. According to the fundamental theory of EFGF, resolution and peak capacity in EFGF with a linear gradient cannot be improved simultaneously, because bandwidth and resolution are inversely proportional to the square root of the field gradient. However, some theoretical work indicates that the peak capacity could be improved using an EFGF device with nonlinear (convex) gradient (curve 2 in Figure 7.1), such as can be approximated with bilinear EFGF.[1,2] All analytes would first be focused in the steeper gradient section to form narrow stacked bands. Then they would be sequentially moved into the shallower gradient section and be resolved by manipulating the counter flow rate or applied voltage. This dynamic improvement of peak capacity is important for further development of the EFGF technique. An ineffective EFGF device with a nonlinear gradient was constructed using a buffer conductivity gradient.[3] This device provided a very steep gradient section followed by a very shallow section. Unfortunately, the first steep segment was too short to significantly improve peak capacity.

In this work, two types of nonlinear EFGF devices, bilinear (convex, curve 2 in Figure 7.1) and concave (curve 3 in Figure 7.1), were fabricated from PEG-functionalized copolymers. A monolith was synthesized in the EFGF channels, and the separation and focusing of proteins in these channels were investigated.

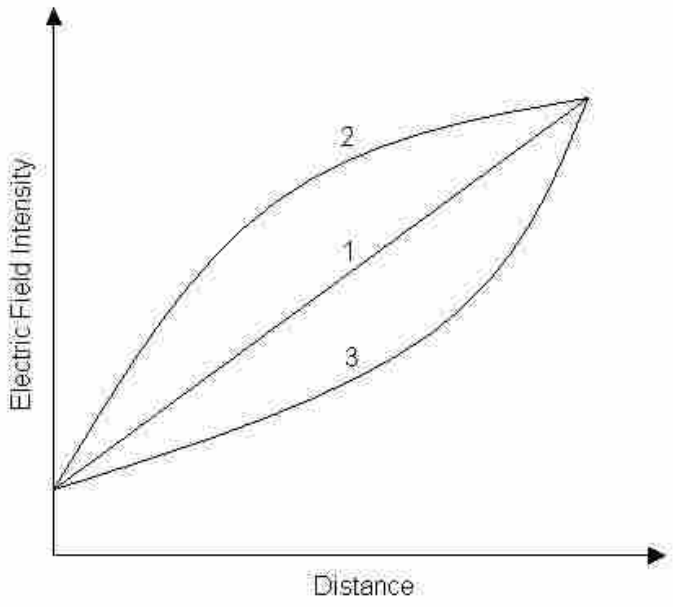

Figure 7.1. Three types of electric field gradient profiles studied for EFGF. (1) Linear, (2) convex, and (3) concave.

7.2 Experimental Section

7.2.1 Materials

Poly(ethylene glycol) diacrylate (PEGDA, MW ~258), poly(ethylene glycol) methyl ether methacrylate (PEGMEMA, MW~1100), methyl methacrylate (MMA, 99%), 2-hydroxyethyl methacylate (HEMA, 99%+), and 2,2'-dimethoxy-2-phenylacetophenone (DMPA) were purchased from Aldrich (Milwaukee, WI). Ethoxylated trimethylolpropane triacrylate (SR 9035) was obtained from Sartomer (Warrington, PA). Anhydrous methanol was purchased from Mallinckrodt Chemicals (Phillipsburg, NJ). Anhydrous ethyl ether was purchased from Fisher Scientific (Fair Lawn, NJ). Fluorescein isothiocyanate (FITC) was purchased from Invitrogen (Carlsbad, CA). Potassium chloride (KCl) and potassium phosphate monobasic (KH_2PO_4) were purchased from EM Science (Gibbstown, NJ). Potassium phosphate dibasic (anhydrous) (K_2HPO_4) was purchased from Mallinckrodt Specialty Chemicals (Paris, KY). Dimethyl sulfoxide (DMSO) and β-lactoglobulin A were ordered from Sigma (St. Louis, MO). R-phycoerythrin (R-PE) was obtained from Polysciences (Warrington, PA). Recombinant, enhanced green fluorescent protein was purchased from Clontech (Palo Alto, CA). All chemicals were used as received without further purification. Deionized water (18.2 MΩ·cm) was prepared using a Milli-Q UF Plus water purification system (Millipore, Billerica, MA). Carbonate buffer (10 mM, pH 9.2) and phosphate buffer (5 mM, pH 8.0) containing KCl (5 mM) were filtered using 0.2-μm syringe filters (Pall, East Hills, NY) before being used. Precleaned microscope slides with dimensions of $70 \times 50 \times 1$ mm^3 and 70

× 25 × 1 mm^3 were obtained from Fisher Scientific (Pittsburgh, PA) and Hardy Diagnostics (Santa Maria, CA), respectively.

7.2.2 Preparation of FITC-Labeled β-Lactoglobulin A

The procedure of labeling β-lactogloblin A was reported previously.[4] In brief, 1 mg/mL β-lactoglobulin A solution was prepared in filtered 10 mM carbonate buffer (pH 9.2). FITC was dissolved in absolute DMSO to form a concentration of 6 mM. Then 600 μL protein solution was thoroughly mixed with 40 μL FITC solution and placed in the dark for 2 days at room temperature. After completion of labeling, the protein solution was stored at 4 ^oC. Before use, the FITC-labeled protein sample was diluted with the running buffer.

7.2.3 Fabrication of EFGF Devices

All EFGF devices were fabricated using a previously reported casting method (Figure 5.1).[4] A prepolymerized top slab plate (65 × 25/50 × 1.5 mm^3) containing two reservoirs, and a bottom plate (65 × 25/50 × 2.5 mm^3) containing a planar horn-shaped cavity were first fabricated using a monomer solution containing PEGDA (85%), PEGMEMA (12%), MMA (3%) and DMPA (0.1% of the total monomer weight). The concave planar horn shape of the cavity could be easily designed to generate the desired electric field gradient, such as linear, convex or concave. Two fused-silica capillaries (150 μm i.d.) were threaded with a nickel wire (120 μm diameter, MWS Wire Industries, Westlake Village, CA) and mounted as inlet and outlet capillaries on the top of the bottom plate containing the cavity, followed by placing the cover plate with two reservoirs on top. The assembly was chemically

bonded together by exposure to UV radiation. After bonding, a hydrogel monomer solution containing SR 9035 (85%), DMPA (0.5% of the monomer weight) and phosphate buffer (5 mM, pH 8.0) containing KCl (5 mM) (15%) was introduced into the planar horn-shaped cavity through the reservoir at the wide end of the cavity and photopolymerized under UV light. Finally, the nickel wire was pulled out of the fused silica capillaries, leaving a small channel through the hydrogel.

7.2.4 Synthesis of a Monolith in the EFGF Channel

A protein compatible (i.e., nonadsorptive) monolith was incorporated into the EFGF channel using a previously reported method.[4] Briefly, a degassed mixture containing PEGDA (crosslinker, 22.5 wt %), HEMA (monomer, 7.5 wt %), methanol (porogen, 25 wt %), ethyl ether (porogen, 45 wt %) and DMPA (photoinitiator, 1% of the total monomer weight) was carefully introduced into the channel to avoid bubble generation. The device was then exposed to UV light for 8 min under a UV dichroic mirror (Navitar, Newport Beach, CA). After polymerization, the device was then connected to an HPLC micro pump (Eksigent, Dublin, CA) and washed with methanol for 5 h at 0.4 μL/min to remove unreacted monomers and porogens, followed by flushing with operating buffer until focusing experiments were performed.

7.2.5 Operation of EFGF and Detection

The general EFGF operating procedure was reported previously.[4] First, the sample was electrokinetically injected into the EFGF separation channel by applying a voltage across the reservoir at the low field end of the device (+) and a sample

solution-filled vial at the high field end of the device (-). The amount of injected sample was controlled by the applied voltage and injection time. After injection, the sample vial was replaced by a buffer-filled vial, and a hydrodynamic flow was created using a syringe pump (Harvard Apparatus) from the low field end to oppose the direction of electrophoretic migration. After focusing, the protein bands were detected using a laser induced fluorescence (LIF) inverted microscope by scanning along the separation channel.[4] The fluorescence signal was detected using a photomultiplier (Hamamatsu, Bridgewater, NJ) and recorded using LabView software (National Instruments, Austin, TX).

7.3 Results and Discussion

7.3.1 EFGF with Bilinear (Convex) Electric Field Gradient

Figure 7.2 A shows the design and dimensions of a bilinear EFGF device that was fabricated and evaluated. The left segment provided a steep gradient, while the right segment gave a shallow gradient. The device was fabricated using a casting method as described in Chapter 5.[4] Both the substrate and conductive hydrogel were PEG-functionalized acrylic copolymers. During photopolymerization of the substrates, the UV exposure time was crucial for controlling the reaction. If the substrates were too soft, they were difficult to handle and the device became deformed during photo-induced bonding of the cover plate to the shaped cavity plate. If the prepolymerized substrates were too hard, the bonding was not robust. To improve ion transport in the hydrogel and obtain stable current and electric field, a phosphate

buffer (5 mM) containing a strong electrolyte (5 mM KCl) was incorporated in the hydrogel as described in Chapter 6. If a higher concentration buffer was mixed with the monomer, the mixture became cloudy, and the device turned opaque after polymerization.

According to Chapter 6, the gradient profile can be predicted by measuring the focused band positions in the channel for different counter flow rates at constant voltage.[5] Figure 7.2 B shows the relationship between the focused R-PE band positions in the bilinear EFGF channel and the corresponding counter flow rates when the applied voltage was 500 V. When the counter flow rate was low, the protein was focused near the end at low electric field. With an increase in counter flow rate, the focused protein band moved toward the high electric field end. As shown in Figure 7.2 B, there was a linear relationship between the band positions and the counter flow rates in the flow rate range of 2 nL/min to 22 nL/min. The slope of the line was approximately 1.2. When the counter flow rate was higher than 22 nL/min, another linear relationship was observed between the same two parameters, with a slope of approximately 0.38. The presence of two linear relationships with different slopes indicates that the fabricated EFGF device provided a bilinear field gradient profile. In addition, the low field segment had steeper gradient than the high field segment. The intersection point was approximately at the midpoint (20 mm) of the channel, which was in agreement with the initial design. Figure 7.2 C shows the movement of the focused R-PE peak along the EFGF channel when changing the applied voltage at constant flow rate (20 nL/min). Movement of the band from the steep to shallow

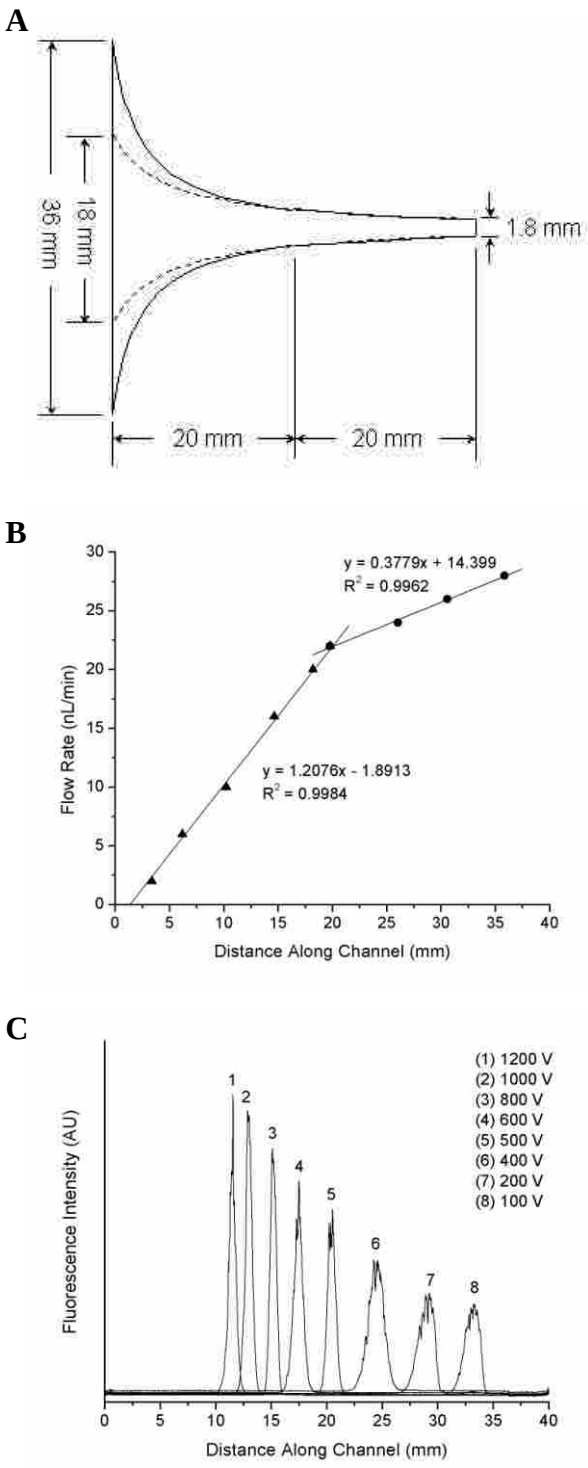

Figure 7.2. (A) Design and dimensions of a bilinear EFGF device (solid line). (B) Plot of counter flow rate versus R-PE peak position in an open bilinear EFGF channel at constant voltage (500 V). (C) Focusing positions of R-PE in an open bilinear EFGF channel for different applied voltages at a constant counter flow rate (20 nL/min).

segments was clearly seen by abrupt peak broadening (i.e., peaks 6-8).

As reported before, dynamic improvement of peak capacity should be realized by increasing the counter flow rate or decreasing the applied voltage to move focused peaks from the steep segment to the shallow segment.[1] The movement of three protein peaks in a monolith-filled bilinear EFGF channel is shown in Figure 7.3. A monolith was incorporated in the EFGF channel to reduce flow dispersion, which narrowed the focused bands. During an experiment, the counter flow rate was increased from 5 nL/min to 20 nL/min while the voltage was kept constant (800 V). When the counter flow rate was low, all proteins were stacked together with narrow bands in the steep segment (Figure 7.3 A). When the counter flow rate was increased, all proteins moved toward the high field end, and the resolution increased gradually (Figure 7.3 B). When samples moved into the shallow segment, they were even better resolved, and minor components in the sample appeared (Figure 7.3 C). When the counter flow rate was increased further, the protein with the smallest electrophoretic mobility (GFP) was eluted (Figure 7.3 D).

7.3.2 EFGF with Concave Electric Field Gradient

EFGF devices with concave electric field gradients were fabricated using a simple design shown in Figure 7.4 A, which looks like an isoceles triangle. Figure 7.4 B shows the movement of the R-PE peak along the EFGF channel as a function of counter flow rate at constant voltage (500 V) using two EFGF devices with different dimensions. When the width of the hydrogel (W_1) at the low field end was larger (i.e., device 1), the field gradient along the channel was greater. For both, the gradient

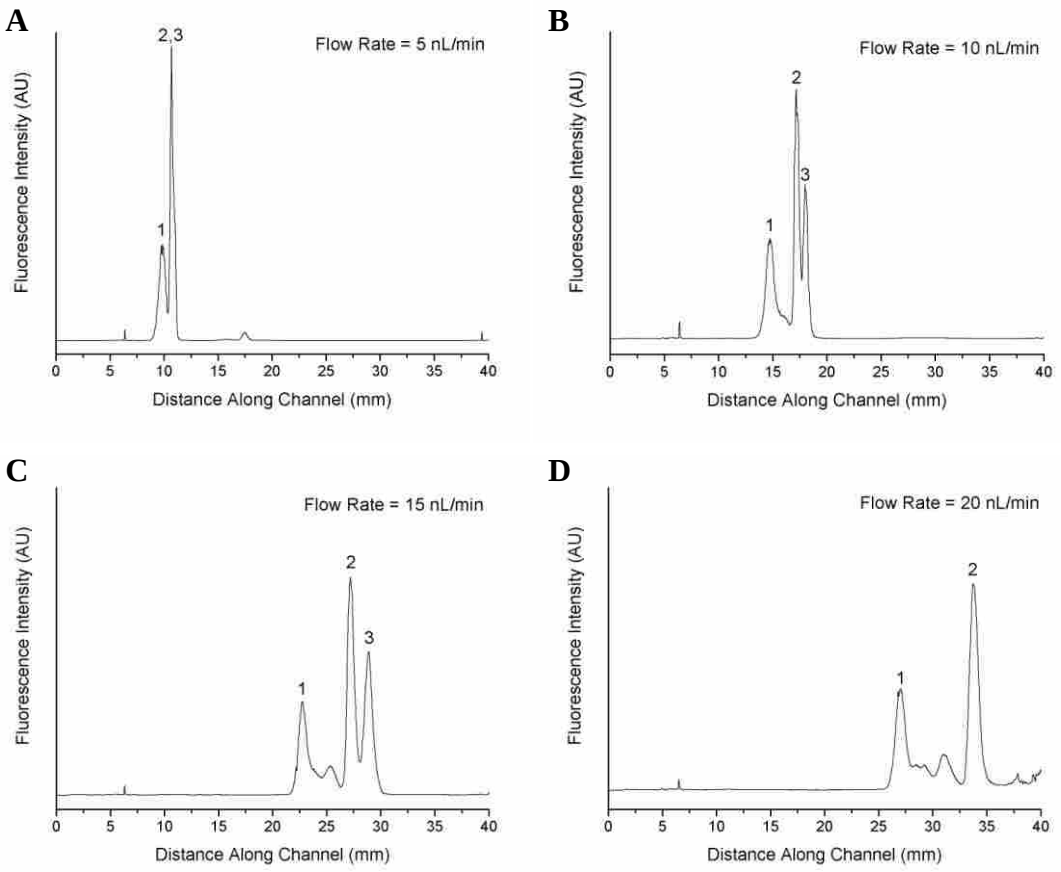

Figure 7.3. Separations of three proteins in a monolith filled bilinear EFGF channel for different counter flow rates at constant voltage (800 V). Peaks: (1) FITC-β-lactoglobulin A, (2) R-PE, and (3) GFP.

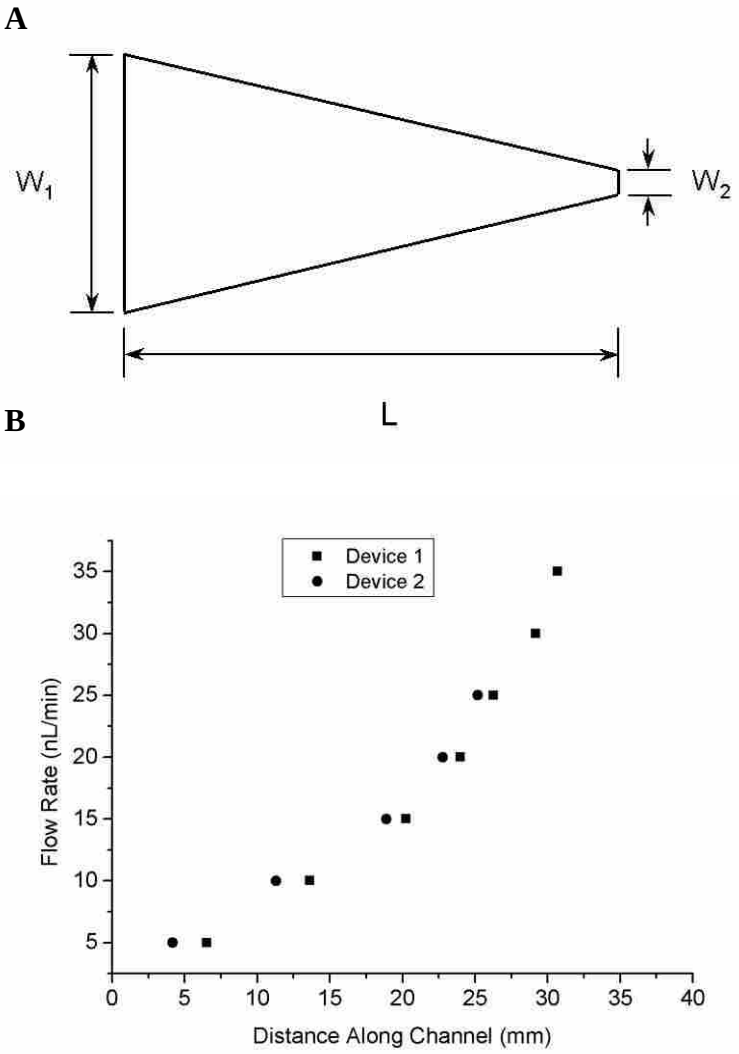

Figure 7.4. (A) Design of an EFGF device with concave gradient profile. (B) Plots of counter flow rate versus peak position for two different EFGF devices with concave gradient profiles. Device 1: W_1 = 20 mm, W_2 = 2 mm, and L = 40 mm. Device 2: W_1 = 15 mm, W_2 = 2 mm, and L = 40 mm.

gradually increased from the low field end to the high field end along the channel. Compared with a linear EFGF device of the same dimensions (W_1, W_2, and L), the gradient was shallower near the low field end and steeper near the high field end. When the counter flow was low, sample bands focused in the low field region were broad but well resolved compared with linear EFGF. When the counter flow was increased to move samples into the high field region, the bandwidths and resolution changed less than for a linear EFGF channel because of the increase in the electric field gradient.

For example, R-PE and GFP were separated in an open-channel EFGF with a concave electric field gradient (device 1) for different counter flow rates at constant voltage (500 V). When the flow rate was 5 nL/min, the resolution was 1.30, which is higher than that obtained in a linear EFGF device (0.76).[4] However, when the flow rate was increased to 10 nL/min, the resolution was 1.74, which is smaller than that measured for a linear EFGF device (3.23).[4] As the flow rate was raised to 15 nL/min and 20 nL/min, the resolution gradually increased to 2.30 and 2.39, respectively.

Figure 7.5 shows the focusing and separation of three proteins in an open EFGF channel with concave field gradient profile. Although the bands are broad, the three peaks are almost completely resolved. Figure 7.6 demonstrates improved focusing with a monolith-filled EFGF channel containing a concave gradient profile. When the counter flow rate was low (5 nL/min), two proteins (R-PE and GFP) were focused in the low field region, and the resolution was 1.12. The bandwidths of these proteins at half height were approximately 0.5 mm. When the flow rate was 15

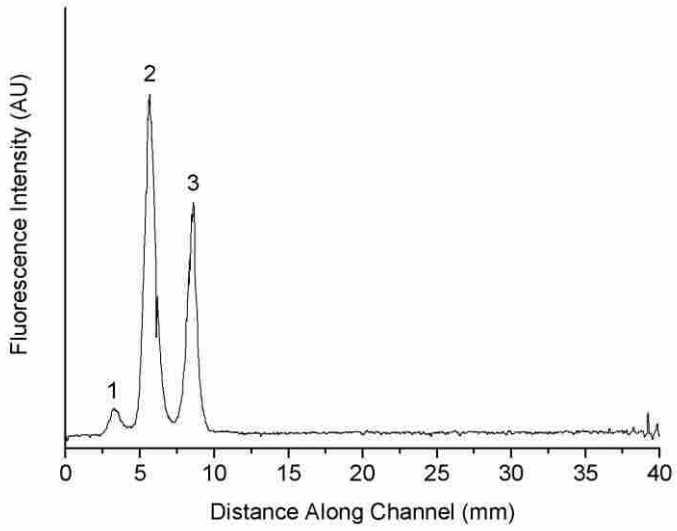

Figure 7.5. Separation of three proteins in an open EFGF channel with concave gradient profile for 5 nL/min counter flow rate and 500 V applied voltage. Peaks: (1) FITC-β-lactoglobulin A, (2) R-PE, and (3) GFP.

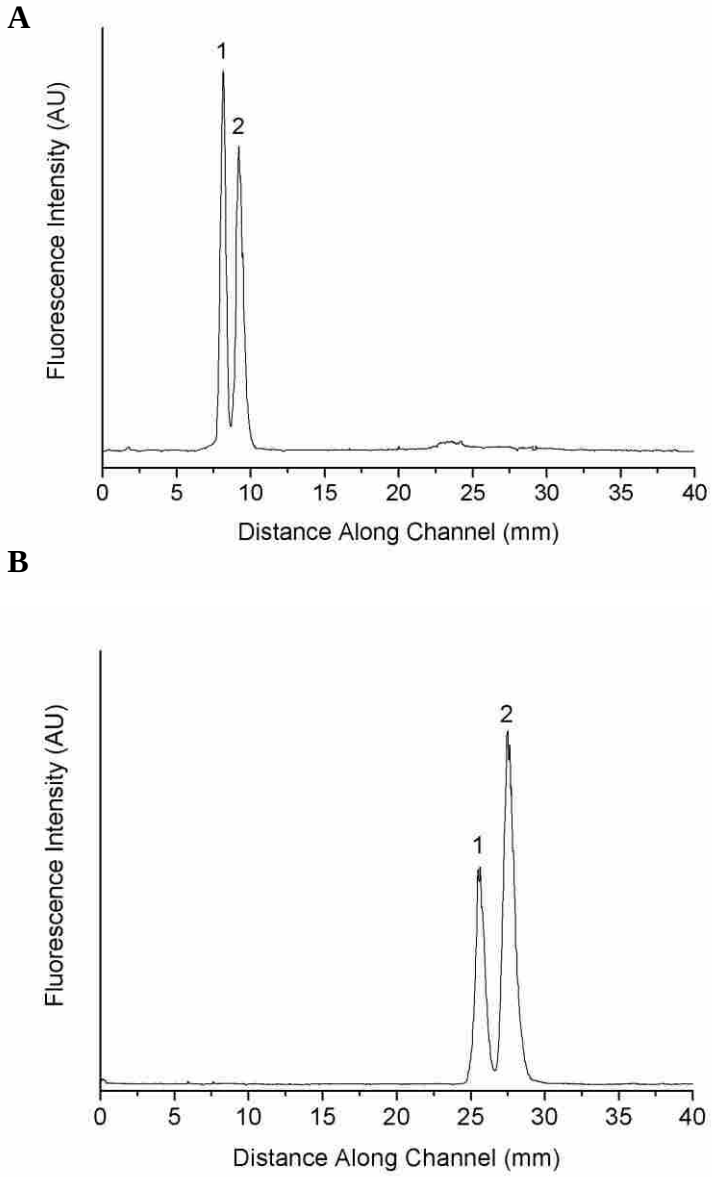

Figure 7.6. Separations of (1) R-PE and (2) GFP in a monolith filled EFGF channel with concave gradient profile at constant voltage (500 V) and different counter flow rates. (A) 5 nL/min and (B) 15 nL/min.

nL/min, the samples were focused in the steeper gradient region. The resolution increased to 1.18 and the bandwidth at half height was approximately 0.8 mm. Compared with the results obtained using an open-channel EFGF device, the bands became narrower.

7.4 Conclusions

I fabricated bilinear EFGF devices using the changing cross-sectional area approach. The presence of two segments with different linear gradients was experimentally confirmed. The steep field segment was near the low field end and the shallow field segment was near the high field end. When samples were focused in the steep field segment, the peaks were narrow and unresolved. After moving them into the shallow field segment by increasing the counter flow rate or decreasing the voltage, the peaks became broader, but better resolved. With a further increase in flow rate, analytes with lower mobilities were sequentially eluted while others were retained. I also fabricated a nonlinear EFGF device with a concave electric field gradient profile, for which the gradient increased along the channel. When the counter flow was increased to move analytes from the low field end to high field end, both bandwidth and resolution changed less than observed for a linear gradient EFGF channel because of an increase in the gradient along the channel.

7.5 References

1. Tolley, H. D.; Wang, Q.; LeFebre, D. A.; Lee, M. L. *Anal. Chem.* **2002**, *74*,

4456-4463.

2. Wang, Q.; Tolley, H. D.; LeFebre, D. A.; Lee, M. L. *Anal. Bioanal. Chem.* **2002**, *373*, 125-135.

3. Wang, Q.; Lin, S.-L.; Warnick, K. F.; Tolley, H. D.; Lee, M. L. *J. Chromatogr. A* **2003**, *985*, 455-462.

4. Sun, X.; Farnsworth, P. B.; Woolley, A. T.; Tolley, H. D.; Warnick, K. F.; Lee, M. L. *Anal. Chem.* **2008**, *80*, 451-460.

5. Sun, X.; Farnsworth, P. B.; Tolley, H. D.; Warnick, K. F.; Woolley, A. T.; Lee, M. L., *J. Chromatogr*. *A* **2009**, *1216*, 159-164

8 FUTURE DIRECTIONS

8.1 PEG-Functionalized Microchips

In Chapter 4, a PEG-functionalized microchip was described. The fabrication was not only easy, but the bonding was strong, which depended on partially polymerized liquid layers remaining on the surfaces. Actually, an unreacted monomer layer on the microchannel wall could facilitate covalent immobilization of a monolith or gel in the channel after quick photo-induced bonding.

Microchip capillary electrochromatography (CEC) can be performed by incorporating a monolith with charges on the surface in the microchannel. For example, a poly(glycidyl methacrylate-co-polyethylene glycol diacrylate) monolith could be prepared in the channel, in which PEGDA is used as a crosslinker to reduce analyte adsorption. Epoxy groups in GMA could be used to attach various functional groups, such as positively charged amine groups or negatively charged acidic groups. Another method would be to directly use functionalized monomers, such as sulfoethyl methacrylate (SEMA), to copolymerize with PEGDA to synthesize monoliths containing the desired functional groups without further treatment.[1,2] A new size exclusion chromatographic monolith could also be integrated in the microchannel which resists protein adsorption and has mesopores for protein separation according to size. In this type of monolith filled microchip, CE separation of proteins would depend on a combination of charge and size, which is similar to gel electrophoresis. It would also be convenient to incorporate a photo curable polyacrylamide gel or PEG-functionalized acrylate gel in a microchannel for gel electrophoresis of proteins.

Microchips with more complicated designs could be fabricated using this material and fabrication method. Various functions could be integrated into one microdevice. As reported previously, a hydrogel with permeation to only small ions could be used to concentrate analytes.[3] An affinity monolith could be used to extract specific target proteins from a complicated sample.[4] Monolith filled microchips could be used for microchip liquid chromatography. This biocompatible material could also be used to fabricate droplet-based microchips to handle single cells in a microchannel. Proteins could be released from the trapped individual cells after lysis, and then digested. The resultant peptides would be separated by CE and analyzed by ESI-MS. This method would be useful for proteomics analysis. For such applications, the major issue would be to use proper solvents, which should not swell, dissolve, or destroy the substrates.

Currently, I can fabricate very thin plates (< 400 μm) using the described microchip fabrication method and material. The thickness of the final microchip was typically less than 1 mm, and it retained sufficient mechanical strength for operation. It is possible that a thin microchip could offer higher efficiency due to good Joule heat dispersion. Furthermore, I could fabricate multiple-layer microdevices for complicated analysis.

8.2 Multi-Electrode EFGF

I fabricated linear, bilinear and concave profile gradient EFGF devices using the changing cross sectional area approach. However, complex changing cross

sectional channels are required to achieve complicated field gradients. Furthermore, the field gradient cannot be easily modified once the device is fabricated. Fortunately, multi-electrode EFGF offers a solution to this problem.

A bottom plate with a rectangular cavity would first be fabricated. A top plate with many small reservoirs would then be bonded to the bottom plate after photopolymerization. Hydrogel monomer solution would be introduced into the cavity and polymerized, and the channel would be formed using a metal wire embedded in the hydrogel. Multiple electrodes would be placed in the buffer filled reservoirs and voltages between adjacent electrodes would be controlled by a computer. Any complicated gradient profile could be obtained by adjusting the voltages to reach the best separation performance. In addition to proteins, cells and viruses could be focused and studied using this technique.

Even though significant progress has been made in EFGF performance as described in this dissertation, it has not reached its expected performance. This is due to current technical difficulties. For example, the hydrodynamic flow rate for focusing is extremely low, and it is difficult to keep it constant during operation. Any slight fluctuation in the flow rate destroys the equilibrium and, thus, affects focusing. Furthermore, I have not been able to precisely control the desired electric field in the channel. When these issues are adequately solved, EFGF could become a powerful analytical technique.

8.3 References

1. Gu, B.; Chen, Z.; Thulin, C. D.; Lee, M. L. *Anal. Chem.* 2006, *78*, 3509-3518.

2. Gu, B.; Li, Y.; Lee, M. L. *Anal. Chem.* 2007, *79*, 5848-5855.

3. Kelly, R. T.; Li, Y.; Woolley, A. T. *Anal. Chem.* 2006, *78*, 2565-2570.

4. Sun, X.; Yang, W.; Pan, T.; Woolley, A. T. *Anal. Chem.* 2008, *80*, 5126-5130.